CHARACTERIZATION OF THE ROLE OF IRISIN IN SKELETAL MUSCLE GROWTH AND REPAIR

MUSARRAT MAISHA REZA

SCHOOL OF BIOLOGICAL SCIENCES

A thesis submitted to the Nanyang Technological University in partial fulfillment of the requirement for the degree of Doctor of Philosophy

2016

Acknowledgements

First and foremost, I would like to express my sincere gratitude to Dr. Craig McFarlane for your excellent supervision and continuous support throughout my PhD. Working under your guidance has definitely enabled me to expand my scientific knowledge and think critically, which would be important for my future scientific career. Your constructive feedback on my experiments and writing has shaped me into a more independent, creative and efficient scientist. Thank you for believing in me and pushing me to reach my best potential. Your contribution to my thesis has been invaluable. It has been my privilege to work in your lab.

Dr. Ravi Kambadur, I would like to extend my heartfelt gratitude to you for being a wonderful mentor. You have ignited the passion for science in me and guided me into a fascinating scientific world. You have equipped me with the strength and confidence to pursue Science. I will always be indebted for your contribution in my life. Dr. Mridula Sharma, you have been a patient and kind advisor to me and have given me valuable scientific feedback on my work, which I appreciate tremendously. A special thank you to Assoc/Prof Thirumaran Thanabalu for the support you have rendered in my thesis completion.

Thank you to Dr. Preeti Chandrashekar and Lee Jing Han Marcus for reading my thesis and giving critical feedback. Thanks to Dr. Ravikumar Manickam for assisting me with the denervation of mice. Thank you to Bhagiradhi Somalanka and Anantha Raj Rengaraj for help with mice dissections and Nesibe Peker for helping me with the Seahorse experiment. I would like to thank Sim Chu Ming for your hard work and dedication towards our project.

I would like to express my sincere appreciation to an amazing leader and mentor, Dr. Ge Xiaojia. I have learnt every scientific technique from you and you have been pivotal in polishing those techniques. You have taught me with so much patience and grace and I have tremendous respect for you. Thank you for all the critical advice and suggestions you have given me for my experiments.

2

One person that I would like to mention specially is Durgalakshmi Sathiakumar for being such a wonderful friend and always being my confidante whenever I needed someone to speak to regarding anything. You have given me so much moral support throughout my PhD and I appreciate that greatly.

To, Nathiya Subramaniyam you are my best friend and we have worked together for the first half of my PhD. I appreciate your support and diligence in all the work that you have done with me and I am so proud of what we have achieved together. We make a perfect team together.

To my dear family, whatever I am today is only because of your unconditional and unwavering support and love. Words cannot justify how grateful I am to have you walking step by step with me throughout every phase of my life, good or bad. You have not just been my pillar of support, but my strongest foundation that I can always depend on. Your kind and loving words of encouragement have been my strength throughout my life. You are irreplaceable.

Table of Contents

List of Figures

List of Tables

List of Abbreviations

5'	5 prime
3'	3 prime
36C15Q	Human myoblast cell line
3T3L1	Murine adipocyte cell line
°C	Degree celsius
aa	Amino acid(s)
A band	Anisotropic band
Ach	Acetylcholine
ActRIIB	Activin receptor type IIB
Alk4/5	Activin receptor like kinase 4/5
Agxt2	Alanine-glyoxylate aminotransferase 2
AMPK	Adenosine monophosphate (AMP)-activated protein kinase
APS	Ammonium persulfate
ATP	Adenosine triphosphate
βMe	β-Mercaptoethanol
BAT	Brown adipose tissue
BCS	Bovine calf serum
Bdnf	Brain-derived neurotrophic factor
BF	Biceps femoris
bFGF	Basic fibroblast growth factor
bHLH	Basic helix loop helix
Bmp4	Bone morphogenic protein 4
BSA	Bovine serum albumin
C1s	Complement C1s
C2C12	Murine myoblast cell line
cAMP	Cyclic adenosine monophosphate
Ccl	C-C motif chemokine ligand
Ccnd1	Cyclin D1
Cdk2	Cyclin dependant kinase 2
cDNA	Complementary deoxyribonucleic acid
CEE	Chick embryo extract
Cidea	Cell death-inducing DFFA-like effector a

12

CK	Creatine kinase
Cpt1b	Carnitine palmitoyltransferase 1b
CSA	Cross sectional area
Cobll1	Cordon-bleu WH2 repeat protein like 1
Cox-2	Cyclooxygenase-2
Crispld2	Cysteine rich secretory protein LCCL domain containing 2
Cxcl	C-X-C motif chemokine ligand
DAPI	4',6-Diamidino-2-phenylindole, dihydrochloride
DB	Dialysis buffer
Dio2	Type II iodothyronine deiodinase
DMD	Duchenne muscular dystrophy
DMEM	Dulbecco's modified eagle's medium
DMSO	Dimethyl sulfoxide
DNA	Deoxyribonucleic acid
EBD	Evans blue dye
E. coli	Escherichia coli
eIF4E	Elongation initiation factor 4E
ECM	Extracellular matrix
EDL	Extensor digitorum longus
EDTA	Ethylenediaminetetraacetic acid
ELISA	Enzyme-linked immunosorbent assay
Ereg	Epiregulin
Erk	Extracellular signal-regulated kinases
EtBr	Ethidium bromide
FNDC 5	Fibronectin type III domain containing 5
FBS	Fetal bovine serum
FCCP	Carbonyl cyanide-4-(trifluoromethoxy)phenylhydrazone
FGF	Fibroblast growth factor
Figf	C-fos induced growth factor
FITC	Fluorescein isothiocyanate
FoxO	Forkhead box class O

g	Gram(s)
Gas	Gastrocnemius
GAPDH	Glyceraldehyde 3-phosphate dehydrogenase
Gap43	Growth associated protein 43
GDF8	Growth and differentiation factor 8
GLUT4	Glucose transporter type 4
Gpd11	Glycerol-3-phosphate dehydrogenase 1-like
GSK-3	Glycogensynthase kinase 3
h	Hour(s)
hADSCs	Human adipose-derived stem cells
H&E	Hematoxylin and Eosin
HCl	Hydrochloric
HEK293	Human embryonic kidney cell line
Heyl	Hairy/enhancer-of-split related with YRPW motif-like
HGF	Hepatocyte growth factor
Hp	Haptoglobin
HRP	Horseradish peroxidase
HS	Horse serum
I band	Isotropic band
IBMX	3-isobutyl-1-methylxanthine
ICC	Immunocytochemistry
Ig	Immunoglobulin
IGF1	Insulin growth factor 1
IHC	Immunohistochemistry
IL6	Interleukin 6
IP	Intraperitoneal
IPTG	Isopropyl β-D-1-thiogalactopyranoside
Irak4	Interleukin 1 receptor associated kinase 4
IRS-1	Insulin receptor substrate 1
JAK	Janus kinase
kb	Kilo base(s)
kDa	Kilo dalton(s)
L	Litre

14

LB	Lennox broth
LIF	Leukemia inhibitory factor
LPS	Lipopolysaccharide
MAFbx50	Muscle atrophy F-box protein, Atrogin-1
MAPK	Mitogen-activated protein kinase
mdx	Dystrophic mice
Megf10	Multiple EGF-like domains 10
MES	2-(N-morpholino)ethanesulfonic acid
MHC	Myosin heavy chain
mg	Milli gram(s)
ml	Milli litre(s)
mM	Milli mole(s)
mRNA	Messenger ribonucleic acid
Mmp	Matrix metallopeptidase
Mnk1/2	MAPK-interacting kinase
MOPS	3-(N-morpholino)propanesulfonic acid
MRF4	Myogenic regulatory factor
MSK1/2	Mitogen- and stress-activated protein kinase
Mt1	Metallothionein 1
mTOR	Mammalian target of rapamycin
MuRF-1	Muscle RING-finger protein-1
mV	Milli volt(s)
Myf5	Myogenic factor 5
NADH	Nicotinamide adenine dinucleotide
NFκB	Nuclear factor-kappa B
ng	Nano gram
NGS	Normal goat serum
Ni	Nickel
No.	Number
NO	Nitric oxide
NRF1	Nuclear respiratory factor 1
Nrg1	Neuregulin 1
Nrp	Neural regeneration protein
NSS	Normal sheep serum

NTA	Nitrilotriacetic acid
O.C.T	Optimal cutting temperature
OCR	Oxygen consumption rate
OD	Optical density
Ogn	Osteoglycin
p90^{rSk}	p90 Ribosomal S6 kinase
P	Probability
p-Akt	Phosphorylated Akt
PAGE	Polyacrylamide gel electrophoresis
Pax3	Paired box gene 3
Pax7	Paired box gene 7
PBS	Phosphate buffered saline
PDGF	Platelet derived growth factor
PFA	Paraformaldehyde
PGC1-α	PPAR-γ co-activator 1-α
PI	Protease inhibitor
PI3-k	Phosphoinosital 3-kinase
Plau	Plasminogen activator, urokinase
PMSF	Phenylmethane sulfonyl fluoride
PPAR-α	Peroxisome proliferator-activated receptor- α
Prdx6	Peroxiredoxin 6
P/S	Penicillin and streptomycin
PTEN	Phosphatase and tensin homolog
Ptx3	Pentraxin 3
Quad	Quadriceps
Rb	Retinoblastoma
RNA	Ribonucleic acid
RNAse	Ribonuclease
rpm	Revolutions per minute
RT	Room temperature
qPCR	Quantitative reverse transcription polymerase chain reaction
s	Second(s)
SC	Santa Cruz

16

SDS	Sodium dodecyl sulfate
Sema3f	Semaphorin 3F
Serpina3g	Serine (or cysteine) peptidase inhibitor, clade A, member 3G
SHIP	SH2-domain-containing inositol 5'-phosphatase
Shq1	H/ACA ribonucleoprotein assembly factor
siRNA	Small interfering ribonucleic acid
Smad	Small mother against decapentaplegic
SOCS	Suppressor of cytokine signaling
Sod3	Superoxide dismutase 3, extracellular
Sol	Soleus
Sox8	SRY-Box 8
STAT	Signal transducer and activator of transcription
TA	Tibialis anterior
TAE	Tris acetate EDTA
Taq	DNA polymerase from *Thermus aquaticus*
TBS-T	Tris buffered saline with Tween 20
TEMED	Tetramethylethylenediamine
TFAM	Transcription factor A, mitochondrial
TGF-β	Transforming growth factor- β
Thbd	Thrombodulin
Timp1	Tissue inhibitor of metalloproteinase
Tiparp	TCDD inducible poly(ADP-ribose) polymerase
Tmem26	Transmembrane protein 26
TNF-α	Tumor necrosis factor-α
Tnfrsf11b	Tumor necrosis factor superfamily, member 11b
Tris	2-amino-2-(hydroxymethyl)-1,3-propanediol
T-tubules	Transverse tubules
Ucp-1	Uncoupling protein-1
Ucp-3	Uncoupling protein-3
μg	Micro gram(s)
μl	Micro litre(s)
WAT	White adipose tissue

Abstract

Exercise stimulates the expression of PPAR-γ co-activator 1-α (PGC1-α), which in turn increases the levels of the myokine, Irisin. Irisin is synthesized as part of a 209 amino acid (aa) long precursor protein, Fibronectin Type III Domain Containing Protein 5 (FNDC5), which is proteolytically cleaved at the C terminal to give rise to the 112 amino acid long Irisin protein. Irisin induced upon exercise, promotes browning of white adipose tissue through binding to CD137+ precursor cells, resulting in increased energy expenditure, reduced adiposity and improved insulin sensitivity.

A novel function of Irisin on skeletal muscle has been reported in this thesis. Recombinant Irisin protein induced a number of pro-myogenic and exercise response genes in myotubes. Moreover, treatment of C2C12 myoblasts with recombinant murine Irisin protein resulted in increased myoblast proliferation and fusion, leading to increased myogenic differentiation. Expression analysis of myoblast differentiation markers showed upregulation of Myosin Heavy Chain (MHC) in response to Irisin treatment, which validated the increased differentiation noted. Moreover, the primary fusion marker, *Myomaker* was also shown to be upregulated by Irisin treatment. In addition, evidence presented in this thesis revealed that the increased myogenic differentiation observed following Irisin treatment is, at least in part, due to IL6. These data reveal that Irisin positively regulates myogenesis through enhancing myoblast growth, differentiation and fusion.

Mice injected with recombinant murine Irisin displayed increased muscle weights, distinct hypertrophy in un-injured muscle and enhanced grip strength, further supporting the pro-myogenic function of Irisin. Mechanistically, Irisin promoted skeletal muscle hypertrophy, through increasing protein synthesis and inhibiting protein degradation pathways. Expression analysis confirmed that Irisin activates the protein synthesis pathways via Akt, Erk and MAPK activation. In addition, Irisin inhibits the protein degradation pathway by reducing the expression of E3 ubiquitin ligases, Atrogin-1 and MuRF-1.

To further study the pro-myogenic capacity of Irisin, we next assessed the effect of Irisin during muscle regeneration. Treatment with Irisin resulted in significant myofiber hypertrophy and increased centrally placed nuclei, further supporting the role of Irisin in promoting myoblast fusion. Immunocytochemistry revealed that injection of Irisin during skeletal muscle regeneration increased Satellite cell activation, as shown by higher numbers of MyoD positive nuclei in the early stages of regeneration. This data was further validated *in vitro*, where we observed a larger population of activated, fusion competent ($Pax7^-MyoD^+$) and proliferating Satellite cells ($Pax7^+MyoD^+$), suggesting a direct role of Irisin on Satellite cells activation. These results reveal that increased circulatory levels of Irisin may further induce skeletal muscle hypertrophy by activating Satellite cells.

In addition to assessing Irisin function during muscle regeneration the effect of Irisin on muscle growth was further assessed in models of muscle atrophy and wasting. We investigated if Irisin could rescue or reverse muscle atrophy associated with denervation. Irisin injection distinctly rescued the loss of skeletal muscle mass and reduced myofiber cross sectional area noted in response to denervation-induced muscle atrophy, which was associated with enhanced Satellite cell activation and reduced protein degradation. The effect of Irisin on dystrophic muscle loss was further assessed using the *mdx* mouse model of Duchenne Muscular Dystrophy (DMD). Results revealed that Irisin treatment resulted in reduced fibrotic tissue accumulation and muscle necrosis as well as improved sarcolemmal stability in *mdx* mice. Furthermore, increased muscle mass and myofiber hypertrophy, was noted upon Irisin treatment of *mdx* mice, which was more significant in adult mice and during prolonged Irisin treatment.

Collectively, the data presented in this thesis underscores the important autocrine/paracrine function of Irisin on skeletal muscle and the potential benefit of Irisin in promoting muscle growth and repair/healing and protection from muscular atrophy.

1. Introduction

1.1 Skeletal Muscle

1.1.1 Skeletal Muscle Structure and Organization

There are three types of muscles in the body; smooth, cardiac and skeletal muscle. Skeletal muscle is one of the largest organs in the human body and contributes to 50% of our body mass[1]. Skeletal muscle is critical for voluntary movement during normal daily activities, such as walking and sitting upright. Skeletal muscles are striated[2], consisting of multinucleated fibers, which are in fact a syncitium that is formed from the fusion of multiple muscle precursor cells, termed myoblasts. Skeletal muscle plays an important role in regulating whole body metabolism[3]. As such, skeletal muscle is a storage site for major metabolites, including glucose in the form of glycogen, amino acids in the form of muscle protein and fatty acids[4]. Skeletal muscle is composed of muscle fibers, blood vessels and nerves and is surrounded by an extracellular matrix (ECM), which is critical for its maintenance and function. The ECM consists of three different layers of connective tissue, the epimysium, perimysium and endomysium. The epimysium surrounds multiple fascicles that are made up of many bundles of muscle fibers. Each fascicle is enclosed by the perimysium. The perimysium contains blood vessels, nerves and collagen. Each muscle fiber found within fascicles is further surrounded by the endomysium, which contains blood capillaries. Collagen and proteoglycans are also major components of the ECM and together, they determine the structural organization of the ECM (Figure 1.1).
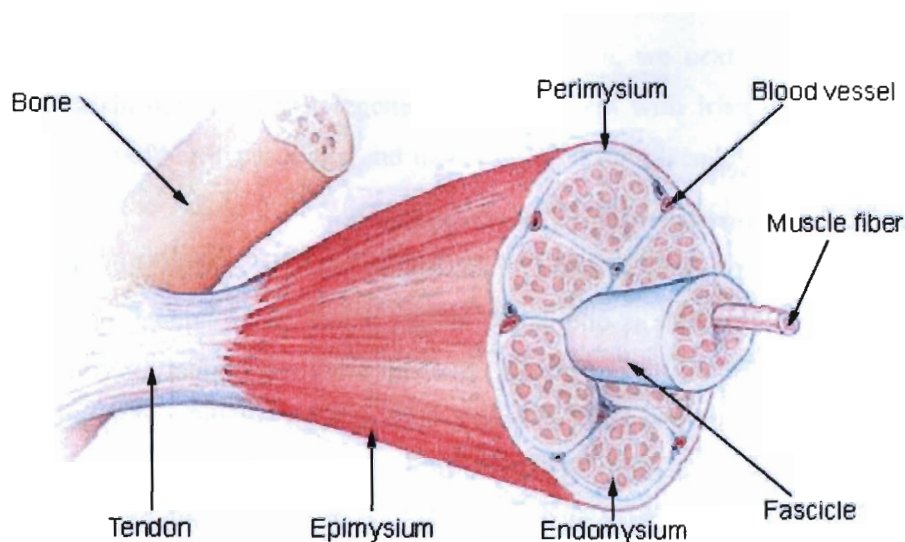
Figure 1.1: Skeletal muscle structure

The entire skeletal muscle is enclosed by the epimysium. Skeletal muscle is made up of fascicles, which are wrapped around by the perimysium. Each fascicle contains muscle fibers, which are in turn, enclosed by the endomysium. Figure was adapted from Wikimedia, https://commons.wikimedia.org/wiki/File:Illu_muscle_structure.jpg#filelinks. (*This image is in the public domain*).

1.1.2 Sarcomeric Structure

Each muscle fiber is enclosed by a plasma membrane, termed the sarcolemma, and are made up of multiple myofibrils. Each myofibril consists of approximately 10,000 contractile units, known as sarcomeres[5]. Sarcomeres are the contractile functional units of skeletal muscle and are responsible for generation of force, which is translated to movement. The sarcomere contains several proteins, such as thin actin filaments and thick myosin filaments and additional proteins that regulate their interaction, such as troponin and tropomyosin[6]. Myosin is made up of 2 globular heads and is arranged in a head-to-tail fashion. Myosin heads contain ATPase activity, which hydrolyses adenosine triphosphate (ATP) required for generation of force during muscle contraction. Approximately, 300 heads are present in each myosin thick filament[7]. On the other hand, actin filaments in the muscle are globular proteins, which form helical filaments after polymerization. Actin molecules contain docking sites for myosin, which interact during muscle contraction[8].
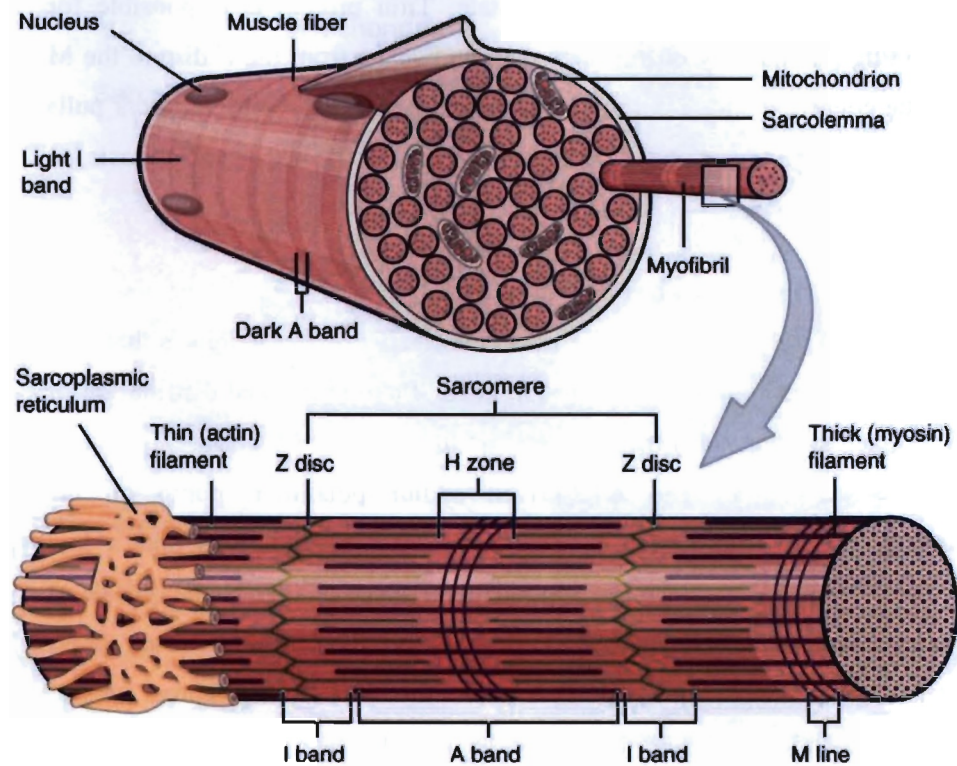
Figure 1.2: Structure of the sarcomere
Diagram a muscle fiber made up of multiple myofibrils, which consist of repeated contractile units, known as sarcomeres. The sarcomere above shows the thick filaments (myosin), thin filaments (actin), I band, A band, Z discs, M line, zone of overlap and H zone. Figure was adapted from OpenStax Wikimedia,
https://commons.wikimedia.org/wiki/File:1022_Muscle_Fibers_(small).jpg.
(*This image is licensed under the terms of the Creative Commons Attribution License*).

The sarcomere structure is highly organized (Figure 1.2). The sarcomere functional unit extends from one Z disc to other. The Z disc is the line which divides the isotropic band (I band) and is the anchoring point for the actin filaments. The I band consists of only actin filaments. The anisotropic band (A band) on the other hand consists of the zone of overlap between actin and myosin filaments and the entire length of myosin filaments. The differences in density and distribution of the filaments make the sarcomere appear as banded regions due to the darker A band and the lighter I band. The M line is the anchoring point for the myosin filaments on either side of the sarcomere (Figure 1.2). During skeletal muscle contraction, the zone of overlap extends and the length of the sarcomere shortens as the thin and thick filaments slide

22

across each other. During the resting state, Titin protein is responsible for maintaining the integrity of the sarcomere and spans from the Z disc to the M line. The concerted shortening of the sarcomere across the muscle fibers pulls on the connective tissue, which in turn pulls on the tendon or aponeurosis, to which they are connected, in order to generate movement[9].

1.1.3 Skeletal Muscle as a Locomotion Organ

Skeletal muscle fibers are highly responsive to neuromuscular signals that lead to muscle contraction. During the resting state, there is unequal distribution of charges across the sarcolemma, which maintains the electric potential difference at -90mV. The ATP-driven sodium-potassium pump on the sarcolemma maintains a high concentration of potassium ions and a low concentration of sodium ions in the intracellular space relative to the outside of the sarcolemma. Acetylcholine (ACh) released from the neurons diffuses across the neuromuscular junctions and binds to the nicotinic ACh receptors present on the sarcolemma[10]. When neuromuscular signals reach the threshold level, the chemically regulated ion channels open, allowing extracellular sodium ions to rush into the muscle cell while less potassium ions leave the muscle cell. This exchange of ions results in the depolarization and subsequent generation of an action potential, which travels rapidly along the sarcolemma. The sarcolemma forms deep invaginations that span across the muscle fibers, known as transverse tubules (T-tubules) (Figure 1.3), which are responsible for transmitting the depolarization signal throughout the muscle fibers uniformly[11]. During the resting state, terminal cisternae, the bulge from the sarcoplasmic reticulum on either side of the T-tubules (Figure 1.3), stores calcium ions, which are released once the action potential reaches them via the T-tubules. The released calcium ions bind to troponin, resulting in a conformation change in the structure of tropomyosin, which normally blocks the myosin binding sites on actin filaments. Hence, allowing for myosin-actin interaction and finally, the contraction of sarcomeres as the actin filaments move closer to the center of the sarcomere, in an ATP-dependent manner[6].
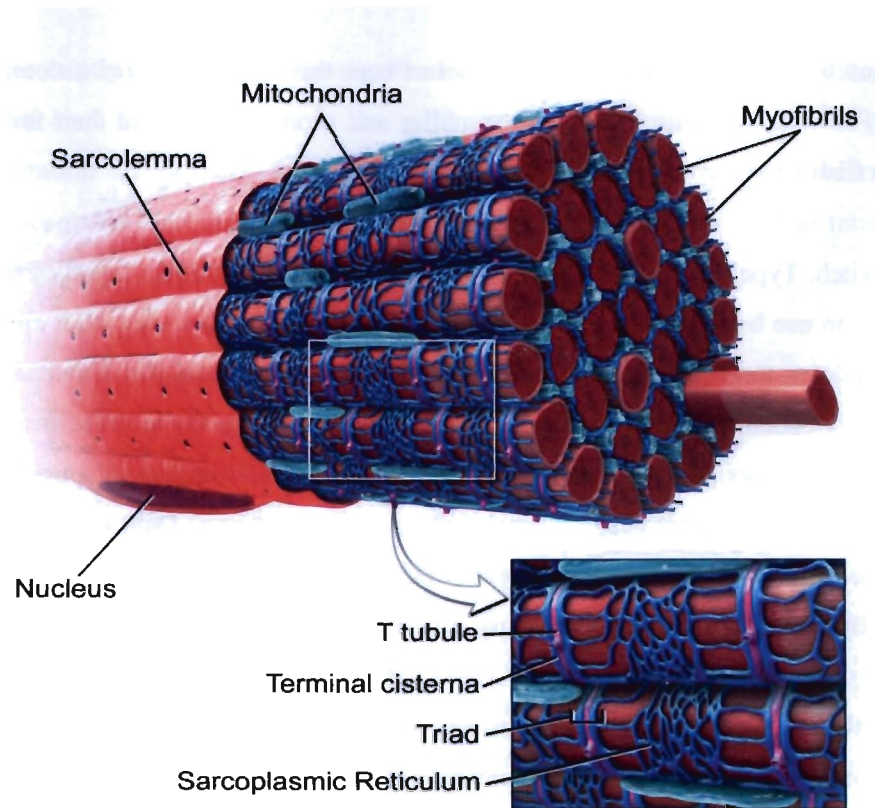
Figure 1.3: Structure of a muscle fiber
Diagram of an individual muscle fiber displaying the myofibrils, sarcolemma, sarcoplasmic reticulum, T-tubules, terminal cisternae, thick filaments (myosin), thin filaments (actin) and myofibrils. Figure was adapted from BruceBlaus, Wikimedia, Blausen.com staff. "Blausen gallery 2014". *Wikiversity Journal of Medicine*. DOI:10.15347/wjm/2014.010.

1.1.4 Muscle Fiber Types

There are primarily three different types of skeletal muscle fibers that are used in response to different forms of physical activity or stress on skeletal muscle. These different muscle fiber types are Type I slow twitch oxidative fibers, Type IIa fast twitch oxidative fibers and Type IIb fast twitch glycolytic fibers.

The Type I slow twitch fibers are used mostly during long periods of endurance exercise, as they are able to produce large amounts of ATP for a prolonged period. Type I slow twitch fibers contract repeatedly over a long period, although slower than that of the fast twitch fibers. Type I fibers are rich in mitochondria and can generate their ATP in the mitochondria via oxidative phosphorylation. Hence, Type I slow twitch muscle fibers are aerobic in nature and are enriched with blood vessels to supply oxygen, carried by myoglobin to

24

the muscle, which also gives these muscle fibers their distinctive red colour. Type I slow twitch muscle fibers are smaller and produce less force than fast twitch fibers, but are the most resistant to fatigue[12 13].

Fast twitch, Type IIa oxidative fibers on the other hand can contract rapidly but are able to use both aerobic and anaerobic energy sources to generate ATP and break it down to provide energy for muscle contraction. Type IIa fibers contain more mitochondria, blood capillaries and myoglobin than Type IIb fibers, giving these fibers their red colour. Type IIa fibers can produce energy quickly by utilizing both aerobic and anaerobic metabolism. However, Type IIa fibers are more prone to fatigue than Type I fibers. As such Type IIa fibers are generally used during moderate training activities[12, 13].

Type IIb fast twitch glycolytic fibers can contract very rapidly (three times faster than slow, Type Ia fibers) to generate a large amount of force over a short period of time, especially during high intensity activities, such as sprinting. Type IIb fast twitch fibers are much bigger in size than slow twitch fibers, as they are packed with myofibers. Type IIb fast twitch fibers are glycolytic in nature and can breakdown glycogen rapidly for high intensity activity and hence, they have little mitochondria. However, Type IIb fast twitch fibers fatigue easily due to lactic acid build up, since these fibers utilize anaerobic respiration to produce small amounts of ATP rapidly, which is then broken down in order to provide energy to contracting muscle fibers. Type IIb fast twitch fibers have little intracellular myoglobin and low capillary density, hence, these muscle fibers appear white in colour[12, 13].

1.2 Myogenesis

1.2.1 Embryonic Myogenesis

Myogenesis is the process in which muscle fibers are formed from myogenic progenitor/precursor cells, termed myoblasts[14]. During embryonic myogenesis, the first muscle fibers are formed from mesoderm-derived structures, termed somites, and are found in the mesodermal germ layer. Additional muscle fibers are subsequently formed along the initial template fibers[15, 16]. Resident myogenic progenitors in skeletal muscle proliferate extensively at first, which is

25

subsequently decreased as the number of myonuclei reaches a steady state, at which time there is a peak in the synthesis of myofibrillar proteins[17]. Upon maturation of skeletal muscle, these myogenic progenitors will become quiescent and function as Satellite cells (Section 1.2.2.1), also known as muscle stem cells.

During embryogenesis, skeletal muscle is formed from somites, which are derived specifically from the paraxial mesoderm germ layer[18]. Increasing retinoic acid concentration enables the distinction of the dorsal and ventral segments of the somites[15]. The dorsal portion of somites gives rise to the dermomyotome, which then forms the hypaxial and epaxial dermomyotome[19]. The hypaxial dermomyotome generates body and limb musculature, while the epaxial dermomyotome generates deep back musculature. The ventral portion of the somites on the other hand, forms the sclerotome which gives rise to cartilage and bone. Apart from head muscles, all skeletal muscles are derived from the dermomyotome[19].

Cells in the dermomyotome express the paired-box transcription factors *Pax3* and *Pax7*[20]. Hepatocyte growth factor (HGF) and subsequent binding of HGF to the receptor tyrosine kinase c-met, promotes the delamination of muscle progenitor cells from the epithelium of the dermomyotome and subsequent migration of progenitor cells into the limb buds[21]. *Pax3* functions upstream of *c-Met* and regulates *c-Met* expression[22]. *Pax3* expressing cells direct cells in the dermomyotome into a myogenic lineage, which subsequently express *Pax7* and become muscle progenitors for embryonic and fetal myogenesis[23, 24, 25].

After migration into the limb buds, muscle progenitor cells start expressing *MyoD* and *Myf5* which are basic-helix-loop-helix (bHLH) transcription factors that play significant roles in embryonic myogenesis. *Myf5* is the first bHLH transcription factor to be expressed in embryogenesis and acts upstream of *MyoD*[22]. However, *Myf5* and *MyoD* have redundant functions and can compensate for the absence of the other. Homozygous *Myf5* knockout results in normal skeletal muscle morphology and expression of muscle specific genes but with reduced muscle fibers size and mass[26]. Similarly, a knockout of *MyoD*

26

results in a significant spike in *Myf5* expression resulting in normal musculature, although myogenesis is delayed[26, 27]. However, a double knockout of both *MyoD* and *Myf5* results in the complete absence of skeletal muscle[27].

Myogenin and *MRF4,* are also part of the same bHLH family. *Myogenin* is required for terminal differentiation while *MRF4* is expressed after the onset of terminal differentiation [28]. Myoblasts undergo repeated cycles of proliferation and upon depletion of growth factors, withdraw from the cell cycle and become committed to differentiation. Committed myoblasts express *myogenin* and align themselves before fusing with one another, or with existing myofibers. While knockout of *myogenin* results in normal myoblast populations, terminal differentiation is absent, underscoring the critical role of myogenin in myogenic differentiation[29]. The final bHLH transcription factor, *MRF4*, functions as a maturation factor for myotubes, promoting mature muscle fiber formation[30].

1.2.2 Post-natal Myogenesis

1.2.2.1 Satellite Cells

Post-natal adult skeletal muscle, like all regenerating tissues, relies on mechanisms that compensate for the turnover of terminally differentiated cells to maintain tissue homeostasis [31, 32]. Post-natal muscle growth and repair is primarily attributed to the function of muscle stem cells (also known as satellite cells), which reside between the sarcolemma and endomysium of muscle fibers[33, 34]. At birth, 30% of the muscle nuclei in mice are satellite cells, but the numbers reduce and stabilize at 5% during adulthood[35].

Satellite cells normally exist in a quiescent state and express high levels of Pax7 and low levels of MyoD (Pax7$^+$MyoD$^-$) but are activated in response to signals resulting from stimuli such as injury or muscle stress[36]. During exercise, stretch or damage skeletal muscle fibers secrete HGF into the extracellular matrix in order to activate Satellite cells via a Nitric oxide (NO)-dependent pathway[37]. Activated satellite cells express the myogenic marker MyoD and become positive for both Pax7 and MyoD (Pax7$^+$MyoD$^+$). Satellite cells re-enter the cell cycle and undergo repeated rounds of proliferation in the presence of growth factors. Growth factors, such as Insulin-like growth factor (IGF) and fibroblast

growth factor (FGF) can stimulate proliferation of activated satellite cells[38, 39]. Activated satellite cells express the early myogenic markers *Myf5 and MyoD*, which are required for proliferation of myoblasts. MyoD is essential for myoblasts to commit to differentiation (Figure 1.4).

Once nutrients like FGF or IGF are depleted, myoblasts withdraw from the cell cycle and secrete fibronectin into the extracellular matrix. Fibronectin is present in the ECM in abundance and plays an important role during myogenesis and muscle regeneration (See Section 1.2.2.2 Skeletal Muscle Regeneration). Secreted fibronectin then binds to the major fibronectin receptor, $\alpha 5\beta 1$ integrin on myoblasts to initiate migration and alignment of myoblasts to facilitate fusion[40, 41]. This enables myoblasts to proceed with differentiation. *Myogenin*, which functions downstream of *MyoD,* is responsible for myoblast differentiation into myotubes[29]. *Myogenin* positive myoblasts fuse and give rise to multinucleated myofibers[42]. The presence of different molecular markers in satellite cells and satellite cell-derived myoblasts during post-natal myogenesis have been extensively characterized (Figure 1.4), which allow for the identification of the different cell types at each stage.
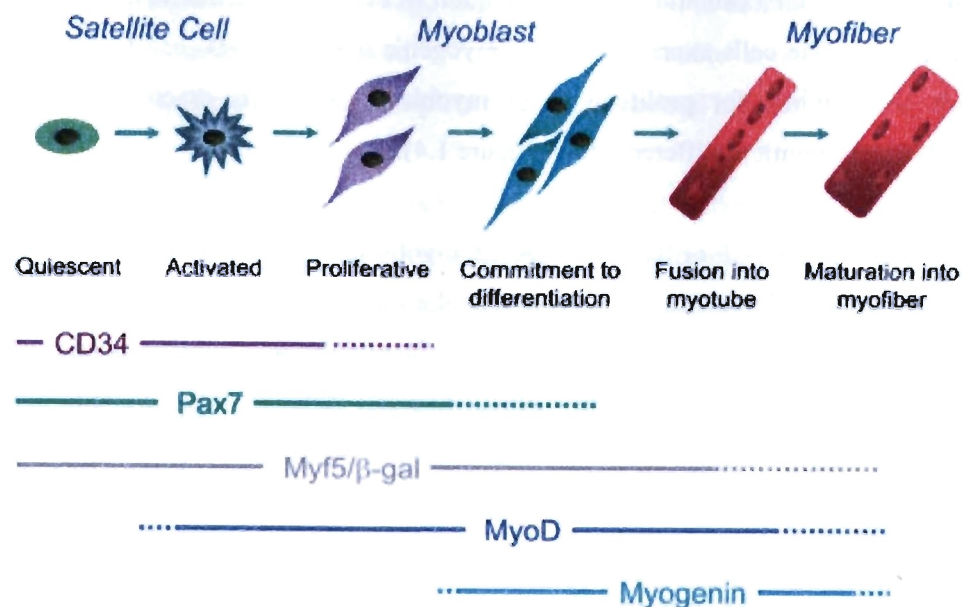
Figure 1.4: Illustration of the different markers that are expressed in satellite cells and myoblasts during different stages of myogenesis

The lines extending from both sides of each marker indicate the different stages of myogenesis that the particular marker is expressed. CD34 and Pax7 are markers of quiescent Satellite cells. Myf5 is the first myogenic marker to be expressed in activated, proliferating myoblasts. MyoD is expressed subsequently in activated, proliferating myoblasts and is required for myoblast commitment to differentiation. Myogenin is expressed downstream of MyoD and is essential for fusion of myoblasts into myotubes. Figure was adapted and modified from Zammit, P. S., Partridge, T. A., & Yablonka-Reuveni, Z. (2006). The skeletal muscle satellite cell: the stem cell that came in from the cold. *Journal of Histochemistry & Cytochemistry, 54*(11), 1177-1191. (*Permission to use this image has been granted by Copyright Clearance Centre, See Appendix 6.1*).

For the Satellite cell population to maintain itself at a steady state, self-renewal is critical. Satellite cells have two potential fates; they can become either fusion competent or fusion incompetent myoblasts. Fusion competent cells, which normally express MyoD and lack Pax7 expression, fuse with one another or fuse with existing myofibers. However, fusion incompetent myoblasts lose MyoD expression while retaining its Pax7 expression and hence, returns to a state of quiescence to maintain the satellite cell pool, a process known as satellite cell self-renewal.

Two models of self-renewal have been proposed to date. Firstly, it is thought that satellite cell self-renewal may occur through symmetric division, where

satellite cells divide to give rise to two identical daughter cells committed to myogenesis or identical daughter satellite cells committed for self-renewal[43, 44]. The second model relies on asymmetric division, where satellite cells divide and give rise to an identical daughter stem cell for self-renewal and a second fusion competent daughter cell, which either fuses to give rise to new muscle fibers or fuses directly with damaged myofibers, to repair the injury and contribute to the pool of nuclei found within skeletal muscle fibers[45, 46]. Approximately 10% of the Satellite cell population undergoes asymmetric division[47].

1.2.2.2 Skeletal Muscle Regeneration

As alluded to above (see section 1.2.2.1 Satellite cells), skeletal muscle has the innate ability to repair and regenerate itself in response to injury. Skeletal muscle regeneration is a highly coordinated process and has several phases, the degeneration phase, inflammation phase, repair phase and finally re-innervation and re-vascularization[48]. During degeneration, muscle fibers undergo necrosis due to stress or muscle damage. Inflammation involves infiltrating monocytes that orchestrate the inflammation process. Myofiber debris is cleared and muscle repair then occurs. During the repair phase, satellite cells are activated. Activated satellite cells proliferate, differentiate and fuse to form new muscle fibers in order to replace damaged ones[49] (See 1.2.2.1 Satellite cells). Rgenerating muscle undergoes re-vascularization and re-innervation as well to enable muscles to function normally[48]. Finally, formation of scar tissue occurs and muscles regain their functional capacity[50] (Figure 1.5).

When skeletal muscle undergoes trauma or injury, myofibers undergo rapid necrosis with a disruption to the sarcolemma, which triggers multiple modes of responses from the muscle. The first mode of response to muscle damage is inflammation[51]. This process involves mainly neutrophils and macrophages[52]. The resident macrophages located in the epimysium and perimysium of the muscle are the first to kick-start the inflammation process[53]. Resident macrophages are involved in clearing bacteria or damaged muscle debris and secrete pro-inflammatory cytokines[54]. These macrophages release chemoattractants, which attract circulating neutrophils[48] . The population of

neutrophils undergoes a distinct increase within the first few hours of muscle injury and secrete pro-inflammatory cytokines, free radicals and proteases[48]. The proteases are involved in the degradation of muscle debris, while free radicals target the necrotic muscle fibers for phagocytosis. Pro-inflammatory cytokines attract circulating macrophages to the site of injury[55].

Infiltrating macrophages are crucial for successful regeneration since depletion of the circulating monocytes has been shown to block muscle regeneration[56]. The infiltrating macrophages are a heterogeneous population with the presence of pro-inflammatory and anti-inflammatory sub-populations. CD68^{+} pro-inflammatory macrophages are key players in the inflammation process and these macrophages secrete high levels of pro-inflammatory cytokines, such as tumor necrosis factor-α (TNF-α), IL1β and IL12[57]. They are also involved in the phagocytosis of necrotic fibers and muscle debris[57]. Pro-inflammatory macrophages can also be induced to synthesize nitric oxide synthase in order to produce nitric oxide, which would be responsible for killing intracellular pathogens[57]. Following the inflammation process, anti-inflammatory CD163^{+} macrophages then dominate the site of regeneration. Anti-inflammatory macrophages deactivate the pro-inflammatory macrophages by secreting anti-inflammatory cytokines, such as IL10[58]. Pro-inflammatory macrophages were shown to promote myoblast proliferation while the anti-inflammatory macrophages promote skeletal muscle regeneration by inducing myoblast differentiation and fusion[56]. Importantly, inhibition of anti-inflammatory macrophages leads to reduced muscle fiber size[56].

During muscle repair, regenerating muscle fibers undergo extracellular matrix remodeling, re-vascularization and re-innervation[48]. Muscle repair involves the rebuilding of the extracellular matrix around the damaged muscle fiber. Macrophages secrete growth factors, such as transforming growth factor- β (TGF-β), basic fibroblast growth factor (bFGF) and platelet-derived growth factor (PDGF), which are essential for attracting fibroblasts to the site of injury[59]. Fibroblasts migrate and proliferate in order to produce new ECM components including, collagen, fibronectin, elastin, proteoglycans and laminin. These components form a scaffold for newly forming myofibers and restore the

integrity of the ECM[60]. Satellite cells use the sarcolemma of damaged muscle fibers and these components of the ECM to ensure muscle fibers are re-formed in the same position and also to direct the formation of neuromuscular junctions for the process of re-innervation[60]. Proteases and the specific inhibitors are what regulate the formation and degradation of the ECM. Protein fragments, which are generated as a result of the degradation of ECM, are also important in ensuring normal muscle tissue repair[61]. In situations of prolonged inflammation where there are high levels of the cytokine TGF-β, myoblasts can be triggered to transform into myofibroblasts, which further contribute to muscle fibrosis[62, 63].

Angiogenesis, the formation of new blood vessels is another crucial process in skeletal muscle regeneration as it helps to re-vascularize skeletal muscle fibers at the injury site, in order to allow new muscle fibers to grow and mature in the presence of oxygen and nutrients [60, 64]. This allows the injured area to become functional again.
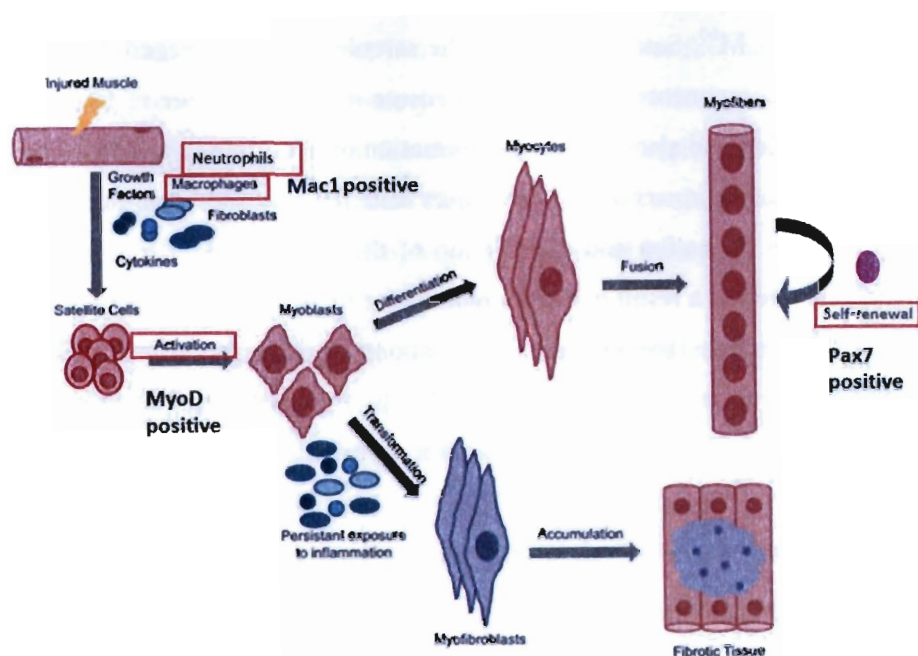
Figure 1.5: Schematic representation of skeletal muscle regeneration
Diagram representing the different stages of regeneration in skeletal muscle including, inflammation involving neutrophils and macrophages, satellite cell activation and fusion to form new myofibers or transformation into myofibroblasts for scar tissue formation. Satellite cells also undergo self-renewal to maintain its population. Image was adapted and modified from Burks, T. N., & Cohn, R. D. (2011). Role of TGF-β signaling in inherited and acquired myopathies. *Skeletal Muscle, 1*(1), 1. (*This image has been obtained from Open Access article distributed under the terms of the Creative Commons Attribution License*)

1.3 Skeletal Muscle Dystrophy

Duchene Muscular Dystrophy (DMD) is a very common form of muscle wasting seen in young boys and is caused by mutations in the *dystrophin* gene[65]. Mutation of the *dystrophin* gene results in the production of defective dystrophin, a sub-sarcolemmal protein leading to membrane fragility and muscle necrosis[66]. Membrane fragility occurs because absence of functional dystrophin prevents the formation of the link between the endomysium and cytoskeleton resulting in the breakdown of protein complexes of the muscle membrane[57].

Multiple rounds of degeneration in dystrophic muscle are accompanied by chronic inflammation in the muscle. TGF-β1, which is highly present during

33

inflammation, is known to be a potent regulator of tissue healing and fibrosis and high levels of TGF-β1 induces the conversion of myoblasts into fibrotic tissue[60, 67]. Moreover, TGF-β1 is known to inhibit the activation of satellite cells and differentiation of myoblasts[38]. Satellite cells are the primary pro-myogenic cells in skeletal muscle and are critical for successful muscle regeneration. However, due to consistent cycles of degeneration and regeneration during DMD, Satellite cells either lose their ability to repair damaged muscle or the population becomes exhausted. Moreover, myofibers are progressively replaced by collagen, which promotes fibrosis and weakening of muscle, as elastic myofibers are replaced by non-elastic connective tissue[68].

The functionality of muscle deteriorates in muscular dystrophy patients over time, which leads to the weakening of muscle in humans[66]. In the late stages of the muscular dystrophy, patients become wheelchair bound since activities like walking become challenging and patients often die prematurely due to heart and respiratory failure[69]. Currently there are no known therapies to overcome DMD or for that matter, any form of muscular dystrophy.

To study the dystrophic phenotype, mdx mice have been used in this thesis. The naturally occurring mdx mouse model of DMD[70] is one of the most widely used models to study the pathophysiology of DMD. At an early stage of the disease (3 weeks of age), mdx mice undergo a sudden onset of muscular necrosis[71]. This acute onset of muscular dystrophy provides a good platform to investigate various potential therapeutics aimed at reducing necrosis and improving muscle strength. Mdx muscle growth is slower than that of wild type controls and hence, they have smaller muscle fibers, reduced myonuclear domains and less myonuclei[72]. Three-week-old young mdx mice undergo severe and repeated rounds of muscle fiber destruction and regeneration. Hence, a large population of necrotic muscle fibers is present[73]. After 8 weeks of age, the extent of muscle fiber necrosis decreases and stabilizes despite repeated rounds of fiber necrosis and regeneration[73]. By 12-14 weeks of age, dystrophic muscle fibers attain the maximum size and become hyper-nucleated, which is evidence of muscle regeneration[72].

1.4 Mechanisms Regulating Skeletal Muscle Mass

Skeletal muscle mass is regulated through the interplay of several factors, which maintain a critical balance between protein synthesis and protein degradation. Protein turnover due to synthesis and degradation is an ongoing process, which maintains skeletal muscle mass in a steady state[74]. Myonuclear accretion and eventual myonuclear loss are also responsible for regulation of skeletal muscle mass[75].

A shift in the balance towards increased protein synthesis, stimulated by circumstances such as resistance exercise, which involves the bearing of a load, can promote skeletal muscle hypertrophy[76, 77, 78]. Skeletal muscle hypertrophy is a phenomenon defined by an increase in muscle fiber size and muscle mass[76]. Increased protein synthesis enables new muscle proteins and contractile filaments to be incorporated into existing myofibers, thus allowing for greater force to be generated[74].

On the other hand, during chronic disease situations, such as cancer, AIDS, sepsis, starvation or denervation, degradation or breakdown of muscle protein ensues, primarily via the ATP-dependent ubiquitin proteasome pathway. This leads to the loss of skeletal muscle mass and strength and hence, muscle undergoes atrophy[74].

Satellite cells have also been shown to play a critical role in regulating skeletal muscle mass. Apart from processes involving muscle repair and regeneration, satellite cells can enhance skeletal muscle mass and promote muscle hypertrophy by fusing to existing muscle fibers and contributing to myonuclear domain expansion[75]. Upon stimuli like exercise, satellite cells can also undergo post-natal myogenesis (See section 1.2.2.1 Satellite cells) to fuse and promote muscle hypertrophy. Although it was previously established that satellite cell activation is necessary for muscle hypertrophy, recent transgenic studies established that hypertrophy of skeletal muscle can occur without the presence of satellite cell activation and fusion[75]. However, in most occurrences of hypertrophy, satellite cell activation is observed.

1.4.1 Protein synthesis

Hypertrophy of skeletal muscle can also be attributed to increased protein synthesis, via the Akt/mTOR[79, 80] and Erk1/2 pathways[80]. Endurance exercise, such as cycling[81] and running[82], increases phosphorylation of Erk1/2. Recently, resistance exercise, such as weight lifting has also been shown to enhance Erk1/2 phosphorylation and activation[83]. Activation of Erk1/2 in turn phosphorylates downstream targets, such as mitogen- and stress-activated protein kinase (MSK1/2), p90 ribosomal S6 kinase (p90[rSk]) and MAPK-interacting kinase (Mnk1/2)[84, 85, 86]. Mnk1/2 activates the elongation initiation factor 4E (eIF4E), which promotes the synthesis of muscle proteins (Figure 1.6).

Several growth factors contribute to the activation of the protein synthesis pathways. Increased muscle load or exercise simulates the expression of the growth factor, IGF-1, which can function in an autocrine or paracrine manner to induce muscle hypertrophy and hence, increase muscle mass[87, 88]. Increased levels of IGF-1, results in binding of IGF-1 to the IGF-1 receptor tyrosine kinase, which induces a conformational change, resulting in receptor trans-phosphorylation and downstream phosphorylation and subsequent activation of insulin receptor substrate-1 (IRS-1). Activation of IRS-1 in turn, activates Phosphoinositide 3-kinase (PI(3)K) and the PtdIns-regulated kinase Akt. Increased phosphorylation of Akt at Ser473 activates Akt, which leads to a cascade of reactions, including activation of the rapamycin sensitive kinase mTOR, which plays a central role in integrating various stimuli (including growth factors and nutritional stimulation) to upregulate protein synthesis[74]. Raptor protein plays an important role in the regulation of mTOR activation. Raptor is a scaffold protein, which enables the recruitment of downstream proteins such as p70*S6K* and PHAS-1/4E-BP1 to the mTOR complex, hence, activating the protein synthesis pathway[89, 90]. However, phosphorylation of raptor at Ser722/792 interferes with its activity as a scaffold protein and hence, fully suppresses the activity of mTOR complex[91]. Activation of p70*S6K* and inhibition of PHAS-1/4E-BP1 by mTOR is known to promote protein synthesis, increase muscle fiber size and repress muscle fiber atrophy[74]. The Akt/mTOR signaling pathway is sufficient to regulate skeletal muscle growth. Activation of the Akt/mTOR pathway gives rise to more contractile filaments being added to

myofibers, which enables skeletal muscle to produce greater force[74]. The levels of Akt and activation of Akt are known to increase during hypertrophy[74]. Akt activation can also promote muscle hypertrophy via phosphorylation and inhibition of glycogen synthase kinase-3 (GSK-3), which prevents the inhibitory effect of GSK-3 on protein synthesis[74] (Figure 1.6).

The activity of Akt can be further regulated by phosphatase and tensin homolog (PTEN) and SH2-domain-containing inositol 5'-phosphatase (SHIP), which are two phosphatases that dephosphorylate and inactivate Akt[74]. The downstream effect of altering Akt activation on muscle growth is well established. Overexpression of PTEN has been shown to inactivate Akt1 and results in reduced cell size[92, 93, 94]. In addition, overexpression of SHIP2 inhibits muscle hypertrophy[79, 95].

1.4.2 Protein degradation

Studies have shown that exercise is able to reverse skeletal muscle atrophy by increasing muscle mass and muscle fiber cross sectional area (CSA), even in the presence of spinal cord injury[96]. In addition, PPAR-γ co-activator 1-α (PGC1-α), which is strongly stimulated during exercise, can protect muscle from denervation-induced atrophy and muscular dystrophy[97] (See section 1.5).

Muscle atrophy results from conditions such as cancer cachexia, aids, fasting, Type 2 diabetes, muscle disuse and in response to denervation[98]. Protein breakdown increases during atrophy, which is primarily linked to activation of the ATP-dependent ubiquitin proteasome pathway[99]. In several models of atrophy, the two ubiquitin E3 ligases, known as muscle ring finger protein 1 (MuRF-1) and muscle atrophy F-box protein (MAFbx), also known as Atrogin-1, are specifically upregulated in skeletal muscle[79, 99, 100, 101, 102]. Increased expression of Atrogin-1 and MuRF-1 leads to increased ubiquitination of muscle proteins and enhanced protein degradation via the ubiquitin proteasome pathway[99]. It was found that inhibiting the expression of Atrogin-1 led to increased MuRF-1 expression and vice versa, which suggested the presence of a mechanism to compensate for the loss of either ubiquitin ligase[103]. Suppression of both Atrogin-1 and MuRF-1 together, promotes myotube

hypertrophy, which was associated with enhanced protein synthesis[103]. In addition, loss of both Atrogin-1 and MuRF-1 also prevented dexamethasone-induced myotube atrophy by preventing protein degradation[103]. Moreover, mice lacking either Atrogin-1 or MuRF-1 showed resistance to muscle atrophy[104].

In addition to regulating protein synthesis, Akt has a crucial role in controlling muscle protein breakdown. Activation of Akt (p-Akt) leads to phosphorylation of the Forkhead BoxO (FoxO) family of transcription factors (FoxO1, FoxO3 and FoxO4)[105], sequestering them in the cytoplasm and effectively rendering them inactive. Inactivation of FoxO transcription factors, in turn leads to decreased expression of downstream effector proteins Atrogin-1 and MuRF-1 (Atrogenes), resulting in a significant reduction in protein degradation and hence, atrophy [99] (Figure 1.6). Several other factors have also been implicated in causing skeletal muscle atrophy. Excess or lack of endocrine factors, such as glucocorticoids or thyroid hormone, can result in atrophy[106]. *In vitro*, TNF-α was able to induce atrophy of muscle cells, which could be rescued by treatment with anti-TNF agents[107]. In addition, the growth factor Myostatin is also a potent inducer of muscle atrophy (See section 1.5.2 Myostatin).
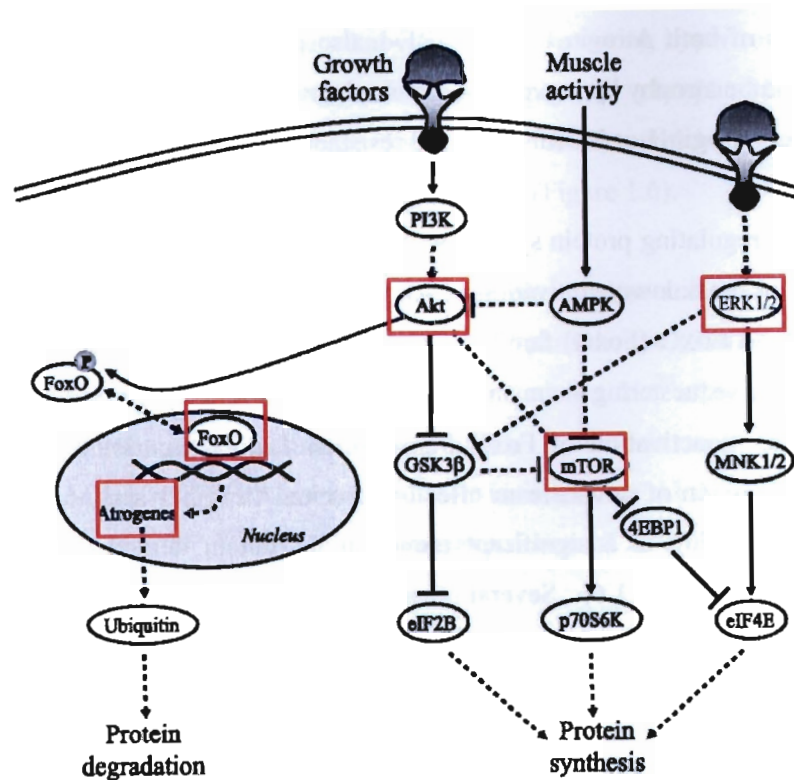
Figure 1.6: Schematic diagram of protein synthesis and protein breakdown pathways in skeletal muscle

Diagram showing different pathways involved in protein synthesis and protein degradation in skeletal muscle. Pathways linked to increased protein synthesis, including PI3-K-Akt, mTOR and MAPK-Erk1/2, and protein degradation, including the ubiquitin proteasome pathway, are depicted. Muscle activity and anabolic growth factors signal to enhance protein synthesis and reduce protein degradation. Image was adapted and modified from Argadine, H. M., Mantilla, C. B., Zhan, W. Z., & Sieck, G. C. (2011). Intracellular signaling pathways regulating net protein balance following diaphragm muscle denervation. *American Journal of Physiology-Cell Physiology*, *300*(2), C318-C327. (*Permission to use this image has been granted by Copyright Clearance Centre, see Appendix 6.2*).

39

1.5 Growth Factors that Regulate Muscle Growth

Skeletal muscle is an endocrine organ that adapts to changes in physical activity, at least in part through the production of growth factors, termed myokines, which include myostatin, IL4, IL6, IL7, IL15, myonectin, follistatin-like 1 and leukemia inhibitory factor (LIF)[108]. Myokines are secreted into the bloodstream as endocrine molecules, which in turn, could regulate several physiological processes in numerous tissues, such as liver, bone, pancreas, adipose tissue and the vascular system (Figure 1.7). In addition, myokines can also act in an autocrine or paracrine manner directly on skeletal muscle (Figure 1.7). The function and mechanism of action of three critical myokines, IL6, myostatin and Irisin, are discussed in this section.
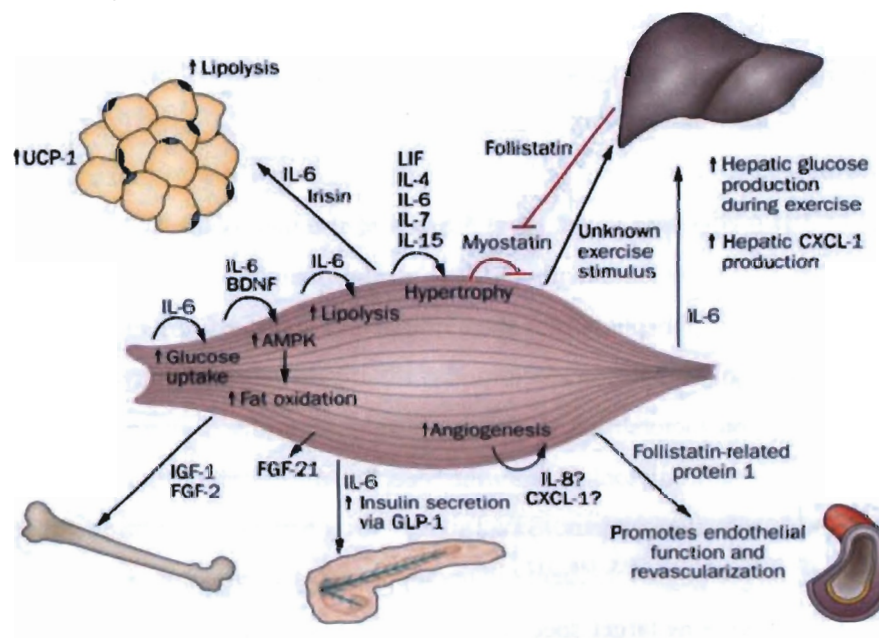
Figure 1.7: Skeletal muscle as a secretory organ
Figure illustrating the effect of different secreted myokines on skeletal muscle and their interaction and cross talk with other organs, such as adipose tissue, bone, liver, pancreas and the vascular system. The secreted factor IL6 has an autocrine/paracrine function and signals to enhance glucose uptake, lipolysis, muscle hypertrophy and fat oxidation. On the other hand, myostatin secreted from skeletal muscle has an inhibitory effect on muscle hypertrophy/growth. Black arrows in this diagram represent upregulation or an activating effect, while red blunted arrows represent an inhibitory effect. Figure was adapted from Pedersen, B. K., & Febbraio, M. A. (2012). Muscles, exercise and obesity: skeletal muscle as a secretory organ. *Nature Reviews Endocrinology*, 8(8), 457-465. (*Permission to use this image has been granted by Copyright Clearance Centre, see Appendix 6.3*).

1.5.1 IL6

Skeletal muscle is an important source of IL6. IL6 is a myokine that is secreted in increased amounts from contracting skeletal muscle, proportional to the length of exercise or the intensity of workload the skeletal muscle is exposed to[109]. *IL6* mRNA transcription undergoes a rapid increase immediately after exercise, suggesting that *IL6* transcription is a consequence of muscle contraction[110]. Although IL6 is also a pro inflammatory cytokine, the expression of IL6 during exercise occurs without exercise-induced local muscle damage and independent of the inflammatory cytokine, TNF-α[110]. Functional overloading of skeletal muscle gives rise to increased muscle-specific IL6 expression, with an associated increase in muscle cross sectional area[111]. Consistent with this, knockdown of *IL6* blunted the hypertrophic effect noted in response to muscle overload, reinforcing the significance of IL6 in mediating hypertrophic growth[112].

In the classical IL6 signaling pathway, IL6 binds to the membrane bound IL6 receptor, which then dimerizes with gp130[113], subsequently activating JAK. Activated JAK in turn, phosphorylates the cytoplasmic region of gp130, which enables the docking of signal transducer and activator of transcription (STAT) cytosolic transcription factors[114]. JAKs then phosphorylate the receptor bound STATs, allowing them to dissociate from the receptor, dimerize and translocate to the nucleus. Inside the nucleus, STATs bind to enhancers promoting the transcription of target genes[115, 116, 117]. The suppressor of cytokine signaling (SOCS) family of proteins target specific members of the JAK/STAT pathway and inhibits the IL6 signalling pathway[118, 119, 120]. Interestingly, it has been shown that activation of the JAK/STAT pathway enables STAT proteins to increase the expression of SOCS3, which forms the basis of a negative feedback mechanism to inhibit JAK/STAT signaling. Several studies have shown that increased circulating IL6 resulted in increased skeletal muscle expression of SOCS3[121, 122].

IL6 regulates satellite cell-mediated skeletal muscle hypertrophy[111]. Previous studies have revealed that IL6 is a critical regulator of satellite cell proliferation. Specifically, IL6 has been shown to enhance satellite cell proliferation via the

STAT3 pathway and subsequent regulation of proliferation markers, including Cyclin D and c-Myc[111]. In addition to enhanced proliferation, increased IL6 concentration has been linked to enhanced myogenic differentiation and fusion of myoblasts[123]. Specifically, siRNA-mediated knockdown of *IL6* has been shown to result in reduced myoblast differentiation and fusion[123], which was reversed upon either overexpression or addition of IL6 protein[123]. Downstream of IL6, the JAK/STAT pathway has also been reported to be involved in promoting myoblast differentiation[124]. Both Erk and PI(3)K/Akt pathways can also be activated by IL6, which result in increased protein synthesis and hence, muscle hypertrophy[123].

1.5.2 Myostatin

The TGF-β superfamily Myostatin, also known as growth and differentiation factor 8 (GDF8), is a potent negative regulator of skeletal muscle growth and myogenesis[125, 126]. Myostatin is expressed predominantly in skeletal muscle but is also expressed to a lesser extent in other tissues[127]. Consistent with Myostatin function as negative regulator of muscle growth, animals that lack *myostatin*, or a functional Myostatin protein, display a 'double muscling' phenotype and hence, have distinctly larger skeletal muscle mass[125, 126]. Myostatin, as a secreted growth factor, binds to receptors to initiate downstream signaling. Specifically, myostatin binds to the Activin receptor type IIB (ActRIIB, type 2 receptor), which dimerizes with Activin receptor like kinase 4/5 (Alk4/5, type 1 receptor), initiating activation of canonical Smad2/3/4 signaling[128].

Myostatin is able to negatively regulate myoblast proliferation and differentiation. Myostatin regulates proliferation by increasing the expression of the cyclin-dependent kinase inhibitor p21, thereby resulting in reduced expression and activity of key cell cycle regulators, including cyclin dependent kinase 2 (Cdk2)[129, 130]. This results in the accumulation of hypo-phosphorylated, active retinoblastoma protein (p-Rb), which blocks the cell cycle at the G1 phase, preventing transition to the S phase[130]. Myostatin also inhibits myogenesis by blocking differentiation and fusion of myoblasts. Myostatin treatment reduces the expression of the myogenic regulatory factors MyoD, Myf5 and Myogenin[131]. Mechanistically, Myostatin binding to its receptor,

phosphorylates Smad3 and inhibits transcription of *MyoD* via Smad3 association with MyoD. Hence, differentiation of myoblasts is inhibited[131].

Myostatin has also been shown to be a potent inducer of skeletal muscle wasting. Previous studies have shown that Myostatin can reduce protein synthesis in skeletal muscle and results in loss of skeletal muscle mass through reducing protein synthesis via inhibition of Akt and mTOR signaling[132, 133].

Another study reported that Myostatin treatment inhibited Akt phosphorylation and activation, which in turn increased the levels of active FoxO1. Hence, increased expression of the downstream targets, including Atrogin-1 and MuRF-1 was observed. As a result, Myostatin reversed the Akt dependent hypertrophy pathway and enhanced protein degradation via the ubiquitin proteasome pathway[134]. Thus, resulting in myotube atrophy (reduction in diameter of myotubes) and muscle wasting[134].

In addition, studies have revealed that Myostatin negatively regulates skeletal muscle regeneration by regulating Satellite cell activation, migration, differentiation and self- renewal[135]. Myostatin also regulates the inflammation phase of muscle regeneration. It is proposed that myostatin inhibits the migration of macrophages to the site of injury[136] while attracting more fibroblasts, which further express myostatin and differentiate into myo-fibroblasts[137, 138]. As a result, collagen and connective tissue accumulates more rapidly, enhancing fibrosis[137, 138]. In agreement with this, absence of myostatin leads to reduced fibrotic tissue accumulation and as such, improved muscle healing[136]. Moreover, regenerating muscle in *myostatin*-null mice showed enhanced migration and accumulation of macrophages and myogenic cells (activated Satellite cells) and hence, improved muscle regeneration[136]. In addition, inflammation subsided more rapidly in injured muscle of *myostatin*-null mice indicating an accelerated inflammatory response in the absence of myostatin[136].

1.5.3 Irisin

1.5.3.1 Discovery of Irisin

Endurance exercise results in the elevated expression of the nuclear transcriptional co-activator, PGC1-α, in skeletal muscle fibers[139]. PGC1-α is known to control mitochondrial biogenesis, oxidative metabolism in various cell types, angiogenesis and fibre-type switching[140]. Increased expression of PGC1-α also provides resistance to muscular dystrophy and muscle atrophy caused by denervation[97]. In addition, increasing PGC1-α expression in muscle prevents muscle wasting during ageing[141]. Overexpression of PGC1-α has also been linked with improved life span in mice and helps to prevent age-related diabetes and obesity[141].

A recent study revealed that PGC1-α induces the expression of the gene Fibronectin type III domain containing 5 (*Fndc5*), which encodes for a 209 amino acid (aa) long, type I precursor membrane protein FNDC5[139]. Boström *et al.*, 2012, further revealed that FNDC5 is cleaved at the C terminus to give rise to a 112 aa long hormone, known as Irisin, which is secreted from skeletal muscle[139] (Figure 1.8). Given the fact that Irisin is secreted form skeletal muscle and that the levels of Irisin increase in response to PGC1-α during exercise, Irisin was initially referred to as a PGC1-α-dependent myokine secreted after endurance exercise (swimming).
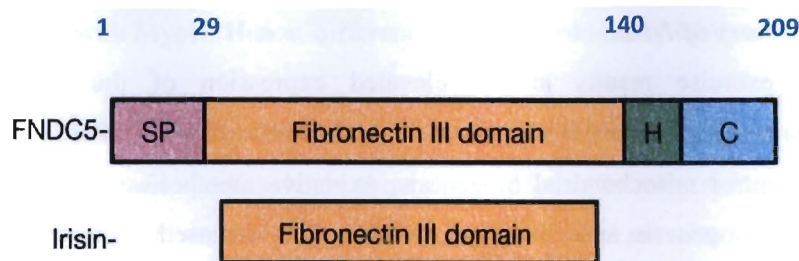
MPPGPCAWPPRAALRLWLGCVCFALVQAD<u>SPSAPVNVTVRHL</u>
<u>KANSAVVSWDVLEDEVVIGFAISQQKKDVRMLRFIQEVNTTT</u>
<u>RSCALWDLEEDTEYIVHVQAISIQGQSPASEPVLFKTPREAE</u>
<u>KMASKNKDEVTMKE</u>MGRNQQLRTGEVLIIVVVLFMWAGVIAL
FCRQYDIIKDNEPNNNKEKTKSASETSTPEHQGGGLLRSKI

Figure 1.8: FNDC5 is proteolytically cleaved and secreted into circulation
FNDC5 is synthesized as a 209-amino acid protein and C' terminally cleaved into a 112-amino acid protein, termed Irisin. The image on the upper panel shows the structure on FNDC5 and the cleaved mature circulating form, Irisin that consists of the Fibronectin III domain. SP: signal peptide, H: hydrophobic region, C: C terminal region. Mature Irisin spans from amino acid 29 to amino acid 140 as labeled above. The lower panel in this figure shows the full sequence of the 209 amino acid protein, FNDC5. The underlined region highlights the amino acid sequence of Irisin. Image was adapted and modified from Boström, P., Wu, J., Jedrychowski, M. P., Korde, A., Ye, L., Lo, J. C., ... & Kajimura, S. (2012). A PGC1-α-dependent myokine that drives brown-fat-like development of white fat and thermogenesis. *Nature*, *481*(7382), 463-468. (*Permission to use this image has been granted by Copyright Clearance Centre, see Appendix 6.4*).

1.5.3.2 Role of Irisin in Adipose Tissue during Obesity and Type 2 Diabetes

There are three types of adipose tissues in the body; white adipose tissue (WAT) and two types of brown adipose tissue, namely, classical brown adipose tissue (BAT) and beige adipose tissue. WAT stores energy in the form of triglycerides. WAT contains a single large lipid droplet (unilocular) and few mitochondria[142]. Conversely, BAT primarily utilizes glucose and fat as opposed to storing it, as such BAT is known to have a high rate of fatty acid oxidation and glucose uptake, potentially protecting against obesity and insulin resistance through increasing energy expenditure[143]. BAT has numerous scattered small lipid droplets (multilocular) and contains numerous mitochondria[143]. BAT expresses elevated levels of mitochondrial uncoupling protein-1 (Ucp-1), which leads to

uncoupling of oxidative phosphorylation from ATP production[144]. This imparts thermogenic capacity to BAT, with excess chemical energy dissipated as heat through non-shivering thermogenesis. Hence, BAT also protects against hypothermia[145]. Developmentally, WAT is developmentally derived from a non-Myf5 lineage, whereas BAT is derived from a $Myf5^+$ lineage common to skeletal muscle[145].

Beige or brown-in-white (Brite) adipose tissue is located within WAT depots. However, beige adipocytes have a distinct gene expression pattern from either white or brown adipose tissue and express specific markers, such as CD137 and TMEM26[145]. In a basal state, beige adipose tissue resembles WAT phenotypically and expresses low levels of the thermogenic marker, Ucp-1. However, just like BAT, beige adipose tissue is highly sensitive to cAMP stimulation. In response to cAMP stimulation, the levels of Ucp-1 and overall respiration rate are increased in beige adipose tissue[145], allowing beige adipocytes to function like BAT.

Although a myokine, the initial discovery of Irisin was associated with the identification of a novel role for Irisin in regulating white adipose tissue metabolism. Importantly, Irisin has been shown to act on beige adipocytes within the WAT population and induce the expression of "brown/beige fat genes", such as Ucp-1, Cidea, Cpt1b and Dio2, which enables beige adipose tissue to function in a similar manner to BAT. Increased expression of these browning genes was shown to be partly mediated by peroxisome proliferator-activated receptor-α (PPAR-α)[139]. Since BAT and beige adipose tissue have greater mitochondrial content, it was suggested that increased beige adipose content in response to Irisin action allows for increased oxygen consumption and energy expenditure in the body[140, 146, 147] (Figure 1.9).
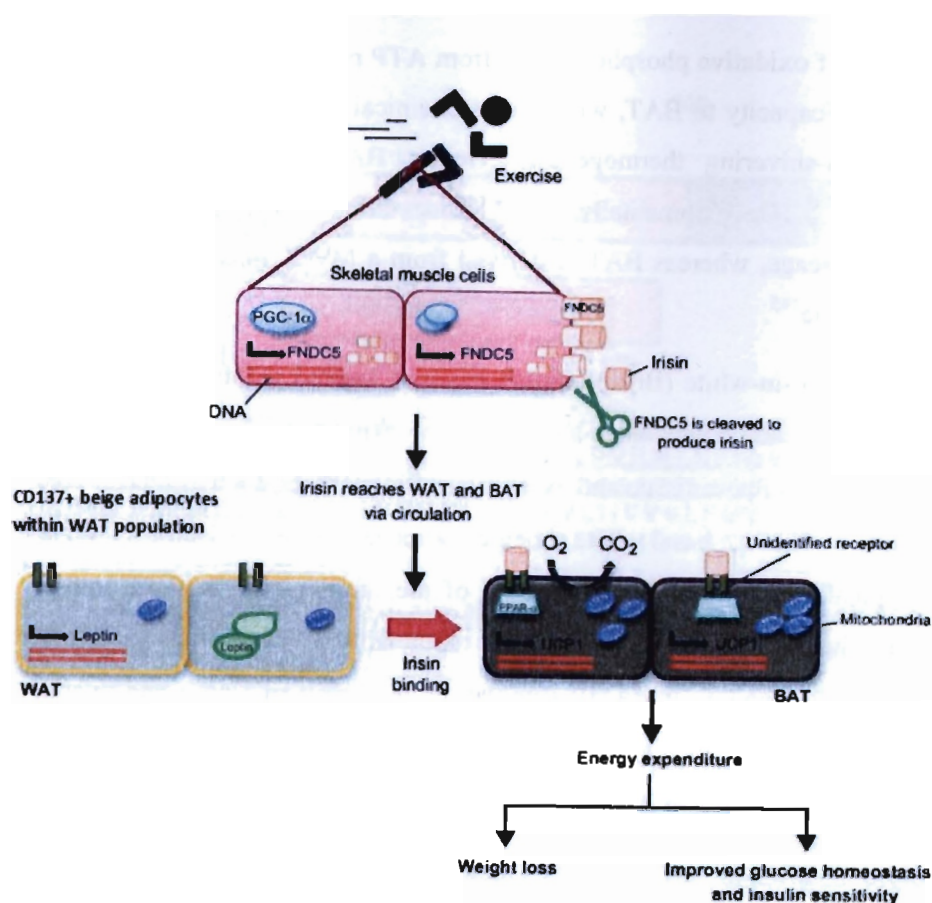
Figure 1.9: Exercise and Irisin induces browning of white adipose tissue

Exercise stimulates the expression of PGC1-α in skeletal muscle, which in turn upregulates the expression of FNDC5. FNDC5 is cleaved at the C terminal region to produce the mature protein Irisin, which is released into circulation. Irisin then binds to a receptor on CD137+ beige adipocytes, which are highly responsive to the myokine. Ucp-1 protein is upregulated as a result, which promotes a BAT-like phenotype in WAT with increased mitochondrial respiration and enhanced energy expenditure. Figure was adapted and modified from Castillo-Quan, J. I. (2012). From white to brown fat through the PGC-1α-dependent myokine Irisin: implications for diabetes and obesity. *Disease Models and Mechanisms*, 5(3), 293-295. (*This image has been obtained from Open Access article distributed under the terms of the Creative Commons Attribution Non-Commercial Share Alike License*)

Subsequent to the initial discovery of Irisin by Boström *et al.*, (2012), several other studies in rodents and in humans have been published to support the role of Irisin in fighting obesity and insulin resistance. Specifically, Irisin was able to reduce body weight and enhance glucose homeostasis[148]. Moreover, Irisin

has been shown to stimulate the expression of "brown fat" genes which could prevent obesity and Type 2 diabetes[148]. In a separate study, reduced levels of Irisin in circulation were also noted in patients with Type 2 diabetes[149, 150]. In mice, Irisin has also been shown to have beneficial effects on Type 2 diabetes by improving glucose utilization and fatty acid oxidation via AMPK regulation[151]. In addition, exogenous addition of Irisin to diabetic mice led to reduced fat mass and lowered levels of triglycerides and total cholesterol in serum[151].

1.5.3.3 Effect of Resistance and Endurance Exercise on Irisin

Irisin has been shown to be upregulated by both endurance and resistance exercise. Several models of exercise have been used in mice and in humans to show the different effects exercise has on the circulating levels of Irisin. Endurance exercise (swimming) was shown to reduce body fat mass and increase the expression of Irisin in Wistar rats fed with high fat diet[152]. Another study revealed that resistance exercise resulted in a significant increase in circulating Irisin. However, an increased level of Irisin was not observed after aerobic training[153]. Mice undergoing a resistance exercise-training regime showed increased serum Irisin levels and increased Irisin expression in the soleus muscle, which was accompanied by improved grip strength[154]. This effect was paralleled in humans undergoing resistance exercise training, where increased Irisin levels in circulation were associated with enhanced muscle strength[154]. Hence, increased levels of Irisin are positively correlated to muscle strength. In another publication, men who underwent resistance exercise displayed higher levels of Irisin in circulation, than those who either underwent endurance exercise or a combination of both types of exercise[155]. These results confirm that Irisin levels are enhanced in response to exercise and further suggest that resistance exercise may result in the greatest increase in circulating Irisin.

1.5.3.4 Controversy Relating to Irisin

1.5.3.4.1 Is Human Irisin a Myth?

While the presence of Irisin and increased expression of Irisin in response to exercise has been well established in mouse models, contrasting results have been reported in humans. While Boström *et al.*, (2012) noted the presence of Irisin in human serum and increased serum Irisin levels in humans after exercise[139]; a study Raschke *et al.*, (2013) reported that the effect of Irisin in humans is unclear, as the gene encoding FNDC5 found in rodents and primates displays a mutation in the conserved start codon in humans. Specifically, the codon is mutated from the typical ATG (Methionine) start codon to ATA, which codes for Isoleucine. It was further shown that transfection of an FNDC5 construct, which used the ATA start codon, into HEK293 cells, resulted in production of only ~1% of the full length FNDC5 protein that was produced in HEK293 cells transfected with an FNDC5 construct containing the ATG start codon[156]. Raschke *et al.*, (2013) also failed to observe any distinct increase in *FNDC5* mRNA expression upon electrical pulse stimulation of primary human myotubes (*in vitro* model of muscle contraction) although there was a significant increase in *PGC1-α* mRNA. Moreover, no increase in *FNDC5* mRNA was noted after endurance or strength training in humans. Hence, it was concluded that it would be unlikely that the beneficial effects of Irisin in mice could be translated to humans[156].

A further report by Albrecht *et al.*, (2015) calls into question all previous reports that use commercial ELISA kits to detect Irisin[157]. In this study, they have reported that antibodies from several ELISA kits have shown cross reactivity with non-specific proteins in the serum of humans and animals. Albrecht *et al.*, (2015) further claimed that Irisin protein transcribed from the mutated ATA start codon would produce a truncated FNDC5 protein from an in-frame ATG codon and hence, lack the first 44 amino acids. It would hence be unlikely that the truncated protein would be translated[157].

Another study by Pekkala *et al.*, (2013) revealed that although there was a robust increase in *PGC-1α* mRNA after a single bout of resistance exercise, only a moderate increase in *FNDC5* mRNA was observed. Pekkala *et al.*, (2013)

claimed that this result demonstrated a poor relationship between PGC-1α and FNDC5. Secondly, Pekkala *et al.*, (2013) reported that *PGC-1α* and *FNDC5* expression in skeletal muscle and Irisin levels in serum do not show a difference after either endurance or aerobic exercise or a combination of both endurance and resistance exercises[158]. No correlation between obesity or fasting glucose/insulin levels and *FNDC5* expression was also noted. However, it was indicated that the glycosylation status of Irisin in serum may affect the analysis of Irisin levels in their study[158].

Kurdiova T *et al.*, (2014) reported that although *PGC1-α* expression doubled in differentiated myotubes post-exercise mimetic treatment, *FNDC5* expression in myotubes and Irisin levels in the medium were reduced[159]. Moreover, myotubes derived from subjects with Type 2 diabetes showed increased *FNDC5 expression* and hence, *FNDC5* showed a negative correlation with insulin sensitivity and a positive relationship with fasting glucose levels[159].

1.5.3.4.2 Human Irisin is Translated from a Non-Canonical Start Codon
In direct response to controversy regarding the existence of human Irisin protein, work by Jedrychowski *et al.*, (2015) has confirmed that the ATA non-canonical start codon does indeed result in the translation of full length FNDC5[160]. Importantly, not only was FNDC5 protein present, but using state-of-the-art tandem mass spectrometry, Jedrychowski *et al.*, (2015) were able to detect Irisin in human serum at a molecular weight of 12kDa[160]. Furthermore, Jedrychowski *et al.*, (2015) showed that in response to aerobic exercise Irisin levels were significantly increased in humans[160]. Baseline circulating levels of Irisin in sedentary individuals was found to be 3.6ng/ml, whereas the levels increased to 4.3ng/ml in circulation in response to exercise. Importantly, Jedrychowski *et al.*, (2015) further pointed out that poor detection limits for ELISA kits (with a minimum detection limit of 100ng/ml) together with incomplete protein deglycosylation could have contributed to the inability to detect circulating levels of Irisin in previous studies[160].

1.5.3.5 Where Does Research on Irisin Stand Today?

Although there have been controversial reports on Irisin function in humans, to date there are close to 400 publications on Irisin (*based on an online PubMed search*) and its multifarious functions on different organs in the body.

1.5.3.5.1 Proposed Mechanism for Irisin Signaling in Beige Adipocytes

A recent study investigated the mechanism of action of Irisin in regulating the expression of Ucp-1 in beige adipocytes. Zhang *et al.*, (2014) proposed that Irisin upregulates Ucp-1 via the phosphorylation and activation of p38 MAPK and Erk pathways. In agreement with this, inhibition of the p38 MAPK and Erk pathways inhibited Irisin-mediated induction of Ucp-1. Therefore, this study identified a novel signaling pathway through which Irisin regulates browning of white adipose tissue[148].

1.5.3.5.2 Evolution of Irisin Secretion from Shivering in Muscle

In a recent study, secretion of Irisin from contracting skeletal muscle during exercise has been recently suggested to evolve from muscle contraction during the process of shivering[161]. Shivering is a phenomenon where muscle contracts in order to generate heat when exposed to cold in order to maintain the body temperature at a homeostatic level[161]. During cold exposure, both shivering and non-shivering thermogenesis is employed to generate heat in the body[161]. Results from Lee *et al.*, (2014) revealed that shivering stimulates the secretion of Irisin from skeletal muscle, while non-shivering thermogenesis induces the secretion of FGF21, an adipokine that also promotes browning of white fat[161]. It was further shown that, both Irisin and FGF21 have the capacity to upregulate the browning programme in human beige adipocytes[161]. In addition, results revealed that the level of Irisin secreted was proportional to the intensity of shivering, which was in a similar magnitude to exercise-induced Irisin secretion[161]. Lee *et al.*, (2014) postulated that exercise might be mimicking contracting muscle during shivering and lead to the secretion of Irisin, so that it could function alongside FGF21 to enhance the browning programme in white fat[161].

1.5.3.5.3 Irisin Secretion from Other Organs

Although initially identified as a Myokine, with ~72% of circulating Irisin secreted from skeletal muscle, recently it has been shown that small amounts of Irisin are synthesized and secreted from white adipose tissue[162] and liver[163]. Within WAT, it has been reported that post-exercise, subcutaneous adipose tissue secretes the highest levels of Irisin, followed by visceral adipose tissue and brown adipose tissue depots[162].

1.5.3.5.4 Role of Irisin in Other Organs/Organelles

Liver

The role of Irisin has been studied in several tissues. Recently, Irisin levels have been associated with intra-hepatic triglyceride content[164], where treatment with recombinant Irisin protein inhibited palmitic acid-induced lipogenic markers and lipid accumulation in liver cells. Irisin was also able to reduce oxidative stress by reducing the expression of inflammatory markers such as NFκB, COX-2, p38 MAPK, TNF-α, IL6 and superoxides. This suggested that Irisin may be able to prevent fatty liver disease due to triglyceride accumulation in the liver and could relieve oxidative stress[165].

Brain

The PGC1-α-FNDC5 pathway has been shown to be upregulated in the hippocampus in mice after exercise. Increased levels of FNDC5 due to exercise and as such, increased levels of circulating Irisin, induces the expression of brain-derived neurotrophic factor (*Bdnf*) and other neuroprotective genes in the brain, indicating that Irisin may have a potential to treat neurodegenerative diseases as well[166].

Kidney

Irisin has been suggested to play a role in chronic kidney disease. Plasma Irisin levels were significantly lower in patients with chronic kidney disease[167, 168, 169] and moreover, the reduction in plasma Irisin was inversely related to blood-urea nitrogen and creatinine levels[169].

Mitochondria

It has been reported that Irisin treatment enhances oxidative metabolism significantly and upregulates expression of PGC1-α, nuclear respiratory factor 1 (NRF1), mitochondrial transcription factor A (TFAM), glucose transporter 4

(GLUT4) and mitochondrial uncoupling protein 3 (Ucp-3)[170] Upregulation of these genes has been linked to increased mitochondrial biogenesis[170].

1.6 Aims and Objectives

Previous studies have attempted to define a role for Irisin in regulating skeletal muscle mass. Circulating Irisin levels have been positively correlated with biceps circumference and IGF-1 levels in humans[163]. Similarly, in *myostatin-null* (*Mstn*-null) mice, which display dramatically increased skeletal muscle mass and pronounced browning of white adipose tissue, increased activation of AMPK-PGC-1α-FNDC5 pathway has been shown to lead to elevated Irisin levels[171]. Activation of AMPK is known to inhibit mTOR activity and hence, protein synthesis, while increasing proteolysis. It is interesting to surmise that activation of the AMPK- PGC-1α-FNDC5- Irisin axis may therefore work downstream of AMPK, as part of a feedback mechanism, to help rebuild and repair skeletal muscle in response to negative energy situations, such as in response to exercise. In addition, recent work has revealed that Irisin is able to stimulate muscle growth-related genes in humans[172]. It has been further shown that Irisin levels are increased during myogenic differentiation and that Irisin treatment results in increased p-Erk expression, which is involved in protein synthesis[172]. Taken together, these previous studies suggest that increased Irisin levels could promote skeletal muscle growth. Given these previous studies and the fact that Irisin is a muscle-secreted growth factor (myokine) I hypothesized that *Irisin may function in an autocrine/paracrine manner to exert beneficial effects on skeletal muscle growth.*

Previously published work is suggestive of beneficial effects of Irisin on skeletal muscle growth. However, to date, no in depth study has clearly defined a specific role for Irisin in regulating skeletal muscle growth, or for that matter, identified signaling pathways involved in Irisin function in skeletal muscle or the potential benefits Irisin might confer to muscle repair. With this in mind the work performed in my thesis aimed to systematically investigate the effect of Irisin on skeletal muscle growth, repair and regeneration and during conditions of muscle atrophy and wasting. To address my hypothesis and overall research

aim, I have undertaken the following objectives:

1. Elucidate the role of Irisin on skeletal muscle myogenesis *in vitro*.

2. Investigate if Irisin acts as a growth factor to induce skeletal muscle hypertrophy in resting muscle.

3. Delineate molecular mechanisms through which Irisin functions in muscle.

4. Investigate the role of Irisin in skeletal muscle regeneration using a mouse model of muscle injury.

5. Study the therapeutic potential of Irisin *in vivo* using atrophy and muscle wasting models.

2. Materials and Methods

2.1 Materials

The following section outlines all materials and composition of materials used for the studies undertaken and described in this thesis.

2.1.1 Composition of Reagents

The compositions of reagents used in this thesis are described in tables provided in the following section.

2.1.1.1 Reagents Used for Irisin purification

Reagents used for the purification of murine recombinant Irisin protein are provided in the following tables. The composition of each reagent is also provided.

Table 2.1: TAE buffer

TAE Buffer	Amount/Volume
Tris-acetate	40mM
EDTA (pH 8.0)	2mM

Table 2.2: 1% DNA gel

1% DNA Gel	Amount/Volume
Ultra Pure™ Agarose	1g
1x TAE buffer	100ml

Table 2.3: DNA loading dye (10x)

DNA Loading Dye (10x)	Amount/Volume
Tris-acetate	40mM
EDTA (pH 8.0)	2mM

Table 2.4: Binding buffer

Binding Buffer	Amount/Volume
1M Tris-Hydrochloric acid (HCl) pH 8.0	25ml
5M Sodium Chloride (NaCl)	20ml
Glycerol	50ml
Imidazole	0.68g
Top up MQ water to	500ml

Table 2.5: Dialysis buffer

Dialysis Buffer	Amount/Volume
1M Tris-HCl pH 8.0	100ml
NaCl	5.844g
Top up MQ water to	1 Litre

Table 2.6: Imidazole

Imidazole	Amount/Volume
1) 50mM Imidazole	0.102g
Binding buffer	50ml
2) 200mM Imidazole	1.25g
Binding buffer	50ml

Table 2.7: Isopropyl β-D-1-thiogalactopyranoside (IPTG)

IPTG	Amount/Volume
IPTG	1.25g
MilliQ water	5ml

Table 2.8: Ampicillin

Ampicillin	Amount/Volume
Ampicillin	1g
MilliQ water	10ml

2.1.1.2: Reagents Used for Methylene Blue Photometric Endpoint Assay

Reagents used for the methylene blue photometric endpoint assay to assess cell proliferation are provided in the following tables. The composition of each reagent is also provided.

Table 2.9: Fixative

10% Formal/ 0.9% Saline	Amount/Volume
NaCl	8.7g
40% Formaldehyde solution	250ml
MilliQ water	750ml

Table 2.10: 1:1 Ethanol/0.1M HCl

1:1 Ethanol/0.1M HCl	Amount/Volume
100% Ethanol	500ml
1M HCl	50ml
MilliQ water	540ml

Table 2.11: Borate buffer

0.01M Borate buffer	Amount/Volume
Sodium Tetraborate	7.63g
MilliQ water	2 Litres
Adjust pH to 8.0 with HCl	As required

Table 2.12: HCl

1M HCl	Amount/Volume
11.6M HCl	43ml
MilliQ water	457ml

Table 2.13: Methylene blue

Methylene Blue	Amount/Volume
Methylene blue powder	4g
0.01M Borate buffer	400ml

2.1.1.3: Reagents for Protein Extraction and Western Blot Analysis

All reagents used for protein extraction and Western Blot (Immunoblot) analysis of protein levels are provided in the following tables. The composition of each reagent is also provided.

Table 2.14: Protein lysis buffer for total protein extraction from myoblasts and myotubes

Protein Lysis Buffer	Amount/Volume
1M Tris-HCl pH 7.5	0.5ml
5M NaCl	0.5ml
0.5M EDTA	0.1ml
IGEPAL CA-630	10µl
Complete with protease inhibitor	½ tablet
Top up with MilliQ water to	10ml

57

Table 2.15: RIPA Buffer for total protein extraction from muscle tissue

RIPA Buffer	Amount/Volume
Aprotinin	400µl
700mM NaVO$_4$	30 µl
500mM NaF	1.4ml
0.5M EDTA	140 µl
Protease inhibitor tablet	½ a tablet
MilliQ water	Top up to14ml
100mM PMSF(to be added before use)	140 µl

Table 2.16: 6% Resolving protein gel (for detection of Utrophin, a high molecular weight protein)

Resolving Gel	Amount/Volume
30% Acrylamide	4ml
Tri-HCl pH8.8	7.5ml
10% SDS	200µl
10% APS	200µl
TEMED	20µl
MilliQ water	8.1ml

Table 2.17: 4% Stacking protein gel (for detection of Utrophin, a high molecular weight protein)

Stacking Gel	Amount/Volume
30% Acrylamide	1ml
Tri-HCl pH6.8	750µl
10% SDS	60µl
10% APS	60µl
TEMED	10µl
MilliQ water	4.1ml

Table 2.18: Tris-glycine SDS running buffer

Tris-Glycine Running Buffer	Amount/Volume
Tris	30g
Glycine	18.8g
10% SDS	10ml
MilliQ water	Top up to 1000ml

Table 2.19: Transfer buffer for Western blots

Transfer Buffer	Amount/Volume
Tris	15.1g
Glycine	75g
Methanol	1000ml
MilliQ water	Top up to 5000ml

Table 2.20: Tris buffered saline- tween (TBS-T)

TBS-T	Amount/Volume
1M Tris-HCL pH 7.5	50ml
5M NaCl	30ml
TWEEN-20	1ml
MilliQ water	Top up to 1000ml

2.1.1.4: Reagents Used for RNA electrophoresis

All reagents used for RNA electrophoresis are provided in the following tables. The composition of each reagent is also provided.

Table 2.21: MOPS buffer (10x)

MOPS Buffer	Amount/Volume
MOPS	41.9g
1M Soidum Acetate	50ml
0.5 M EDTA	10ml
MilliQ water	Top up to 500ml
Adjust pH to 7, filter sterilize and protect from light	

Table 2.22: 1% RNA gel

1% RNA Gel	Amount/Volume
Ultra Pure™ Agarose	1g
Formaldehyde	18ml
10x MOPS	10ml
MilliQ water	Top up to 100ml

Table 2.23: RNA loading dye (2x)

RNA Loading Dye	Amount/Volume
MOPS (10x)	10%
Deionized formaldehyde	20%
Deionized formamide	50%
Bromophenol blue	0.02%
Glycerol	5%
EDTA (pH 8.0)	1mM
Ethidium bromide (EtBr)	40μg/ml

2.1.1.5: Reagents used for Immunohistochemistry (IHC) and Immunocytochemistry (ICC)

All reagents used for IHC and ICC are provided in the following tables. The composition of each reagent is also provided.

Table 2.24: Carrageenan λ (0.35%)

Carrageenan λ	Amount/Volume
Carrageenan λ	0.175g
1xPBS	Top up to 50ml

Table 2.25: Triton X-100 (0.1%) used for IHC staining

Triton X-100 (0.1%)	Amount/Volume
Triton X-100	10μl
MilliQ water	10ml

Table 2.26: 20:2:1 Fixative used in Differentiation assay

20:2:1 Fixative	Amount/Volume
70% Ethanol	20ml
Formalin	2ml
Acetic acid	1ml

Table 2.27: Scott's tap water for H&E staining

Scott's Tap Water	Amount/Volume
Sodium Bicarbonate	3.5g
Magnesium Sulphate	20g
MilliQ water	Top up to 1000ml

Table 2.28: 4% Paraformaldehyde used as fixative for IHC staining

4% Paraformaldehyde (4% PFA)	Amount/Volume
Paraformaldehyde	40g
1x PBS (heated to 70°C)	800ml
Sodium hydroxide (NaOH)	As required to dissolve PFA
Hydrochloric acid (HCl)	As required for solution to reach pH 6.9
MilliQ water	Top up to 1 Litre

2.1.1.6: Reagents Used for In Vivo Studies

All reagents used for *in vivo* animal studies are provided in the following tables. The composition of each reagent is also provided.

Table 2.29: Notexin solution for in vivo muscle injury model

Notexin	Amount/Volume
Notexin powder	100μg
Saline	1ml

Table 2.30: Dialysis buffer used as vehicle control for in vivo studies

Dialysis Buffer	Amount/Volume
1M Tris-HCl pH8.0	100ml
NaCl	5.844g
Top up MQ water to	1 Litre

Table 2.31: Evans blue dye injected in young (5-week-old) mdx mice

Evans Blue	Amount/Volume
Evans blue powder	50mg
1x PBS	5ml

Table 2.32: Anesthetic mixture injected in mice prior to sciatic nerve injury

Anesthetic Mixture	Amount/Volume
20mg/ml Ketamine	1ml
100mg/ml Xylazine	0.5ml
1x PBS	8.5ml

2.1.1.7: Reagents Used for Adipogenic Differentiation

All reagents used for adipogenic differentiation of Human Adipose-Derived Stem Cells (hADSCs) and 3T3L1 cells are provided in the following tables. The composition of each reagent is also provided.

Table 2.33: Red blood cell (RBC) lysis buffer

RBC Lysis Buffer	Amount/Volume
Ammonium chloride (NH_4Cl)	824mg
Potassium bicarbonate ($KHCO_3$)	100mg
EDTA	4mg
1x PBS	Top up to 100ml
Filter sterilize before use	

Table 2.34: 0.2% Gelatin used to coat cell culture plates

0.2% Gelatin	Amount/Volume
Gelatin powder	2g
MilliQ water	1000ml

DMEM/F12 was used for hADSCs cultures while DMEM + GlutaMAX was used for 3T3L1 cultures.

Table 2.35: Induction medium

Induction Medium	Amount/Volume
FBS	10%
P/S	1%
IBMX	0.5mM
Dexamethasone	1μM
Insulin	0.01mg/ml
DMEM (F12 for hADSCs/GlutaMAX for 3T3L1)	In 200ml

Table 2.36: Insulin medium

Insulin Medium	Amount/Volume
FBS	10%
P/S	1%
Insulin	0.01mg/ml
DMEM (F12 for hADSCs/GlutaMAX for 3T3L1)	In 200ml

2.1.2 Antibodies

Details of primary, secondary and tertiary antibodies used in this thesis are given in this section.

Table 2.37: Antibodies used for Western blot Analysis

Primary Antibody	Company/ Catalogue No.	Dilution	Animal	Secondary Antibody	Company/ Catalogue No.	Animal	Dilution
MyoD	Santa Cruz (USA) sc-304	1:500	Rabbit	Anti-Rabbit HRP	Bio-Rad (USA) 1706515	Goat	1:5000
P21	BD Pharmingen 556430	1:200	Mouse	Anti-Mouse HRP	Bio-Rad (USA) 1721011	Goat	1:5000
Myogenin	Santa Cruz (USA) sc-576	1:400	Rabbit	Anti-Rabbit HRP	Bio-Rad (USA) 1706515	Goat	1:5000
MHC (MF20)	DSHB (USA) AB 2147781	1:400	Mouse	Anti-Mouse HRP	Bio-Rad (USA) 1721011	Goat	1:5000
p-Akt (Ser473)	Santa Cruz (USA) sc-7985	1:500	Rabbit	Anti-Rabbit HRP	Bio-Rad (USA) 1706515	Goat	1:5000
p-Erk	Santa Cruz (USA) sc-16982	1:500	Goat	Anti-Goat HRP	Bio-Rad (USA) 1721034	Rabbit	1:5000
p-Raptor (Ser792)	Cell Signalling (USA) 2083	1:500	Rabbit	Anti-Rabbit HRP	Bio-Rad (USA) 1706515	Goat	1:5000
Atrogin-1 (H-300)	Abnova (Taiwan) PAB1562	1:500	Goat	Anti-Goat HRP	Bio-Rad (USA) 1706515	Rabbit	1:5000
MuRF-1 (H-145)	Regeneron (Gift)	1:500	Mouse	Anti-Mouse HRP	Bio-Rad (USA) 1721011	Goat	1:5000
FoxO1	Santa Cruz (USA) sc-11350	1:500	Rabbit	Anti-Rabbit HRP	Bio-Rad (USA) 1706515	Goat	1:5000
p-FoxO1	Santa Cruz (USA) sc-101681	1:500	Rabbit	Anti-Rabbit HRP	Bio-Rad (USA) 1706515	Goat	1:5000
Utrophin	Santa Cruz (USA) sc-33700	1:200	Mouse	Anti-Mouse HRP	Bio-Rad (USA) 1721011	Goat	1:5000
Vinculin	Sigma-Aldrich (USA) V9131	1:5000	Mouse	Anti-Mouse HRP	Bio-Rad (USA) 1721011	Goat	1:5000
Ucp-1	Abcam Ab 10983	1:500	Rabbit	Anti-Rabbit HRP	Bio-Rad (USA) 1706515	Goat	1:5000
GAPDH	Santa Cruz (USA) sc-32233	1:10.000	Mouse	Anti-Mouse HRP	Bio-Rad (USA) 1721011	Goat	1:5000
α-Tubulin	Sigma- Aldrich (USA) T9026	1:10.000	Mouse	Anti-Mouse HRP	Bio-Rad (USA) 1721011	Goat	1:5000

Table 2.38: Antibodies used for MyoD IHC staining on regenerating muscle sections

Antibody	Catalog No.	Dilution	Antibody Type
MyoD	Santa Cruz (USA) 304	1:50	Primary
Goat Anti-rabbit IgG Alexa Fluor® 568	Thermo Fisher Scientific (USA) A11011	1:300	Secondary
DAPI	Molecular Probes, Invitrogen (USA) D1306	1:1000	-

Table 2.39: Antibodies used for Pax7 and MyoD ICC staining on primary myoblast cultures

Antibody	Catalog No.	Dilution	Antibody Type
Pax7	DSHB (USA) AB528428	1:100	Primary
MyoD	Santa Cruz (USA) 304	1:100	Primary
Sheep Anti- Mouse IgG Biotin	GE Healthcare Life Sciences (USA) RPN1001	1:300	Secondary
Goat Anti-rabbit IgG Alexa Fluor® 594	Thermo Fisher Scientific (USA) A-11037	1:300	Secondary
Streptavidin Alexa Fluor® 488 conjugate	Thermo Fisher Scientific (USA) S11223	1:400	Tertiary
DAPI	Molecular Probes, Invitrogen (USA) D1306	1:1000	-

Table 2.40: Antibodies used for IgM staining on adult (6-week-old) mdx mice

Antibody	Catalog No.	Dilution	Antibody Type
Goat anti-mouse IgM-FITC conjugated	Sigma-Aldrich (USA) F9259	1:100	-
DAPI	Molecular Probes, Invitrogen (USA) D1306	1:1000	-

2.1.3 Enzymes

Details of enzymes used in this thesis are given in this section. Details of the company are also provided.

64

Table 2.41: List of enzymes used in this thesis

Enzymes	Company
T4 DNA ligase	New England Biolabs (NEB)
Taq DNA polymerase	Thermo Fisher Scientific
BamHI	New England Biolabs (NEB)
NdeI	New England Biolabs (NEB)
Reverse Transcriptase	Bio-Rad (iScript™ cDNA Synthesis Kit)
RNase H	Bio-Rad (iScript™ cDNA Synthesis Kit)
Trypsin	Gibco

2.1.4 Oligonucleotides

All oligonucleotides (primers) were synthesized and purchased from Sigma-Aldrich, Singapore and were stored at -20°C. Primers were diluted 40-fold from 100μM to 2.5μM for subsequent quantitative real time polymerase chain reactions (qPCR). Oligonucleotide information is listed below in Table 2.42. 'F' denotes forward primers, while 'R' denotes reverse primers.

Table 2.42: Oligonucleotides used for quantitative real-time PCR (qPCR) reactions

Primer	Sequence (5' - 3')
Sox8-F	5'-CTG TGG CGC TTG CTG AGT-3'
Sox8-R	5'-CGG CCA GTC TTC ACA CTC TT-3'
Heyl-F	5'-TGC CTT TGA GAA ACA GGC T-3'
Heyl-R	5'-AGG CAT TCC CGA AAC CCA AT-3'
Hp-F	5'-TTC TAC AGA CTA CGG GCC GA-3'
Hp-R	5'-CCC ACA CAC TGC CTC ACA TT-3'
IL6-F	5'-GGG ACT GAT GCT GGT GAC AA-3'
IL6-R	5'-TGC CAT TGC ACA ACT CTT TTC T-3'
Cxcl1-F	5'-CCG AAG TCA TAG CCA CAC TCA-3'
Cxcl1-R	5'-GTG CCA TCA GAG CAG TCT GT-3'
Ptx3-F	5'-CCC GCA GGT TGT GAA ACA G-3'
Ptx3-R	5'-TAG GGG TTC CAC TTT GTG CC-3'
Myomaker-F	5'-GAC AGT GAG CAT CGC TAC CA-3'
Myomaker-R	5'-GTT CAT CAA AGT CGG CCA GT-3'
Caveolin- 3-F	5'-GGA TCT GGA AGC TCG GAT CAT-3'
Caveolin- 3-R	5'-TCC GCA ATC ACG TCT TCA AAA T-3'
GAPDH-F	5'-ACA ACT TTG GCA TTG TGG AA-3'
GAPDH-R	5'-GAT GCA GGG ATG ATG TTC TG-3'

Primer	Sequence (5' - 3')
Irisin-F	5'-CAT ATG GAC AGC CCC TCA GCC CCT-3'
Irisin-R	5'-GGA TCC TCA CTC CTT CAT GGT CAC CTC-3'
Ucp-1-F	5'-ACT GCC ACA CCT CCA GTC ATT -3'
Ucp-1-R	5'- CTT TGC CTC ACT CAG GAT TGG-3'

2.1.5 List of Chemicals

A comprehensive list of chemicals used in this thesis is provided below. Details of the company where the chemicals were purchased from are also provided.

Table 2.43: List of chemicals used in this thesis

Chemicals	Company
1kb Plus DNA Ladder	Thermo Fisher Scientific
4x LDS sample loading dye	Invitrogen
6x DNA loading dye	Thermo Fisher Scientific
Acetic acid	Sigma-Aldrich
Acrylamide	Biorad
Ammonium chloride (NH_4Cl)	Sigma-Aldrich
Ammonium persulfate (APS)	Biorad
Ampicillin	Sigma-Aldrich
Aprotinin	Sigma-Aldrich
Bovine serum albumin	Sigma-Aldrich
Bovine calf serum	Thermo Fisher Scientific
Bromophenol blue	Sigma-Aldrich
B-mercaptoethanol (β-ME)	Sigma-Aldrich
Carrageenan λ	Sigma-Aldrich
Chloroform	Merck, Millipore
Collagenase type 1A	Sigma-Aldrich
Coomassie blie	Biorad
Chick embryo extract (CEE)	Biomed Diagnostics
DAPI	Molecular Probes
DEPC water	1st Base
Dexamethasone	Sigma-Aldrich
DharmaFECT 1	Dharmacon
Dulbecco's Modified Eagle Medium (DMEM) + GlutaMAX	Gibco
Dulbecco's Modified Eagle Medium (DMEM)/ F12	Gibco
DPX	Sigma-Aldrich
Ethylenediaminetetraacetic acid (EDTA)	1st Base
Eosin	Merck Millipore
Ethanol	Merck Millipore
Ethidium bromide (EtBr)	Biorad
Evans blue dye	Sigma-Aldrich
Fetal Bovine Serum	Gibco
Formaldehyde	Sigma-Aldrich
Gelatin	Sigma-Aldrich
Glycerol	Invitrogen
Glycine	Biorad
Hematoxylin	Merck Millipore
Horse serum	Gibco
Hydrochloric acid (HCl)	Merck Millipore
IGEPAL	Fluka
Imidazole	Sigma-Aldrich

Chemicals	Company
3-isobutyl-1-methylxanthine (IBMX)	Sigma-Aldrich
Isopentane	Sigma-Aldrich
Isopropanol	Merck
Isopropyl β-D-1-thiogalactopyranoside (IPTG)	Sigma-Aldrich
Insulin solution from Bovine pancreas	Sigma-Aldrich
Ketamine	Parnell Pharmaceuticals
Lennox Broth(LB)	BD Biosciences
L-glutamine	Sigma-Aldrich
Magnesium sulphate	Sigma-Aldrich
Matrigel	Corning
Methanol	Merck Millipore
Methylene blue	Sigma-Aldrich
3-(N-morpholino)propanesulfonic acid (MOPS)	Sigma-Aldrich
Normal goat serum (NGS)	Sigma-Aldrich
Normal sheep serum (NSS)	Sigma-Aldrich
Notexin	Latoxan
NuPAGE®(20x) MES buffer	Novex
O.C.T	Sakura Finetek
OPTI-MEM 1 reduced serum media	Gibco
Paraformaldehyde (PFA)	Sigma-Aldrich
Penicillin/Streptomycin	Gibco
Phenylmethylsulfonyl fluoride (PMSF)	Sigma-Aldrich
OXOIDTM Phosphate buffered saline	Thermo Fisher Scientific
Ponceau S	Sigma-Aldrich
Potassium bicarbonate (KHCO3)	Sigma-Aldrich
Prolong Gold Anti-Fade	Invitrogen
Protease Inhibitor (PI)	Roche
Protein assay dye reagent concentrate (5x)	Biorad
SeeBlue Plus 2 protein ladder	Invitrogen
Sirius Red/Fast Green collagen staining kit	Chondrex
Skim milk	Sigma-Aldrich
Slowfade gold anti-fade with DAPI	Invitrogen
Sodium acetate	Sigma-Aldrich
Sodium bicarbonate	Sigma-Aldrich
Sodium chloride (NaCl)	1st Base
Sodium dodecyl sulfate (SDS)	Sigma-Aldrich
Sodium fluoride (NaF)	Sigma-Aldrich
Sodium hydroxide (NaOH)	Merck
Sodium orthovandate (NaVO4)	Sigma-Aldrich
Sodium tetraborate	Sigma-Aldrich
SsoFast EvaGreen supermix	Biorad
Tetramethylethylenediamine (TEMED)	Biorad
Tris	1st Base
Triton X-100	Promega
Trizol®	Thermo Fisher Scientific
Tryphan blue	Sigma-Aldrich
Tween 20	Promega
Xylazine	Troy Laboratories
Xylene	Sigma-Aldrich

2.2 Methods

2.2.1 Expression and Purification of Recombinant Irisin Protein

Recombinant murine Irisin protein was expressed and purified using the pET expression system (Novagen, USA). Mouse Irisin cDNA (encoding amino acids 29-140 of FNDC5 protein: ds psapvnvtvr hlkansavvs wdvledevvi gfaisqqkkd vrmlrfiqev ntttrscalw dleedteyiv hvqaisiqgq spasepvlfk tpreaekmas knkdevtmke) were PCR amplified and cloned into the pET-16b expression vector in frame with 10 Histidine residues using standard molecular biology techniques as explained in detail below. Mature mouse Irisin cDNA was PCR amplified using total RNA from mouse muscle as a template. The primers used for cloning are given below: 5' CAT ATG GAC AGC CCC TCA GCC CCT 3', 5' GGA TCC TCA CTC CTT CAT GGT CAC CTC 3'. The resulting PCR product was resolved on a DNA gel and purified using the QIAquick Gel Extraction Kit, according to the manufacturer's protocol (Qiagen, Cat # 28704). Subsequently, TA cloning was performed to insert the PCR product with A and T overhangs into the pGEM-T easy cloning vector. The ligated vector was then transformed into DH5α *E. coli* competent cells and positive transformants (white colonies) were selected for plasmid DNA extraction and purification. Plasmid DNA extraction and purification was performed using the QIAprep spin miniprep kit (Qiagen kit, Cat # 27104), after which the plasmid DNA was sequence verified to ensure that no mutations were present in the sequence.

To sub clone the Irisin fragment into the pET-16b expression vector, the pGEM-T easy vector containing the Irisin insert was double digested with BamHI and NdeI restriction enzymes and was subsequently resolved using DNA gel electrophoresis. The band corresponding to the expected size of Irisin was extracted and purified from the gel using the QIAquick Gel Extraction Kit. The purified fragment was then cloned into BamHI and NdeI restriction sites of the pET-16b expression vector. The Irisin containing pET-16b vector was transformed into DH5α cells and positive transformants were selected and subjected to DNA extraction/purification and sequencing, to ensure the vector was mutation free. The Irisin-pET-16b vector construct was then transformed into the BL21 *E. coli* strain (Agilent Technologies, USA), with another round of DNA extraction/purification and sequencing performed. Transformed BL21

68

cells were cultured in Lennox broth (LB) (BD Biosciences, USA), containing Ampicillin (Sigma Aldrich, USA) (100mg/liter), overnight as a starter culture. The starter culture was diluted into 4L of LB medium plus Ampicillin and was further grown to an optical density (OD) of 0.8 at 595nm. Bacteria were then induced to produce Histidine-tagged Irisin protein through addition of 1mM isopropyl-1-thio-β-D-glalactopyranoside (IPTG) (Thermo Fisher Scientific, USA) for 2.5h. Bacteria were then harvested by centrifugation for 20 minutes at 6000rpm, resuspended in 100ml of binding buffer, sonicated and centrifuged for 30minutes at 10,000g to pellet cell debris. The resulting supernatant was stirred gently with Ni-NTA agarose resin (Qiagen, Germany) for 2 hours at 4°C. Ni-NTA agarose beads with Histidine-tagged Irisin bound were centrifuged for a further 15 minutes at 5000rpm. The resin was then washed with binding buffer and centrifuged at 2500rpm for 2 minutes, for a total of 5 times. The Ni-NTA agarose beads with Histidine-tagged Irisin were then packed into an affinity column and non-specific proteins were removed with 1x wash of 50mM Imidazole (Sigma Aldrich, USA). Fractions containing recombinant Irisin protein were eluted from the Ni-NTA agarose column using 200mM Imidazole. Eluted Histidine-tagged Irisin protein was pooled and dialyzed against three changes of Dialysis buffer for a period of 3h and filter sterilized before use for *in vitro* and *in vivo* experiments. Endotoxin levels in the recombinant Irisin protein was estimated uaing the ToxinSensor Chromogenic LAL kit (GenScript, USA), according to the manufacturer's protocol.

2.2.2 DNA Agarose Gel Electrophoresis

DNA agarose gels were made by boiling Ultra pure^{TM} agarose powder in 1x TAE buffer (1st base, Ultra pure grade) for 2 minutes or until completely dissolved. The mixture was then cooled under running water at RT and 2μl of Ethidium Bromide (EtBr) was added/50ml of 1x TAE buffer /agarose mixture. The gel was then poured into the horizontal gel electrophoresis system (Thermo Fisher Scientific, USA) and allowed to solidify for 30 minutes. Samples were loaded onto the gel using a 6x DNA gel loading dye (Thermo Fisher Scientific, USA) to a final concentration of 1x. The DNA gel was then resolved at 90V for 40 minutes.

2.2.3 Animal Care and Treatment

Wild-type C57BL/6J and *mdx* male mice used were obtained from the Nanyang Technological University (NTU) Animal house, A*STAR Biological Resource Centre, Singapore or InVivos, Singapore. All experiments were performed on 3-8-week-old mice according to NTU Institutional Animal Care & Use Committee (IACUC) approved protocols. All mice were maintained on standard chow diet at a constant temperature of 20°C under an artificial 12h light and 12h dark cycle with *ad libitum* access to food and water at the NTU animal house. To assess the pro-myogenic function of Irisin, 5-week-old C57BL/6J mice were injected with 2.5µg/g body weight of Irisin twice a week intraperitoneally (IP) for 4 weeks and control animals were injected with Dialysis Buffer (DB), as the vehicle control. For the control peptide animal trial, we used the N-terminal His-tag portion of the recombinant Irisin fusion protein coded by the pET-16b vector. The 20-amino acid long peptide (MGHHHHHHHHHHHSSGHIEGR) was synthesized by Merck, Sigma Aldrich. Similar to the previous animal trial, 5-week-old C57BL/6J mice were injected with 2.5µg/g body weight of His-tag peptide three times-a-week intraperitoneally (IP) for 4 weeks and control animals were injected with Dialysis Buffer (DB), as the vehicle control. Body weight, food consumption and water intake were measured. Following the trial, mice were sacrificed by CO_2 asphyxiation and *M. tibialis anterior* (TA), *M. extensor digitorum longus* (EDL), *M. gastronemius* (Gas), *M. soleus* (Sol), *M. Quadriceps* (Quad), *M. biceps femoris* (BF) were collected for further experiments. TA muscle tissue was also embedded in optimum cutting temperature compound (O.C.T) (Sakura Finetek, USA), frozen in liquid nitrogen cooled isopentane (Sigma Aldrich, USA) and stored at -80°C for subsequent sectioning and staining.

Injury of resting muscle was performed through injection of Notexin. 100µg of Notexin powder (Latoxan, L8104) was dissolved in 1ml of autoclaved saline, which was further diluted to 10µg/ml before injection. The hind limb area was shaved using an electric shaver and mice were anesthetized through IP injection of a mixture of ketamine (Parnell Pharmaceuticals, Australia) and xylazine (Troy Laboratories, Australia) at 0.1ml/10g of body weight. A small incision

was made on the left TA muscle and 15μl of 10μg/ml Notexin was injected along the longitudinal axis of left TA muscles of 6-week-old C57BL/6J wild-type mice using a 28-gauge needle (Hamilton Co., USA). The right TA muscle was used as an uninjured control. Mice were injected IP with either DB or recombinant Irisin protein (2.5ug/g body weight) three times-a-week, one week prior to the injury and also following Notexin injury for the duration of the trial. TA muscles were weighed and O.C.T embedded as mentioned above from mice at Days 1, 2, 3 and 10 post-Notexin-induced injury.

In order to investigate if Irisin reduces denervation-induced atrophy of skeletal muscle, 8-week-old C57BL/6J male mice were anesthetized through IP injection of a mixture of ketamine and xylazine at 0.1ml/10g of body weight. Hair on the hind limb was shaved using an electric shaver. A small incision was made and the sciatic nerve of the left leg was isolated and transected using surgical scissors. The skin was glued to close the wound. The contra-lateral (right) leg was used as the uninjured control. Mice were IP injected with either DB or Irisin (2.5μg/g body weight) for one week prior to injury and two weeks post-injury, at a frequency of three times-a-week. Following conclusion of the trial, mice were sacrificed by CO_2 asphyxiation and TA, EDL, Gas and Sol muscles were collected for further experiments. TA muscle tissue was also embedded in O.C.T. as mentioned above for subsequent sectioning and staining.

Experiments to assess the effect of Irisin on muscular dystrophy were performed on 3-6-week-old male *mdx* mice. To monitor the effect of Irisin on dystrophic muscle growth, three trials were performed. In the first trial, young 3-week-old *mdx* mice were injected three times-a-week for two weeks and all hind limb muscles were collected for extensive characterization of the *mdx* phenotype. Cross sectional area and extent of muscle fiber damage was analyzed. A second trial was performed in order to assess muscle cross-sectional area and fibrotic tissue accumulation by injecting 6-week-old adult *mdx* mice with either DB or recombinant Irisin protein (2.5μg/g body weight) three times-a-week for a total of 2 weeks. In the final trial using the *mdx* mouse model, 4-week-old *mdx* mice were injected IP with either DB or recombinant Irisin protein (2.5μg/g body weight) three times-a-week for a total of 4 weeks to

71

analyze if a longer period of treatment enhances muscle weights and grip strength.

The grip strength for all *mdx* mice in the 4-week trial was measured immediately prior to dissection. Six readings were obtained for each mouse, with a 30 second rest between each reading. The highest three values were used to calculate the average grip strength for each mouse in both the DB and Irisin injected groups. For *mdx* mice studies, food intake was measured before every injection. Following conclusion of each trial, mice were sacrificed by CO_2 asphyxiation and TA, EDL, Gas, Sol, Quad, BF muscles were harvested, weighed and stored for further experiments. TA muscle tissue was embedded in O.C.T, as mentioned above for subsequent sectioning and staining.

2.2.4 Muscle Fiber Cross Sectional Area Measurement

Transverse sections (10μm) were cut from the midbelly region of O.C.T embedded TA muscles using a Cryostat (Leica CM 1950, Germany) and muscle sections were mounted on Superfrost Plus Microscope Slides (Thermo Fisher Scientific, USA) and subsequently stained with Gill's Haematoxylin and counterstained with 1% Eosin (Merck) (H&E), as per the protocol described in Table 2.44

Table 2.44: Myofiber H&E staining procedure

Reagent	Duration of exposure
Haematoxylin	1 minute
Rinse with tap water	Until clear
Blue with Scott's Tapwater	2 minutes
Rinse with tap water	Until clear
1% Eosin	2 minutes
Rinse with tap water	Until clear
50% Ethanol	3 dips
70% Ethanol	3 dips
95% Ethanol	2 minutes
100% Ethanol	2 minutes x 2
Xylene	5 minutes x 2
Mount with DPX mountant	

Mounted and stained TA muscle sections were imaged and tiled using the Leica CTR 6500 microscope equipped with the Leica DFC 420 camera, Image Pro Plus software (Media Cybernetics, Bethesda, MD) and a 10x objective. The CSA of 200 muscle fibers from 5 random fields (1000 fibers per mouse) from both DB treated and Irisin treated mice were measured using Image Pro Plus software and data was analyzed using Microsoft Excel.

2.2.5 Immunohistochemical Staining of Muscle Sections

Muscle sections were fixed with 4% paraformaldehyde (PFA) (Sigma Aldrich, USA) in Phosphate Buffered Saline (PBS) (pH 7.4) for 10min and then permeabilized with 0.1% Triton X-100 (Promega, USA) for 10 min. Sections were blocked with 5% Normal Sheep Serum (NSS) (Sigma Aldrich, USA), 5% Normal Goat Serum (NGS) (Sigma Aldrich, USA) and 0.35% Carrageenan lambda (Cλ) (Sigma Aldrich, USA) in PBS for 1 hour at room temperature and incubated with anti-MyoD (Santa Cruz 304 [1:50]) primary antibody overnight at 4°C. Sections were then incubated with secondary antibody (Alexa Fluor® 568 goat anti-rabbit [1:300]) for 1 hour at room temperature. Sections were counterstained with DAPI (Molecular Probes, USA) [1:1000] for 5 min in PBS and mounted using Prolong Gold Anti-Fade (Thermo Fisher Scientific, USA). Stained samples were analyzed and MyoD positive nuclei were counted, with the number of MyoD positive nuclei expressed as a percentage of total DAPI positive nuclei. Images from twenty random microscopic fields for each treatment were analyzed per mouse using the Leica CTR 6500 microscope equipped with the Leica DFC 420 camera and ImageJ software (NIH, USA).

2.2.6 Cell Culture

ATCC murine C2C12 myoblasts (Yaffe and Saxel, 1977)[173] were maintained in proliferation medium, consisting of Dulbecco's Modified Eagle's Medium (DMEM) (Invitrogen, USA), 10% Fetal Bovine Serum (FBS) (HyClone, Thermo Scientific, USA) and 1% Penicillin/Streptomycin (P/S) (Gibco, Invitrogen, USA). 36C15Q primary human myoblasts were a gift from Drs. Vincent Mouly and Gillian Butler-Browne from the Institut de Myologie, Paris, France and were maintained in proliferation medium, consisting of DMEM, 20% FBS, 10% Horse Serum (HS), 1% Chicken Embryo Extract (CEE) and 1% P/S.

36C15Q human myoblasts were always grown/plated on Matrigel Basement Membrane Matrix (Corning, USA) coated plates/coverslips.

2.2.6.1 Myoblast Proliferation Assay

C2C12 myoblasts were seeded at a density of 1000 cells/well in 96-well-plates in proliferation medium and incubated at 37°C in a 5% CO_2 incubator. Proliferating myoblasts were treated with either DB or increasing concentrations of recombinant Irisin protein (250ng/ml, 1000ng/ml and 2000ng/ml) and fixed at 0h, 24h, 48h and 72h proliferation. The point at which myoblasts attached was taken as 0h. Myoblasts were fixed with 200µl of fixative solution per well [10% formaldehyde (Sigma- Aldrich, USA) and 0.9% NaCl]. Plates were wrapped in aluminum foil and stored at room temperature (RT) until assessment of proliferation was performed using the methylene blue photometric end point assay (Thomas *et al.,* 2000)[130]. Initially, fixative was removed from each cell culture plate. After washing with PBS, 100µl of methylene blue (1% methylene blue in 0.01M borate buffer, pH 8.5) was added to each well and incubated for 30 minutes at RT. Methylene blue was removed and each well was washed with 200µl borate buffer [0.01M sodium tetraborate (Sigma Aldrich, USA, pH 8.5)] four times. 200µl of 0.1M HCl: Ethanol 1:1 was added to each well to release the blue dye bound to the cell membrane. The absorbance of each well was read using a microplate reader (model 3550, Bio Rad, USA) at 655nm. Absorbance at 655nm is directly proportional to the total cell number. Each treatment for each time point was performed in sixteen wells.

2.2.6.2 Myoblast Differentiation Assay

C2C12 myoblasts were seeded on plastic thermanox cover slips (Nalge Nunc International, USA) in 24-well-plates at a density of 15,000 cells/cm^2; while 36C15Q human primary myoblasts were seeded at a density of 25,000 cells/cm^2. After overnight cell attachment, myoblasts were induced to differentiate in low serum differentiation medium [DMEM with 2% Horse Serum (HS) (Hyclone, Thermo Scientific, USA) and 1% P/S] at 37°C, 5% CO_2 and were treated with either DB or recombinant Irisin protein (250ng/ml or 1000ng/ml) during differentiation. At 0h, 24h, 48h, 72h and 96h post-induction of differentiation,

74

myotubes were fixed with 70% ethanol, formalin and acetic acid in a 20:2:1 ratio and washed with 1ml of PBS three times before H&E staining was performed. Each treatment was performed in triplicates per time point. Images of non-over-lapping areas from three cover slips were taken in a bright field microscope at each time point (Leica CTR 6500 microscope equipped with the Leica DFC 420 camera). To analyze myotube number, 10 random images were obtained per coverslip at a 10x magnification and the total number of myotubes was counted in each image using the ImageJ software (NIH, USA). Fusion index was measured by dividing the number of nuclei found within the myotubes by the total number of nuclei in each image.

2.2.6.3 Immunocytochemistry of Primary Myoblast Cultures

Primary cultures were isolated from mouse hind limb muscle tissue. Muscle tissues collected from wild type mice were minced well in PBS and centrifuged for 10 minutes at 3000rpm to remove the PBS. Minced muscles were resuspended in filter sterilized 0.2% Collagenase Type IA (Sigma Aldrich, USA) in DMEM (Muscle tissues collected from each mouse was resuspended in 3ml of Collagenase mix) and incubated at 37°C for 90 minutes on a shaker at 70rpm (low shaking). The suspension was centrifuged at 3000rpm for 10 minutes and collagenase liquid was removed. The pellet was resuspended in 12ml of PBS and triturated for 5 minutes before passing the suspension through a 100μM nylon cell strainer (BD Falcon, USA). The filtered suspension was further centrifuged at 3000rpm for 10 minutes and the pellet was resuspended in 8ml of warm Satellite cell proliferation media (DMEM, 20% FBS, 10% HS, 1% Chick embryo extract (CEE) (Biomed Diagnostics, Singapore), 1% P/S). The suspension was pre-plated on a non-coated 10cm dish and left at 37°C and 5% CO_2 for 3 hours for removal of fibroblasts from the culture. Subsequently, the "fibroblast free" cell suspension was plated onto a 10cm cell culture dish coated with 10% Matrigel (Corning, USA) and incubated overnight at 37°C, 5% CO_2. After overnight attachment, primary myoblasts were trypsinized and seeded at a density of 10,000 cells/well in 8-well chamber slides (Thermo Fisher Scientific, USA).

Primary myoblasts cultures were treated with recombinant Irisin protein (250ng/ml, 700ng/ml or 1000ng/ml) and were fixed 24h post-Irisin treatment with 4% paraformaldehyde in Phosphate Buffered Saline for 15 minutes. Fixed primary myoblasts were then treated with 0.1% Triton X-100 for 10 min to permeabilize the cells. Cells were blocked with 5% Normal Sheep Serum (NSS), 5% Normal Goat Serum (NGS) and 0.35% Cλ in PBS for 1 hour at room temperature and incubated with primary antibodies, anti-Pax7 (DSHB AB528428) [1:100] and anti-MyoD (Santa Cruz, SC-304) [1:100] overnight at 4°C. After washing, myoblasts were incubated with Sheep anti-mouse IgG biotinylated secondary antibody (1:300) for 1 hour at room temperature. Lastly, cells were incubated with Streptavidin conjugated Alexa Fluor® 488 tertiary antibody (1:400) and Goat anti-rabbit Alexa Fluor® 594 (1:300) secondary antibody for 1 hour at room temperature in the dark. DAPI staining was performed for 5 min (1:1000 dilution in PBS) and slides were mounted using Prolong Gold Anti-Fade. Stained cells were analyzed for the numbers of Pax7$^+$ and MyoD$^+$ myoblasts. Images from ten random microscopic fields per treatment were analyzed using the Leica CTR 6500 microscope (10x objective) equipped with the Leica DFC 420 camera and ImageJ software (NIH, USA).

2.2.6.4 Transient Transfection of C2C12 Myoblasts

C2C12 myoblasts were seeded on 6-well-plates or on plastic thermanox cover slips in 24-well-plates at density of 12,500cells/cm^2 in antibiotic-free proliferation medium (without P/S). After overnight attachment, 400µl of medium was removed and replaced with 400µl of transfection reagent. The preparation of the transfection reagent is as follows: For each well, 8µl of DharmaFECT 1 transfection reagent was added to 192µl of filter sterilized OPTI-MEM® medium (Life Technologies, USA). In a separate tube, an appropriate volume of the 5µM stock of either *IL6* targeting siRNA (*IL6-siRNA*) or control non targeting siRNA (scramb-siRNA) (Dharmacon, Inc, USA) suspension was added to OPTI-MEM medium (total of 200µl), such that the final concentration of siRNA in each well would be 25nM. The mixtures were then incubated for 5 minutes at RT. The siRNA-OPTI-MEM® suspension mix was then added to DharmaFECT 1-OPTI-MEM® mix and incubated at RT for 20 minutes. The final mixture of 400µl was added to each well in the plates

76

and rocked vigorously. C2C12 myoblasts were transfected for 24h.The target sequences for the *IL6* targeting siRNA are as follows: 1) CCU AGU GCG UUA UGC CUA A; 2) UUA CAC AUG UUC UCU GGG A; 3) GGA CCA AGA CCA UCC AAU U and 4) CUA CCA AAC UGG AUA UAA U.

Following transfection, C2C12 myoblasts were switched to differentiation medium and treated with either DB or Irisin (1000ng/ml) for 48h and myotubes were collected with 1ml of Trizol® reagent/well. RNA was extracted from myotubes and quantitative real-time PCR (qPCR) was used to measure gene expression changes (see section 2.2.8 below). Myotubes differentiated for 72h with either DB or Irisin (1000ng/ml) was stained with H&E for histological analysis. Each treatment was performed in triplicates per time point. Images of non-over-lapping areas from three cover slips with H&E stained myotubes were taken in a bright field microscope at each time point (Leica CTR 6500 microscope equipped with the Leica DFC 420 camera). To analyze myotube number, 10 random images were obtained per coverslip at a 10x magnification and the total number of myotubes was counted in each image using the ImageJ software (NIH, USA). Fusion index was measured by dividing the number of nuclei found within the myotubes by the total number of nuclei in each image.

2.2.7 Isolation of Human Adipose-Derived Stem Cells (hADSCs) and Adipogenic Differentiation

Details regarding establishment of the human primary ADSCs has been described below. The collection of white adipose tissue biopsies and generation of human primary ADSCs cultures has been approved by the Domain Specific Review Board (DSRB: #2013/00171) of National University Hospital, Singapore. Approximately 1g of white adipose tissue was digested with Type IA collagenase (1mg/ml) in BSA (20mg/ml) for 90 minutes at 37°C with shaking (120rpm). The suspension was centrifuged for 10 minutes at 800g and the cell pellet was suspended in 9ml of red blood cell lysis buffer and incubated for 10 minutes. The cells were centrifuged again for 10 minutes at 800g and resuspended in growth medium, consisting of DMEM/F-12 (Gibco, Thermo Fisher Scientific, USA), supplemented with 20% FBS and 1% P/S, and subsequently filtered through a 100μm nylon cell strainer. The filtrate was

77

further centrifuged for 10 minutes at 800g and the pellet was resuspended with hADSC growth medium.

To induce adipogenic differentiation, hADSC cells were seeded on 10cm dishes coated with 0.2% gelatin and grown in DMEM/F12, 10% FBS and 1% P/S. Cells were grown to confluence for 3 days before treatment with Induction medium (DMEM/F-12, 10% FBS, 1% P/S, 0.5mM IBMX, 1µM dexamethasone, 0.01mg/ml Insulin) containing DB or Irisin for a further 48 hours. The induction medium was then replaced with Insulin medium (DMEM/F-12, 10% FBS, 1% P/S, 0.01mg/ml insulin) for another 48 hours in the presence of either DB or Irisin. hADSCs were differentiated for 21 days in the presence of either DB or recombinant murine Irisin protein at a concentration of 4µg/ml.

The murine embryonic fibroblast cell line 3T3L1 (ATCC-CL173), which can be induced to differentiate into adipocytes in culture, was also used in this study. 3T3L1 cells were maintained in growth medium consisting of DMEM + GlutaMAX, 10% Bovine Calf Serum (BCS) (Gibco, Thermo Fisher Scientific) and 1% P/S. To induce adipogenic differentiation, 3T3L1 cells were seeded on 10cm dishes coated with 0.2% gelatin and grown in DMEM with 2mM L-glutamine, 10% FBS and 1% P/S. Cells were grown to confluence for 72 hours and kept at that state for another 48 hours to arrest cell division. 3T3L1 cells were then treated with Induction medium (DMEM+ GlutaMAX, 10% FBS, 1% P/S, 0.5mM IBMX, 1µM dexamethasone, 0.01mg/ml Insulin) containing DB or Irisin for a further 48 hours. The induction medium was then replaced with Insulin medium (DMEM+ GlutaMAX, 10% FBS, 1% P/S, 0.01mg/ml insulin) for another 48 hours in the presence of either DB or Irisin. 3T3L1 cells were induced to undergo adipogenic differentiation for 4 days (after addition of induction medium) in the presence of either DB or recombinant murine Irisin protein at a concentration of 0.5µg/ml.

2.2.8 Protein Extraction and Western Blot (Immunoblot) Analysis

To isolate total muscle proteins, 50mg of muscle tissue was homogenized in RIPA buffer (1x Phosphate buffered saline, 1% IGEPAL CA-630 (v/v), 0.1%

Sodium dodecyl sulfate (w/v), 0.5% Sodium deoxycholate (w/v)), 50mM Sodium fluoride) using the Tissue Lyser II instrument (Qiagen, USA) at 30Hz (3 x 1 minute). To isolate total cell proteins from *in vitro* experiments, C2C12 cultures were re-suspended in protein lysis buffer (1M Tris HCl pH 7.5, 5M NaCl, 0.5M EDTA, IGEPAL CA-630, Protease Inhibitor, MilliQ Water) and syringed 20 times with a 1ml syringe and 26-gauge needle. Subsequently, both muscle homogenates and C2C12 myoblasts/myotubes lysates were centrifuged at 12,000rpm for 10 minutes at 4°C and the supernatant was collected. Protein estimations were performed using Protein assay dye reagent concentrate (5x) (BioRad, USA). 5-20μg of protein was resolved by SDS-PAGE (NuPage 4-12% gradient, Bis-Tris pre-cast polyacrylamide gels, Invitrogen, USA) and transferred to nitrocellulose membrane by wet transfer using the Trans-Blot® Cell system (BioRad, USA) for 2 hours at 4°C. For *mdx* mice studies, 50μg of total protein was resolved by SDS-PAGE (8% Tris-Glycine acrylamide gel) and transferred to nitrocellulose membrane by wet transfer for 2 hours at 4°C. Membranes were stained with Ponceau S (Fluka, Sigma-Aldrich, USA) to confirm equal loading of protein samples.

For Western Blot analysis membranes were blocked for 1 hour at room temperature with 5% milk (Sigma, USA) in T-BST and subsequently incubated with primary antibodies overnight at 4°C (for details of primary antibodies and dilutions see Table 2.37). The membranes were then washed with TBS-T (3 x 10 minutes), followed by secondary antibody incubation for 1 hour at room temperature (RT. (for details of secondary antibodies and dilutions see Table 2.37). Following secondary antibody incubations, membranes were washed as stated above and HRP activity was detected using Western Lightning Chemiluminescence Reagent Plus (NEL104; Perkin Elmer Life Sciences, USA). Kodak films were exposed to the membranes and detected bands were subsequently quantified using Quantity One imaging software and a Calibrated Densitometer (Bio-Rad GS-800, USA). In addition, bands were also detected using the ChemiDoc Touch Imaging System (BioRad, USA) and were analyzed using Image Lab software (BioRad, USA).

2.2.9 Total RNA Extraction, Reverse Transcription and Quantitative Real-Time PCR (qPCR)

Total RNA was isolated from C2C12 myotubes using TRIzol® reagent (Invitrogen, USA). Samples were incubated for 5 minutes at RT before 200µl of chloroform was added for every 1ml of TRIzol® reagent added. Tubes were shaken vigorously for 15 seconds by hand and further incubated at RT for 3 minutes. Samples were then centrifuged at 12,000g for 15 minutes at 4°C. The aqueous phase was separated and 500µl of 100% isopropanol was added to the aqueous phase (for every 1ml of TRIzol® added to the sample) followed by incubation at RT for 10 minutes. Samples were centrifuged again at 12,000g for 10 minutes at 4°C. The supernatant was removed and the pellet was washed with 1ml of 75% ethanol (for every 1ml of TRIzol® added to the sample). Samples were then vortexed briefly before centrifuging at 7500g for 5 minutes at 4°C. The ethanol wash was discarded and the pellet was air dried for 10 minutes. Pellets were re-suspended in 30-50µl of DEPC water (1st Base, Singapore), depending on the size of the pellet, and incubated at 60°C for 10 minutes before utilizing the RNA for downstream applications.

RNA integrity was monitored by RNA electrophoresis. 1µg of total RNA was used to synthesize cDNA according to the iScript cDNA Synthesis kit protocol (Bio-Rad, USA, Cat # 1708891). All reactions were performed according to the iScript protocol: Priming for 5 minutes at 25°C, reverse transcription for 20 minutes at 46°C and reverse transcription inactivation for 1 minute at 95°C. Quantitative real-time PCR (qPCR) reactions were carried out in triplicates using SsoFast EvaGreen Supermix (Bio-Rad, USA) and the CFX96 Real-Time System (Bio-Rad, USA). All reactions were performed using the following thermal cycle conditions: 95° C for 3 minutes, followed by 40 cycles of a three-step reaction, denaturation at 95° C for 10 seconds, annealing at 60° C for 10 seconds, elongation at 72° C for 20 seconds, followed by a melting curve from 65° C to 95° C in 10 second increments of 0.5° C. Gene expression fold change was calculated using the $\Delta\Delta C_t$ method, normalized against the expression of *Gapdh*. Primer stocks (100µM; Sigma-Aldrich, Singapore) were diluted to 2.5µM prior to qPCR. The sequences of the primers used in this study are provided in Table 2.42 (See Materials section).

2.2.10 Microarray Analysis

C2C12 myoblasts were seeded at a density of 20,000 cells/cm^2 in a 10cm cell culture dish and induced to differentiate in low serum differentiation medium (DMEM, 2% HS and 1% P/S) at 37°C, 5% CO_2 for 72h and further treated with either DB or Irisin (1000ng/ml) for 6h, 12h, 24h and 48h. RNA was collected using 2ml of TRIzol® for each 10cm dish and RNA isolation was performed according to the manufacturer's protocol, as described in section 2.2.9. Purified isolated RNA was then subjected to sequencing on a standard Illumina MouseRef8- V2.0 expression bead chip. Both coding and non-coding transcripts were analyzed. This platform is able to analyze about 24,000 coding genes and 300 non-coding genes. However, microRNAs were not analyzed. Data analysis was performed, as per in-house protocols (Sciencewerke, Singapore). In the microarray experiment, a total of 20,000 genes were detected. Only genes that were upregulated or downregulated by $\geq$1.5-fold were considered significant. For genes that had multiple probes (with different accession numbers), the probe that displayed the greatest change (either up- or down-regulation) was considered. Approximately 1000 genes were downregulated by more than 1.5 fold and another 1000 genes were upregulated more than 1.5 fold after Irisin treatment of differentiated myotubes.

2.2.11 Assessment of Mitochondrial Function

C2C12 myoblasts were seeded equally at a density of 15,000 cells/well in an XF^{e}24 plate (Seahorse Biosciences, USA) and induced to differentiate in differentiation medium (DMEM 2%HS, 1%P/S) for 72h. Myotubes were treated with either DB or Irisin (1000ng/ml) for a further 24h or 48h. The oxygen consumption rate (OCR) was measured using the XF^{e}24 extracellular Flux Analyzer, according to the manufacturer's protocol (Seahorse Biosciences). Differentiated myotubes were equilibrated in pre-warmed (37°C) assay medium (DMEM containing 0.45g of glucose and 1ml of 100mM Sodium pyruvate at a pH of 7.4). Baseline OCR and OCR following sequential addition of Oligomycin (1μM), Carbonyl cyanide-4(trifluoromethoxy) phenylhydrazone FCCP (0.5μM) and Rotenone/Antimycin (0.5μM) were assessed. Each of these drugs targets different components of the mitochondrial electron transport chain,

81

which enables the calculation of, ATP-linked respiration, maximal respiration and non-mitochondrial respiration, respectively.

Oligomycin specifically targets and inhibits the function of complex V, which is ATP synthase, resulting in reduced OCR. The difference between the basal OCR and the resulting OCR after Oligomycin treatment of the myotubes determines ATP-linked respiration (ATP production) in the myotubes (Figure 2.1). OCR due to proton leak can also be calculated by deducting the OCR values after Oligomycin injection from the non-mitochondrial respiration rate. FCCP is an uncoupling agent that disrupts mitochondrial membrane potential thereby removing the proton gradient. As a result, electrons flow freely allowing for maximum oxygen consumption, as such, calculation of maximal respiration can be made (Figure 2.1). Spare respiratory capacity can be determined by deducting basal respiration from maximal respiration (Figure 2.1). Injection of Antimycin A and Rotenone blocks complex III and complex I function, respectively. As a result, this completely inhibits mitochondrial respiration and as such non-mitochondrial respiration can be determined (Figure 2.1).
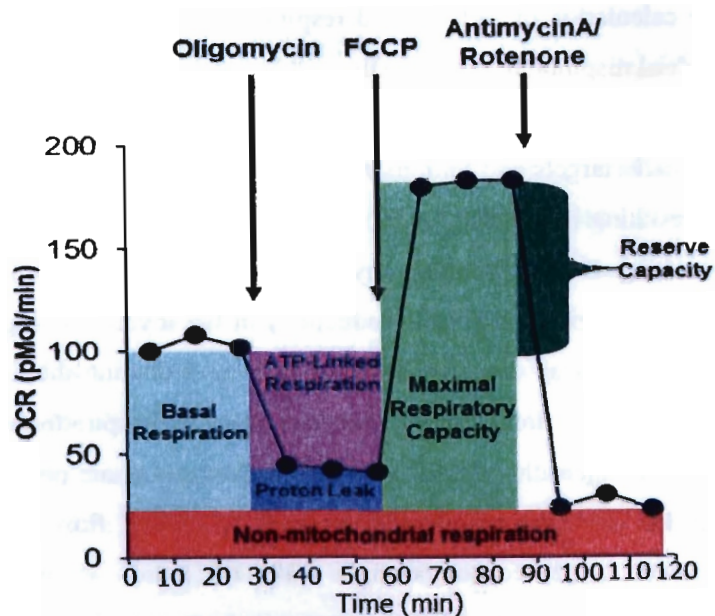
Figure 2.1: Seahorse XF Cell Mito Stress Test profile displaying the key parameters that can be measured during mitochondrial respiration
Graph displays a typical profile of mitochondrial respiration (OCR; pmol/min) in cultured cells over time. Oligomycin, FCCP and a mixture of Antimycin A & Rotenone are injected sequentially to target different components of the electron transport chain, which enables the determination of Basal Respiration, ATP-linked respiration, Proton Leak, Maximal Respiration, Spare Respiratory Capacity and Non-mitochondrial Respiration in cultured cells. Image adapted and modified from Rose, S., Frye, R. E., Slattery, J., Wynne, R., Tippett, M., Pavliv, O., ... & James, S. J. (2014). Oxidative stress induces mitochondrial dysfunction in a subset of autism lymphoblastoid cell lines in a well-matched case control cohort. *PLoS One*, *9*(1), e85436. (*This image has been obtained from Open Access article distributed under the terms of the Creative Commons Attribution License*)

2.2.12 Measurement of Fibrosis

Muscle sections were stained using the Sirius Red/Fast Green collagen staining kit (Chondrex Inc, WA). Muscle sections mounted on glass slides were washed with PBS and immersed in Sirius Red/Fast Green Dye solution for 30 minutes at room temperature. Excess dye was washed off with distilled water. Stained sections were then dried and mounted using DPX mounting medium (Merck, USA). Images of the stained tissue sections were captured and tiled using the Leica CTR 6500 microscope, equipped with the Leica DFC 420 camera, Image Pro Plus software and a 10x objective. The extent of collagen deposition (red stain) was quantified by determining the total area that was stained red across

83

the entire muscle cross section using Image Pro Plus software. The total area stained red was normalized to the total TA muscle cross sectional area and expressed as a percentage, to represent percentage fibrotic area.

2.2.13 Measurement of Fibers with Centrally Placed Nuclei and Necrotic Area in *mdx* Muscle Sections

Transverse sections (10µm) were cut from the midbelly region of O.C.T embedded TA muscles from *mdx* mice injected with either DB or Irisin using a Cryostat. Sections were subsequently stained with H&E (refer to Table 2.44 for protocol details). The CSA of 200 myofibers from 5 random fields were analyzed per section (1000 myofibers in total per mouse). Centrally placed nuclei is a hallmark of regenerated muscle fibers and indicative of the extent of fusion. The number of myofibers with centrally placed nuclei were counted and expressed as a percentage of total myofiber number in the muscle section. Analysis for centrally placed nuclei was performed using the ImageJ software (NIH, USA). Necrotic myofibers were identified based on areas of fragmented sarcoplasm, influx of mononucleated cells and hyper-contracted muscle fibers. The total area of necrotic myofibers was quantified and normalized against the total muscle cross sectional area and expressed as a percentage, to represent percentage necrotic fiber area using Image Pro Plus software. All images of the H&E stained tissue sections were captured and tiled using the Leica CTR 6500 microscope, equipped with the Leica DFC 420 camera, Image Pro Plus software and a 10x objective.

2.2.14 IgM Immunohistochemical Staining of Muscle Sections

IgM is produced by B cells and is restricted to the circulation. IgM accumulates in damaged muscle fibers due to leaky membrane and is proportional to the extent of muscle damage. To detect IgM positive myofibers in *mdx* mouse muscle, sections were fixed with ice-cold acetone for 2 minutes and washed 3 times with 1xPBS for 5 minutes each. Blocking was performed for 1 hour at room temperature with 1% BSA (Sigma Aldrich, USA) and 5% Horse serum in 1xPBS. Sections were subsequently incubated with Goat anti-mouse IgM-FITC conjugated antibody (1:100, Sigma Aldrich, F9259) for 1 hour and washed again 3 times with 1xPBS for 5 minutes each. Sections were mounted with

Slowfade Gold Anti-Fade reagent, containing DAPI (Molecular Probes, USA), and visualized using the Leica CTR 6500 microscope equipped with the Leica DFC 420 camera and Image Pro Plus software. Stained samples were analyzed and the area of the IgM positive muscle fibers were quantified and expressed as a percentage of the total cross sectional area of the muscle section using Image Pro Plus software. All images of the IgM stained tissue sections were captured and tiled using the Leica CTR 6500 microscope, equipped with the Leica DFC 420 camera, Image Pro Plus software and a 10x objective.

2.2.15 Injection of Evans Blue Dye

5-week-old male *mdx* mice were injected IP with a solution of 1% Evans Blue Dye (EBD) (Sigma Aldrich, USA) at a volume of 10µl per gram body weight 24h prior to hind limb muscle collection. EBD forms a conjugate with serum albumin, which is restricted to circulation but accumulates in damaged muscle fibers. The extent of EBD accumulation is indicative of muscle damage and was assessed based on the area of the muscle section that showed red fluorescence divided by the total area of the muscle section. All images of the Evans Blue dye stained tissue sections were captured and tiled using the Leica CTR 6500 microscope, equipped with the Leica DFC 420 camera, Image Pro Plus software and a 10x objective.

2.2.16 Creatine Kinase Assay

A creatine kinase (CK) assay was performed to assess the extent of muscle damage in the *mdx* mice injected with either DB or Irisin. CK is usually present in muscle, but leaks into serum in response to myofiber damage. Blood collected from the heart of *mdx* mice injected with either DB or Irisin was centrifuged at 1500g for 10 minutes and serum was collected. Assessment of CK levels in serum was performed using the Creatine Kinase Activity Assay Kit (Abnova, KA3766), according to the manufacturer's protocol. The CK enzyme converts Creatine and ATP (*provided in kit*) to phosphocreatine and ADP. The resulting ADP forms an intermediate product via the action of the CK enzyme mix (*provided in kit*). CK developer (*provided in kit*) then converts the intermediate product into a colored product that can be detected at a wavelength of 450nm. The color intensity determines the absorbance reading,

which is proportionate to the level of CK present in serum and hence, the extent of muscle damage. In a clear bottom 96-well-plate, 50µl of serum from either DB or Irisin injected mice, diluted 500 times in CK assay buffer (*provided in the kit*) and 50µl of reaction mix (34µl CK Assay Buffer + 2µl CK Enzyme Mix + 2µl CK Developer + 2µl ATP + 10µl of CK Substrate) was incubated for 40 minutes at 37°C and absorbance was measured every 2 minutes. NADH standards were made by adding 0, 2, 4, 6, 8 and 10µl of 1mM NADH standard to 50, 48, 46, 44, 42 and 40µl of CK Assay Buffer respectively, and subsequently topping up the wells with 50µl of reaction mix. Absorbance readings obtained from standard wells were used to plot the standard curve and the amount of NADH was calculated from the curve. Creatine kinase activity was determined using the following formula: ***Amount of NADH calculated from standard curve/ (reaction time*volume of sample added into well)*dilution factor.***

Creatine kinase levels were measured at a wavelength of 450nm using a Microplate Spectrophotometer (BioRad, USA) and the MPM 6 software (BioRad, USA). Calculations were performed according to the manufacturer's instructions as explained above and CK values were represented as mU/mL.

2.2.17 Statistical Analysis

Statistical analysis was performed using two-tailed Student's t-test to compare differences between two treatment groups in one categorical variable. An F-test was performed prior to Student's t-test to assess for equal variance between two groups. Variance between two groups was considered equal when the F-value was smaller than F-critical and unequal if F-value was larger than F-critical values.

One-way-ANOVA, followed by a Tukey's post-hoc test was performed for all experiments that required multiple comparisons between three or more groups from one categorical variable.

Two-way-ANOVA, followed by Scheffe's post-hoc test was performed for all experiments that required the comparison between two categorical variables that could influence the numerical output. For all experiments, results were considered significant at $p < 0.05$ (*), $p < 0.01$ (**) and $p < 0.001$ (***). All data is presented as mean ± S.E.M.

3. Results

The results in this section has been communicated to Nature Communications

3.1 Irisin Treatment Induces the Expression of *Ucp-1*

To study the role of Irisin in skeletal muscle we expressed and purified a Histidine tagged recombinant Irisin protein. Polyacrylamide gel electrophoresis and Coomassie blue staining revealed a single purified Irisin band running at ~15KDa (Figure 3.1a). At 1:100 dilution of the purified recombinant Irisin protein, we observed a low endotoxin level of 1 in the recombinant protein[174]. Previously published work revealed that Irisin induces the expression of Ucp-1[139]. In order to test the biological activity of our recombinant murine Irisin protein, we treated differentiated human adipose-derived stem cells (hADSCs) with recombinant Irisin protein. A significant ~4-fold increase in *Ucp-1* expression was noted in hADSCs after treatment with Irisin (Figure 3.1b). We further noted a significant ~18% increase in *Ucp-1* expression in Irisin treated 3T3L1 fibroblasts during adipogenic differentiation (Figure 3.1c). These data suggested that the purified recombinant murine Irisin was biologically active and as such, this recombinant protein was further utilized to understand the role of Irisin in skeletal muscle.
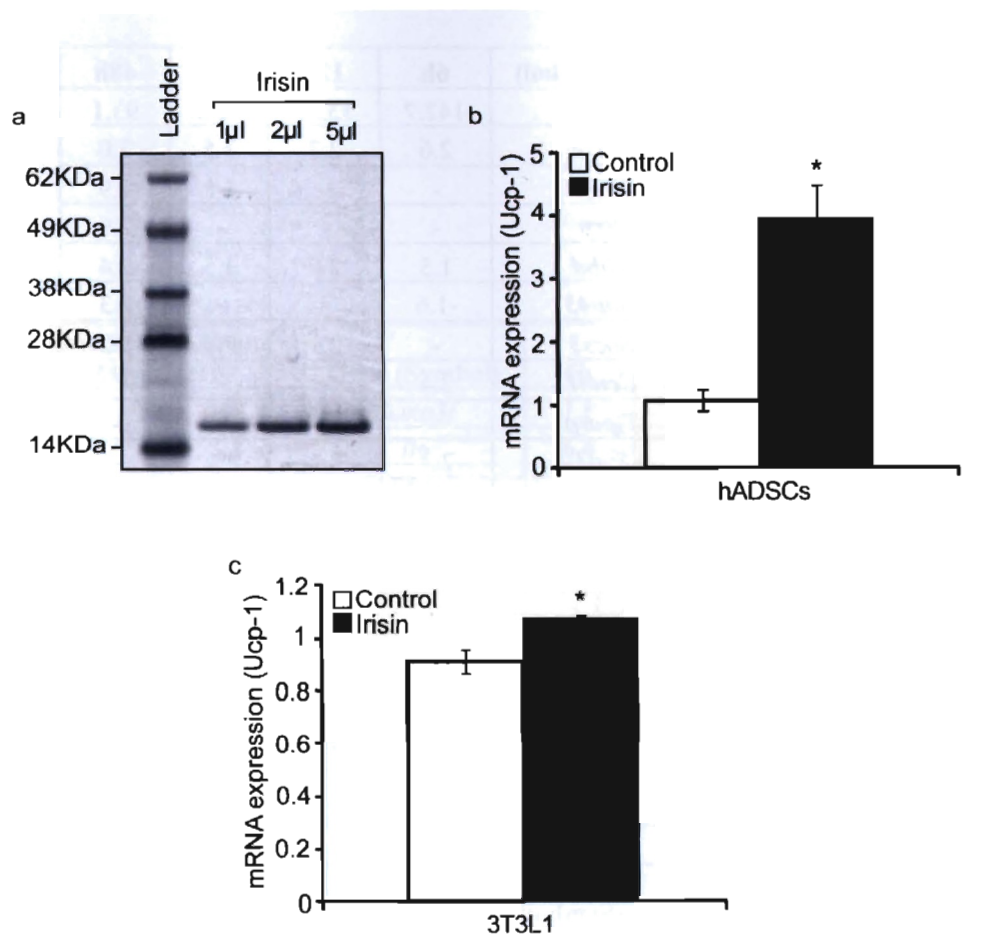
Figure 3.1: Purified recombinant Irisin protein enhances the expression of Ucp-1

(a) Image of Coomassie stained polyacrylamide gel showing recombinant His-tagged Irisin protein. Recombinant Irisin protein was detected as a single band at ~15kDa. Lane 1 shows the SeeBlue Plus 2 Pre-Stained ladder. Lanes 2, 3 and 4 show 1μl, 2μl and 5μl of the purified His-tagged Irisin protein, respectively. (b) Graph displaying qPCR analysis of *Ucp-1* expression in human subcutaneous white adipose-derived stem cells (hADSCs) after 21 days of adipogenic differentiation in the presence of either dialysis buffer (DB; Control) or Irisin (4μg/ml) (n=2 biological replicates). (c) Graph displaying qPCR analysis of *Ucp-1* in 3T3L1 fibroblasts after 4 days of adipogenic differentiation in the presence of either DB (Control) or Irisin (0.5μg/ml) (n=3 biological replicates). Error bars represent mean ± SEM. Student's T-test and one-way ANOVA was performed for Figure 3.1b and Figure 3.1c respectively. Significance is indicated with * ($p < 0.05$).

Exercise Regulated	Gene (Symbol)	6h	12h	24h	48h
Upregulated	*Cxcl1*	142.7	153.0	76.8	93.1
	Cd74	2.6	2.7	3.5	3.0
	Nrg1	-	-	1.8	2.9
	Nrp	-	-	-	2.9
	Thbd	1.5	2.0	1.5	2.4
	Gap43	-1.6	-	-	2.3
	Socs3	-	2.1	3.1	2.2
	Ccnd1	2.4	-	-	-1.6
	Tiparp	-	-	2.9	-
	Sod3	2.3	2.4	1.7	-
	Timp1	2.1	1.6	-	1.5
	Mmp10	3.3	-	-	-
	Hp	-	1.8	3.4	-
	Prdx6	-	-1.5	3.3	-
	Ptx3	2.5	5.1	8.9	6.8
Downregulated	*Crispld2*	-1.8	-	-3.0	-3.5
	Cobll1	-	-1.6	-2.6	-
	Irak4	-	-	-1.6	-
	Gpd1l	-	-2.1	-	-
	Pdgfb	-	-	-1.6	-1.6
Satellite Cell Regulation	Gene (Symbol)	6h	12h	24h	48h
Inhibit Differentiation of Satellite Cells	*Heyl*	-2.9	-3.6	-3.1	-3.4
	Ogn	-2.3	-1.5	-1.9	-1.6
	Sox8	-1.5	-2.0	-2.6	-1.6
Skeletal Muscle Regeneration	Gene (Symbol)	6h	12h	24h	48h
Upregulated	*C1s*	1.6	1.6	1.8	3.9
	Ccl2	38.5	40.7	13.2	3.9
	Ccl7	10.4	18.7	7.6	4.9
	Cxcl16	10.6	10.8	7.4	3.2
	Mmp9	22.6	10.6	5.2	-
	Ereg	3.5	-	-	-
	Figf	-1.6	2.6	2.2	1.9
	Mt1	2.9	2.3	1.9	1.7
	Cxcl12	-	2.8	4.3	2.5
	Megf10	-1.6	-1.8	-1.7	-2.0
Downregulated	*Plau*	-1.8	-2.0	-1.6	-

Muscle Growth and Myogenesis	Gene (Symbol)	6h	12h	24h	48h
Hypertrophy and Growth Factors	Sema3f	1.8	-	1.5	1.6
	Il6	6.4	6.7	2.5	3.6
	Il6ra	1.6	-		
	Shq1	2.4	-	-	-
	Il7	2.0	1.5	1.7	2.4
	Serpina3g	17.8	7.1	8.4	7.9
	Tgfbi	-	-	1.7	2.4
	Bmp4	-4.3	1.9	2.6	2.1
	Tnfrsf11b	-	-	2.0	1.7
	Agxt2	-	2.6	3.4	-

Table 3.1: Irisin treatment promotes the expression of pro-myogenic and exercise-related genes in myotubes
Table listing differentially expressed genes, identified through microarray analysis, between myotubes treated with either DB (Control) or Irisin for 6h, 12h, 24h and 48h. Genes have been manually separated into Exercise Regulated, Satellite Cell Regulation, Skeletal Muscle Regeneration and Muscle Growth and Myogenesis categories. Gene symbols and fold changes at each treatment time point are given. Negative numbers reflect fold repression of gene expression. Only genes that were upregulated or downregulated by $\geq$ 1.5-fold were selected.

3.2 Irisin Treatment Induces Transcriptome Changes That Are Consistent with Exercise and Enhanced Myogenesis

To identify gene expression changes induced by Irisin, we performed microarray on RNA isolated from either DB or Irisin treated C2C12 myotubes. Only genes that were upregulated or downregulated by ≥1.5-fold were analyzed for each time point. Of these selected genes, we noted that genes involved in exercise, satellite cell regulation, skeletal muscle regeneration, muscle growth and myogenesis were differentially expressed between DB and Irisin treated myotubes (Table 3.1). A number of target genes identified from the microarray were validated through qPCR. Subsequent qPCR analysis confirmed reduced expression of negative regulators of myogenic differentiation, including *Sox8* (Figure 3.2a) and *HeyL* (Figure 3.2b), following treatment with Irisin. Moreover, exercise-induced and secreted factors, such as *Haptoglobin (Hp)* (Figure 3.2c) and *Interleukin 6* (*IL6*) (Figure 3.2d), which promote skeletal muscle hypertrophy, were significantly upregulated by Irisin treatment. The expression of *Cxcl1*, a chemokine highly expressed in skeletal muscle and secreted during exercise, was elevated at all time points analyzed, with a sharp significant increase in *Cxcl1* noted 6 hours post Irisin treatment (Figure 3.2e). Another exercise-secreted factor, Pentraxin-3 (*Ptx3*) (Figure 3.2f) also showed a marked upregulation at all Irisin treatment time points. Overall, these data reveal that Irisin treatment results in gene expression changes associated with both exercise and improved myogenesis in muscle cells.
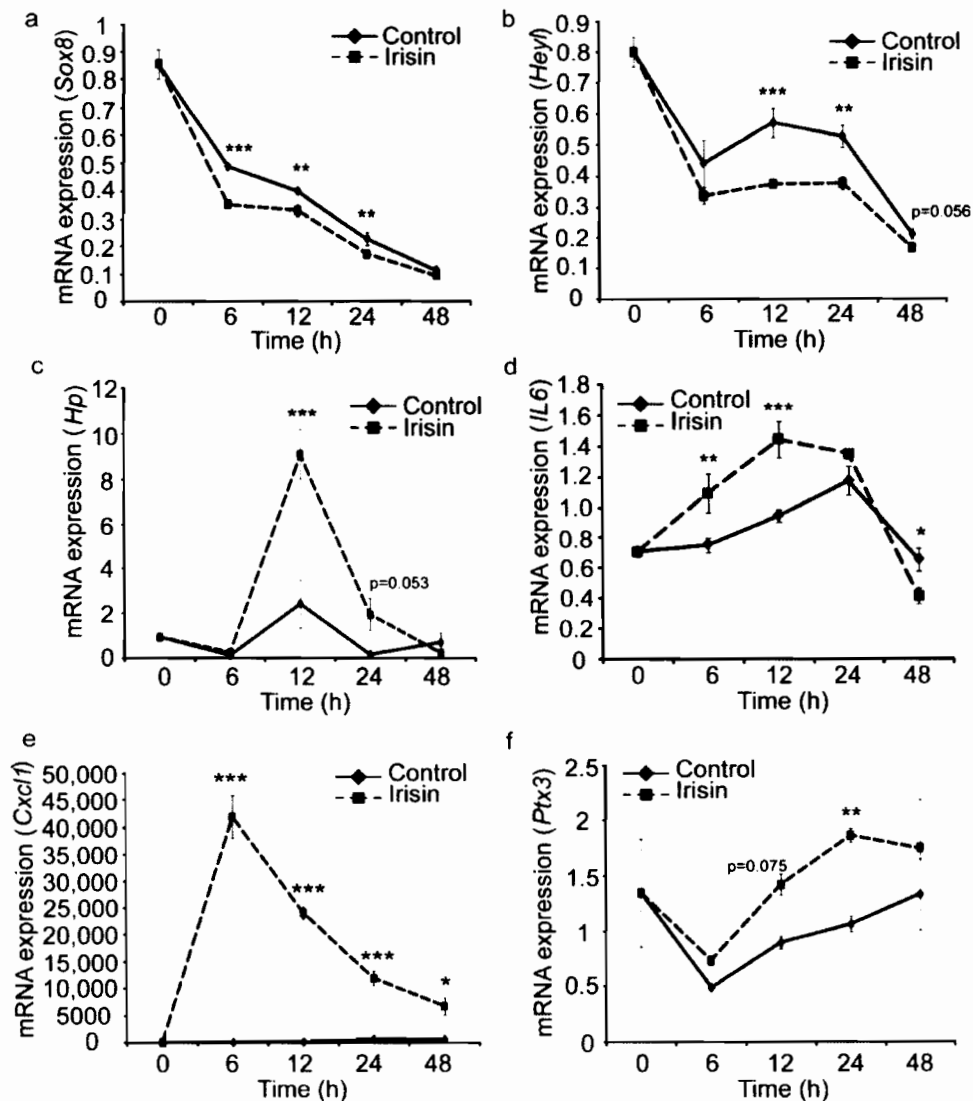
Figure 3.2: Irisin treatment results in gene expression changes consistent with exercise and improved myogenesis

Graphs displaying qPCR analysis of *Sox8* (a), *HeyL* (b), *Hp* (c), *IL6* (d), *Cxcl1* (e) and *Ptx3* (f) in 72h differentiated C2C12 myotubes treated with DB (Control) or recombinant Irisin protein for 0h, 6h, 12h, 24h and 48h. All qPCR graphs show gene expression normalized to *gapdh* (n=3 biological replicates for all figure panels above). Error bars represent mean ± SEM. For all figure, two-way ANOVA was performed and significance is indicated with * ($p < 0.05$), ** ($p < 0.01$) and *** ($p < 0.001$).

92

3.3 Irisin Enhances Myoblast Proliferation and Myoblast Fusion during Myogenic Differentiation

In order to investigate if Irisin enhances myoblast proliferation, a methylene blue photometric end point assay, where the absorbance at 655nm is proportional to myoblast number, was performed. A significant increase in the number of myoblasts at 48h and 72h of proliferation was noted after treatment with Irisin (Figure 3.3a). Moreover, we observed a dose dependent increase in the number of myoblasts at 48h after treatment with increasing concentrations of Irisin (250ng/ml, 1000ng/ml and 2000ng/ml), when compared to DB treated control (Figure 3.3a).

To further investigate the effect of Irisin on myogenesis, differentiating C2C12 myotubes were treated with Irisin. A significant increase in the number of myotubes was noted at both 72h and 96h of differentiation in C2C12 myotubes treated with Irisin, when compared to DB treated controls (Figure 3.3b and 3.3c). The significant increase in myotube number could be due to enhanced fusion. Consistent with this, a significant increase in myoblast fusion index was observed at both 72h and 96h of differentiation following Irisin treatment (Figure 3.3d). We further analyzed the gene expression of fusion markers. Irisin treatment resulted in significantly increased expression of the primary fusion marker, *Myomaker*, at 72h differentiation (Figure 3.3e). Although we observed an increasing trend of the secondary fusion marker, *Caveolin-3* (Figure 3.3f), the increase was not statistically significant. Taken together, these data suggest that Irisin improves myoblast fusion and myogenesis.
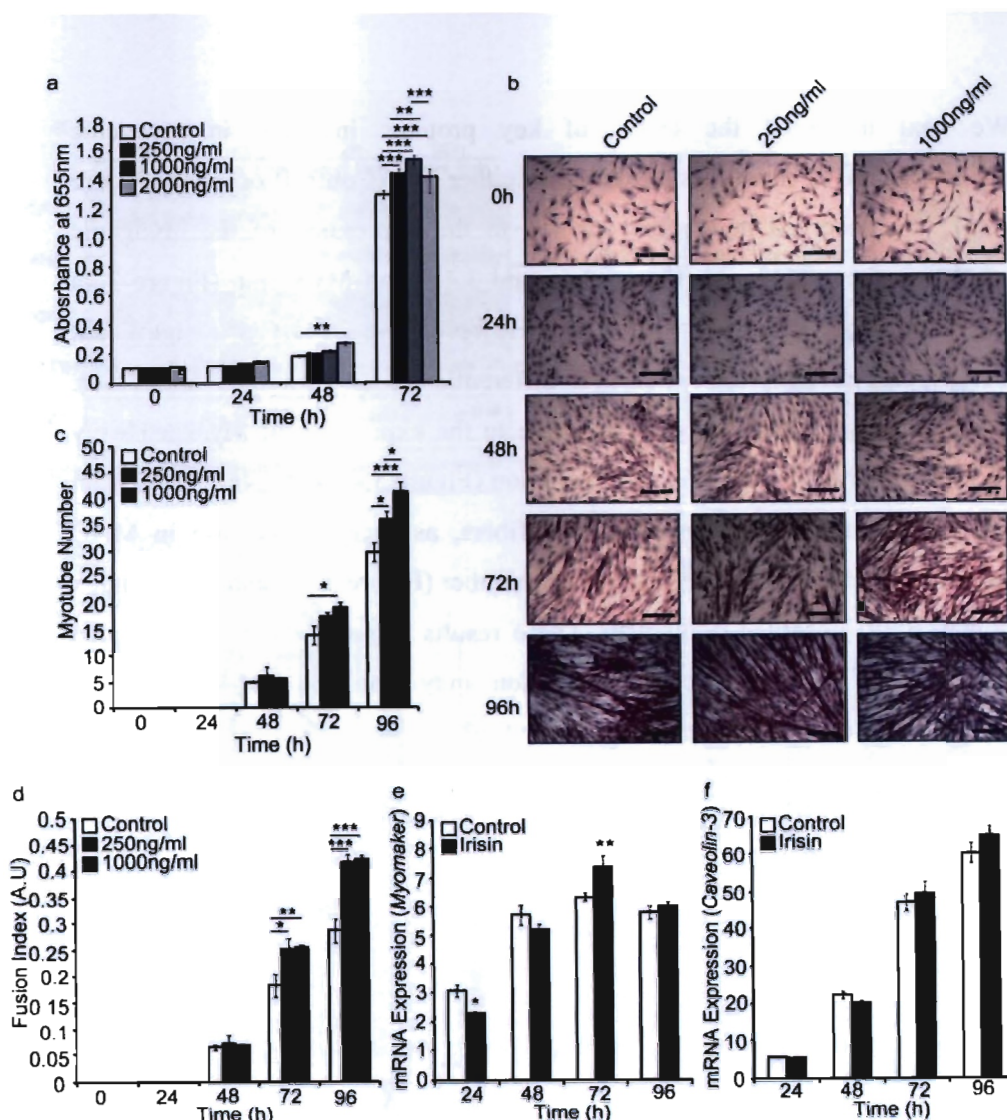
Figure 3.3: Irisin promotes skeletal muscle differentiation by enhancing myoblast fusion

(a) Graph showing absorbance readings of cells treated with DB (Control) or increasing concentrations of Irisin (250ng/ml, 1000ng/ml and 2000ng/ml) at 0h, 24h, 48h and 72h proliferation. Absorbance reading at 655nm is proportional to the number of cells present and hence, indicative of myoblast proliferation (n=16 biological replicates). (b) Representative images of H&E stained myoblasts at 0h, 24h, 48h, 72h and 96h differentiation in the presence of DB (Control) or Irisin (250ng/ml and 1000ng/ml). (c) Graph showing quantification of myotube number at 0h, 24h, 48h, 72h and 96h differentiation in the presence of DB (Control) or Irisin (250ng/ml and 1000ng/ml) (n=3 biological replicates). (d) Graph showing quantification of fusion index at 0h, 24h, 48h, 72h and 96h differentiation in the presence of DB (Control) or Irisin (250ng/ml and 1000ng/ml) (n=3 biological replicates). Graphs displaying qPCR analysis of (e) *Myomaker* and (f) *Caveolin-3* expression normalized to GAPDH in differentiating myoblasts (24h, 48h, 72h and 96h) treated with DB (Control) or Irisin (1000ng/ml) (n=3 biological replicates). Error bars represent mean ± SEM. For all relevant figures, two-way ANOVA was performed and significance is indicated with * ($p < 0.05$), ** ($p < 0.01$) and *** ($p < 0.001$).

94

We next measured the levels of key proteins involved in myogenic differentiation, in myotubes treated with either DB (Control) or Irisin (Figure 3.4a). We observed no distinct change in the expression of the myogenic regulatory factors, MyoD (Figure 3.4a and 3.4b) and Myogenin (Figure 3.4a and 3.4c) after treatment with Irisin. However, we observed a significant increase in p21 expression at 96h differentiation (Figure 3.4a and 3.4d). Importantly, we noted a distinct increase in the expression of Myosin Heavy Chain (MHC) at 72h and 96h differentiation (Figure 3.4a and 3.4e). MHC is an essential contractile protein of muscle fibers, as such an increase in MHC further supports the increase in myotube number (Figure 3.3c) and fusion index (Figure 3.3d) observed previously. These results suggest that Irisin-mediated enhancement of myogenic differentiation may not be due to increased expression of critical myogenic regulatory factors.
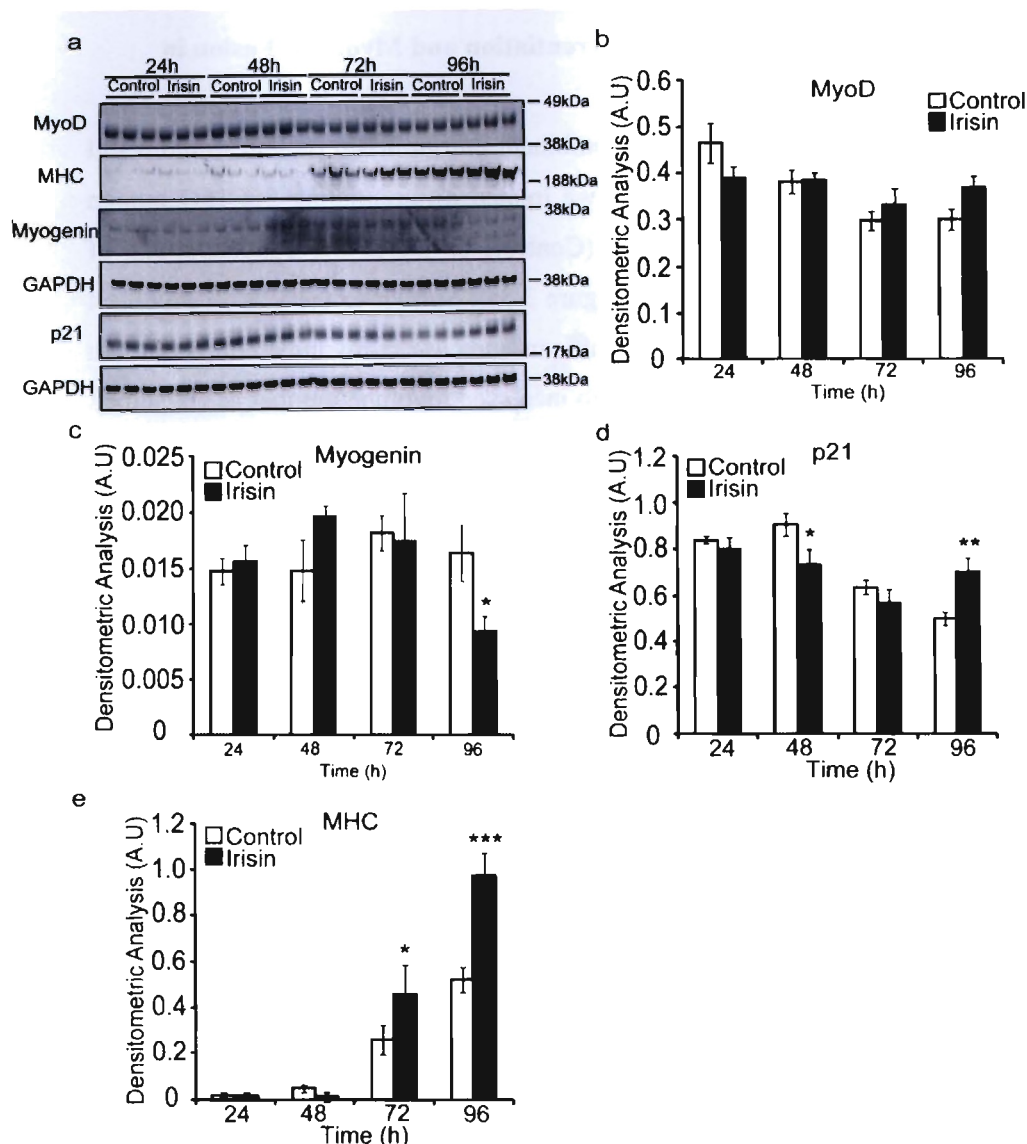
Figure 3.4: Irisin enhances the levels of myosin heavy chain during differentiation

(a) IB analysis of MyoD, MHC, Myogenin and p21 protein levels. The levels of GAPDH were assessed as a loading control. Graphs show densitometric analysis of (b) MyoD, (c) Myogenin (d) p21 and (e) MHC levels in arbitrary units (A.U), normalized to GAPDH. Since MyoD, Myogenin and MHC IB analysis was performed on the same membrane, the same GAPDH was used to normalize the results. All IBs were performed on proteins collected from differentiating myotubes at 24h, 48h, 72h and 96h treated with either DB (Control) or Irisin (1000ng/ml) (n=3 biological replicates for all figure panels above). Error bars represent mean ± SEM. For all relevant figures, two-way ANOVA was performed and significance is indicated with * (p<0.05) and ** (p<0.01).

96

3.4 Irisin Enhances Myogenic Differentiation and Myoblast Fusion in Human Primary Myoblasts

To understand if treatment with recombinant murine Irisin protein would result in a similar phenotype in humans, we treated differentiating 36C15Q human primary myotubes with either DB (Control) or increasing concentrations of Irisin (250ng/ml and 1000ng/ml) (Figure 3.5a). Similar to the C2C12 myoblast differentiation assay, we noted a significant increase in myotube number at 48h and 72h differentiation, with a trend to increased myotube number at 96h, albeit not statistically significant (Figure 3.5b). The fusion index of differentiating myotubes was also enhanced at 48h and the increase became statistically significant at 72h differentiation after Irisin treatment (Figure 3.5c). These data suggest that murine recombinant Irisin protein is able to enhance myogenic differentiation in both mouse and human myotube cultures.
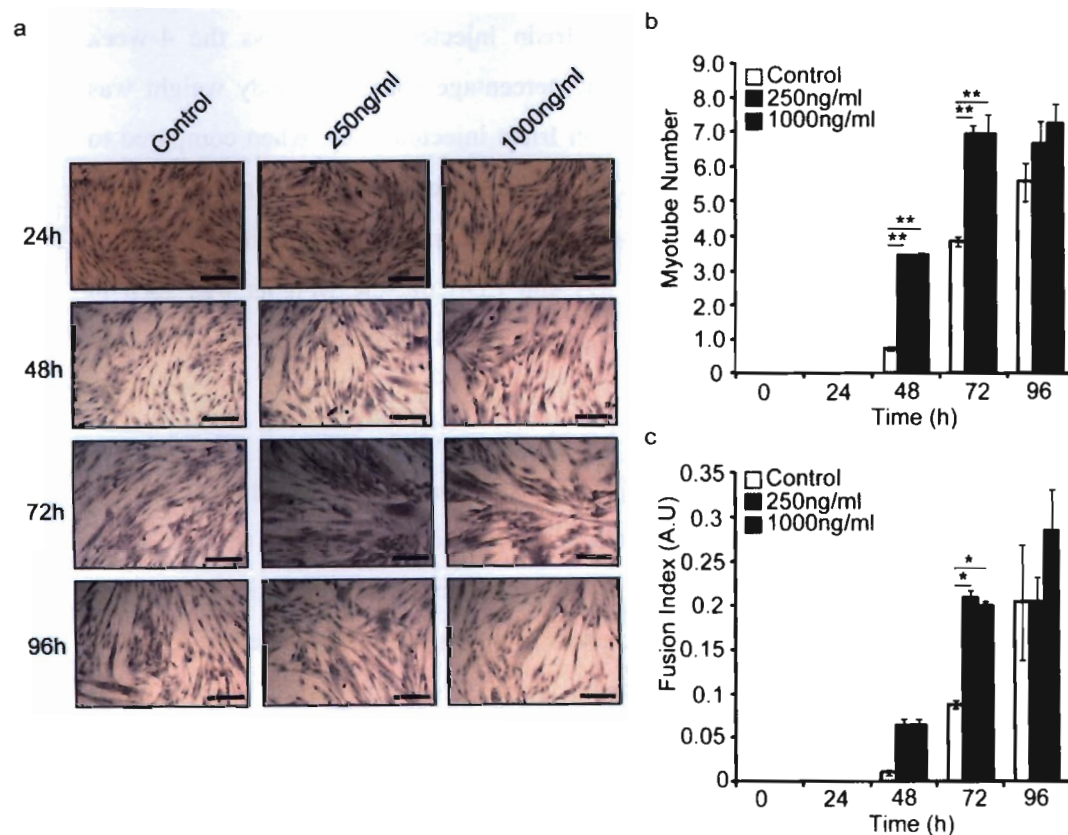
Figure 3.5: Irisin enhances myogenesis in primary human myoblast cultures
(a) Representative images of H&E stained 36C15Q human primary myoblasts at 24h, 48h, 72h and 96h differentiation in the presence of either DB (Control) or Irisin (250ng/ml and 1000ng/ml). (b) Graph showing quantification of myotube number at 0h, 24h, 48h, 72h and 96h differentiation in the presence of either DB (Control) or Irisin (250ng/ml and 1000ng/ml). (c) Graph showing quantification of myotube fusion index at 0h, 24h, 48h, 72h and 96h differentiation in the presence of either DB (Control) or Irisin (250ng/ml and 1000ng/ml) (n=2 biological replicates for all figure panels above). Error bars represent mean ± SEM. For all relevant figures, two-way ANOVA was performed and significance is indicated with * ($p < 0.05$) and ** ($p < 0.01$).

98

3.5 Irisin Injection Increases Muscle Mass, Induces Muscle Hypertrophy and Enhances Grip Strength in Mice

To assess if the pro-myogenic function of Irisin is maintained *in vivo*, we injected 5-week-old C57BL/6J male mice with either DB (Control) or recombinant Irisin protein twice a week, for 4 weeks. As expected, body weights increased in both DB and Irisin injected mice across the 4-week regimen (Figure 3.6a). However, the percentage change in body weight was significantly greater and more rapid in Irisin injected mice, when compared to DB injected controls (Figure 3.6a). We speculated that this increase in body weight could be due to an increase in muscle mass. In agreement with this, a significant increase in Quad, BF, TA and EDL muscle weights was seen in mice injected with Irisin, when compared to DB injected mice (Figures 3.6b and 3.6c).

Measurement of grip strength further indicated that the increased muscle mass translated into enhanced grip strength in mice injected with Irisin (Figure 3.6d). Since Irisin is an exercise-induced hormone, we next analyzed if injecting Irisin promotes hypertrophy of skeletal muscle. Subsequent analysis clearly revealed noticeable hypertrophy of myofibers upon Irisin injection (Figure 3.6e). Moreover, a marked reduction in the number of myofibers with smaller CSA ($<2000\mu m^2$), concomitant with a distinct increase in the number of myofibers with larger CSA ($>2000\mu m^2$), was noted in mice subjected to 4 weeks of Irisin injection, when compared to DB injected mice (Figure 3.6f).

To ensure the increased muscle mass noted upon Irisin injection was specific to the injected Irisin protein, we next performed an *in vivo* trial where mice were injected with either DB (Control) or a His-tag peptide. Unlike the Irisin animal injection trial, we did not observe any significant difference in percentage body weight change between mice injected with either DB or His-tag peptide (Figure 3.7a). Furthermore, there was no significant difference in hind limb skeletal muscle weights between DB and His-tag peptide injected mice (Figure 3.7b and 3.7c). To further confirm that injection of the His-tag peptide had no effect on skeletal muscle fiber size, we performed histological analysis (Figure 3.7d) and quantified the cross-sectional area of TA muscle myofibers from both DB and

His-tag peptide injected mice. Results confirmed no significant difference in myofiber CSA between TA muscles extracted from DB or His-tag peptide injected mice (Figure 3.7d and 3.7e). Collectively, these data confirm that injection of Irisin specifically resulted in the hypertrophy of skeletal muscle observed.
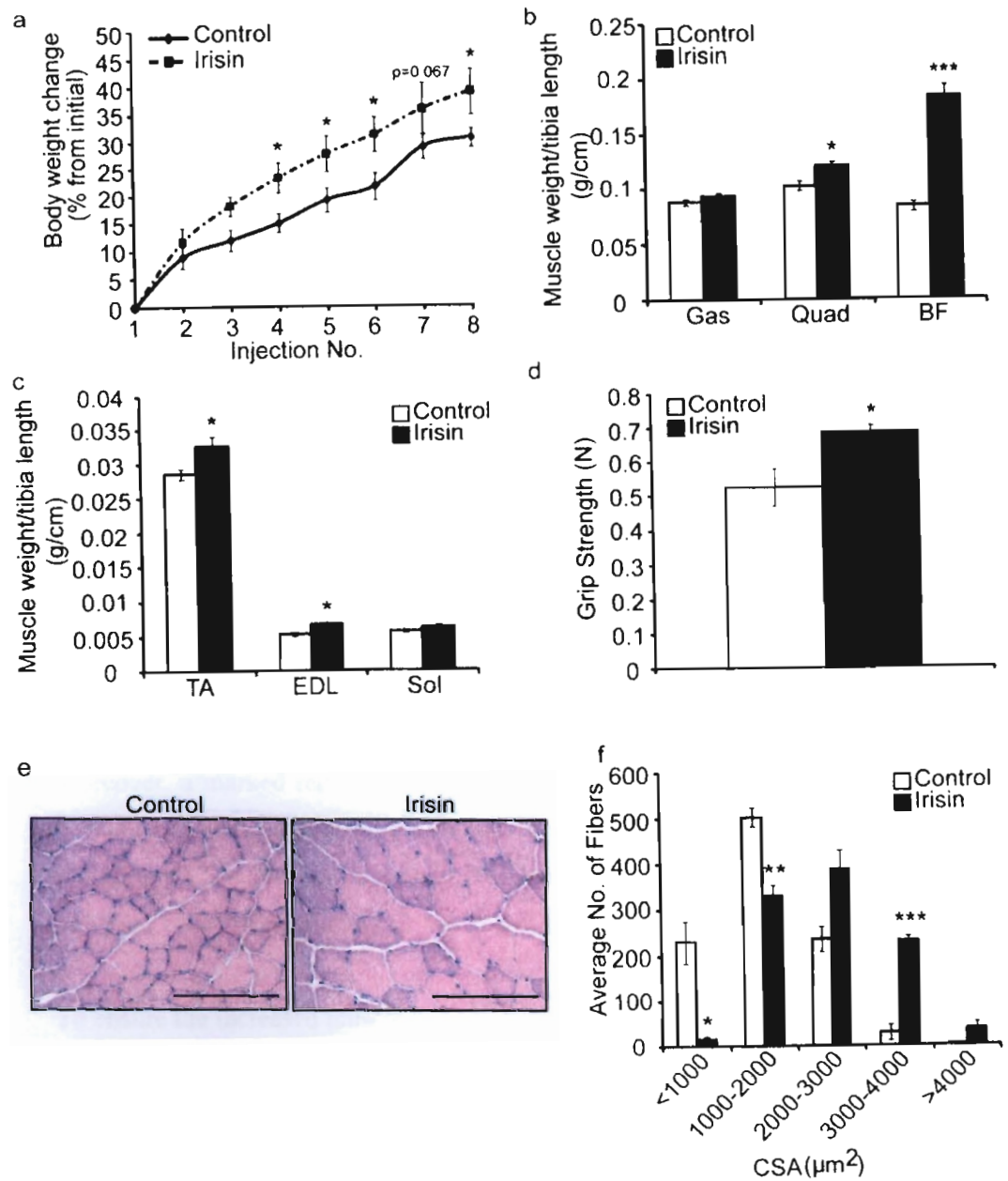
Figure 3.6: Irisin injection results in increased skeletal muscle mass and strength

(a) Graph showing body weight change (% from initial) in mice injected with either DB (Control) or recombinant Irisin protein (2.5µg/g body weight) twice a week for 4 weeks. Body weights were measured prior to each injection. Graphs displaying (b) Gas, Quad, BF and (c) TA, EDL and Sol muscle weights of mice injected with either DB (Control) or Irisin (2.5µg/g body weight) twice a week for 4 weeks. All hind limb muscle weights were normalized to tibia length (d) Graph showing the grip strength of mice (in Newtons; N) injected with either DB (Control) or Irisin (2.5µg/g body weight) twice a week for 4 weeks (n=5 mice for DB injected group and n=4 mice for Irisin injected group for all figure panels above). (e) Representative images of H&E stained TA muscle from mice injected with either DB (Control) or Irisin (2.5µg/g body weight) twice a week for 4 weeks. Images were captured using a 20x objective. Scale bar represents 100µm. (f) Graph showing the distribution of TA myofiber cross sectional area (CSA) in mice injected with either DB (Control) or Irisin (2.5µg/g body weight) twice a week for 4 weeks. (n=3 mice per group). Error bars represent mean ± SEM. Two-way ANOVA was performed in Figure 3.6a and Student's T-test was performed for the remaining relevant figures. Significance is indicated with * ($p<0.05$), ** ($p<0.01$) and *** ($p<0.001$).
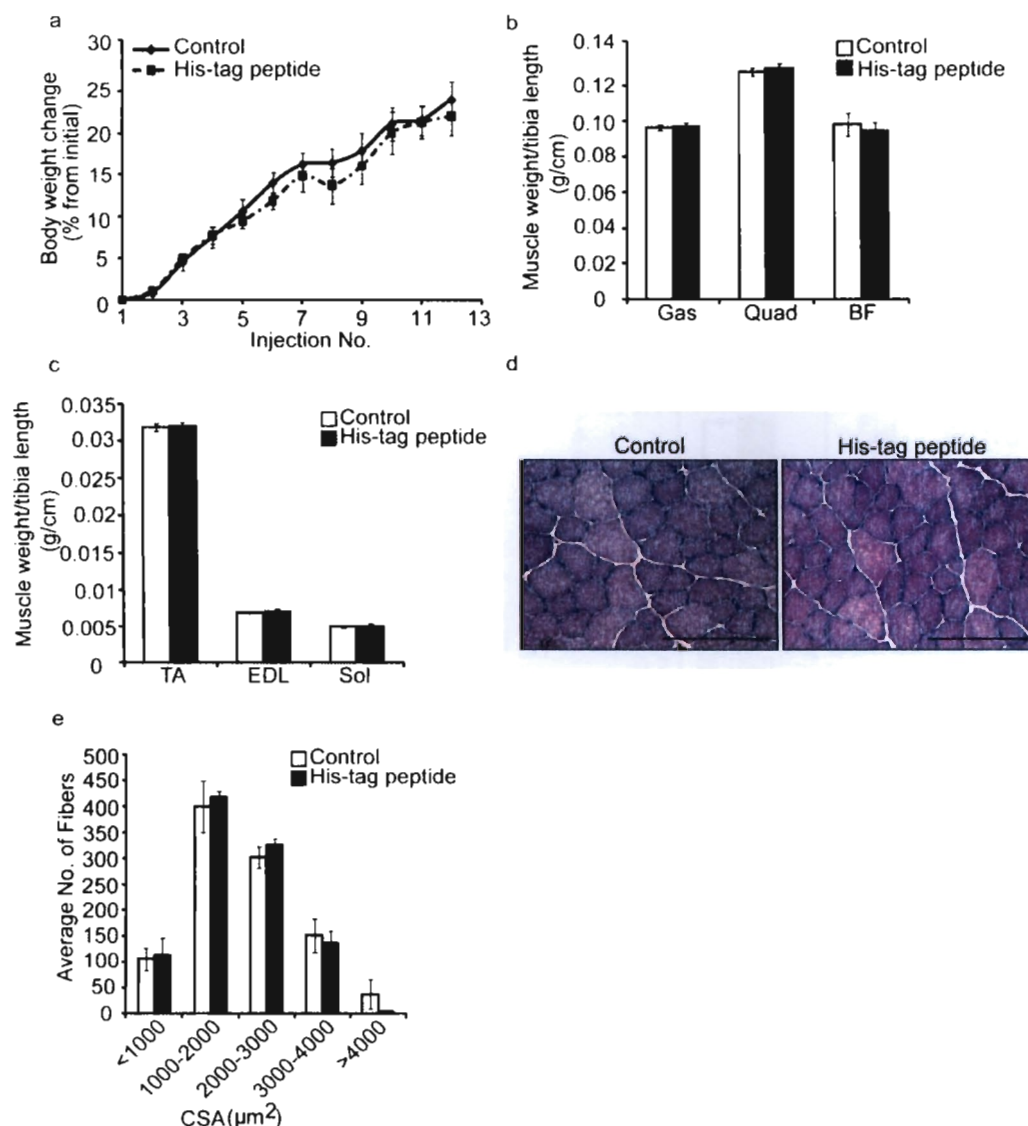
Figure 3.7: Injection of a control His-tag peptide neither increases skeletal muscle mass nor promotes myofiber hypertrophy

(a) Graph showing body weight change (% from initial) in mice injected with either DB (Control) or Histidine-tagged (His-tag) peptide (2.5µg/g body weight) three times-a-week for 4 weeks. Body weights were measured prior to each injection. Graphs displaying (b) Gas, Quad, BF and (c) TA, EDL and Sol muscle weights of mice injected with either DB (Control) or His-tag peptide (2.5µg/g body weight) three times-a-week for 4 weeks. All hind limb muscle weights were normalized to tibia length (n=5 mice for each group). (d) Representative images of H&E stained TA muscle from mice injected with either DB (Control) or His-tag peptide (2.5µg/g body weight) three times-a-week for 4 weeks. Images were captured using a 20x objective. Scale bar represents 100µm. (e) Graph showing the TA myofiber CSA distribution of mice injected with either DB (Control) or His-tag peptide (2.5µg/g body weight) three times-a-week for 4 weeks (n=3 mice per treatment group). Error bars represent mean ± SEM. Two-way ANOVA was performed in Figure 3.7a and Student's T-test was performed for the remaining relevant figures.

We next analyzed the levels of components of three main pathways that activate protein synthesis; Akt, mTOR and Erk1/2, since activation of these pathways have been shown to promote skeletal muscle hypertrophy. Treatment of C2C12 myotubes with recombinant Irisin protein resulted in a significant increase in the levels of p-Akt (Ser473) (Figure 3.8a and 3.8b). As p-Akt in turn activates mTOR, we next analyzed the activity of mTOR by studying the phosphorylation of Raptor. We noted a significant reduction in the phosphorylation of Raptor (Ser792) upon treatment with Irisin (Figure 3.8a and 3.8c), which is indicative of mTOR activation. Irisin treatment also resulted in a significant increase in the levels of active p-Erk1/2 (Figure 3.8a and 3.8d). Taken together these data suggest that Irisin promotes skeletal muscle hypertrophy through activating pathways that promote protein synthesis.

The Akt pathway is closely linked to protein degradation[175], where increased levels of p-Akt have been shown to phosphorylate and inactivate FoxO transcription factors, resulting in reduced expression of the ubiquitin E3 ligases, Atrogin-1 and MuRF-1 and reduced ubiquitin proteasome pathway-mediated protein degradation. Therefore, we next analyzed the levels of p-FoxO1, Atrogin-1 and MuRF-1 in Irisin treated myotubes. Subsequent analysis revealed increased levels of inactive p-FoxO1 following treatment with recombinant Irisin protein (Figure 3.8e and 3.8f). Although the increase in the level of p-FoxO1 was not statistically significant, we observed a significant reduction in the levels of both Atrogin-1 (Figure 3.8e and 3.8g) and MuRF-1 (Figure 3.8e and 3.8h) following Irisin treatment. These data reveal that Irisin not only activates anabolic pathways but may also reduce catabolic pathways in skeletal muscle, which we suggest would contribute to the hypertrophy of skeletal muscle observed.
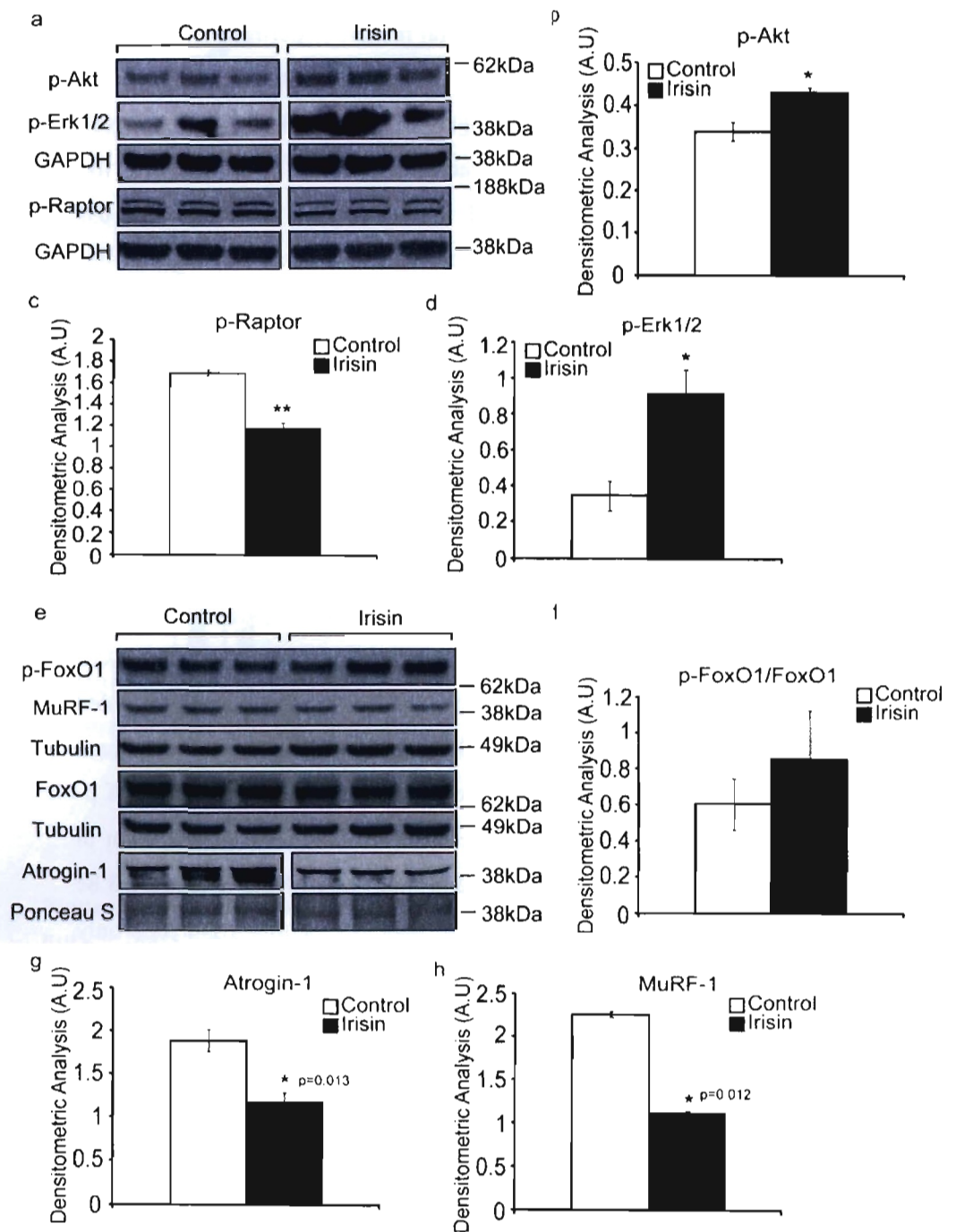
Figure 3.8: Irisin treatment activates protein synthesis pathways and reduces protein degradation

(a) IB analysis of p-Akt, p-Raptor and p-Erk1/2 protein levels. The levels of GAPDH were assessed as a loading control. Graphs show densitometric analysis of p-Akt (b), p-Raptor (c) and p-Erk1/2 (d) levels in arbitrary units (A.U), normalized to GAPDH. Since p-Akt and p-Erk1/2 IB analysis was performed on the same membrane, the same GAPDH was used to normalize the results. (e) IB analysis of FoxO1, p-FoxO1, Atrogin-1 and MuRF-1 protein levels. The levels of either Tubulin or Ponceau S were assessed as loading controls. Graphs show densitometric analysis of p-FoxO1 levels normalized to total FoxO1 (p-FoxO1/FoxO1) (f), Atrogin-1 (g) and MuRF-1 (h) levels in arbitrary units (A.U), normalized to either Tubulin or Ponceau S. Since p-FoxO1 and MuRF-1 IB analysis was performed on the same membrane, the same Tubulin was used to normalize the results. All IBs were performed on proteins collected from 72h-differentiated myotubes treated with either DB (Control) or Irisin (1000ng/ml) for a further 48h. Wherever necessary, intervening irrelevant bands were removed from the IBs, which is denoted by a gap between boxes in the figures (n=3 biological replicates for all figure panels above). Error bars represent mean $\pm$ SEM. For all relevant figures, Student's T-test was performed. Significance is indicated with * ($p<0.05$) and ** ($p<0.01$).

106
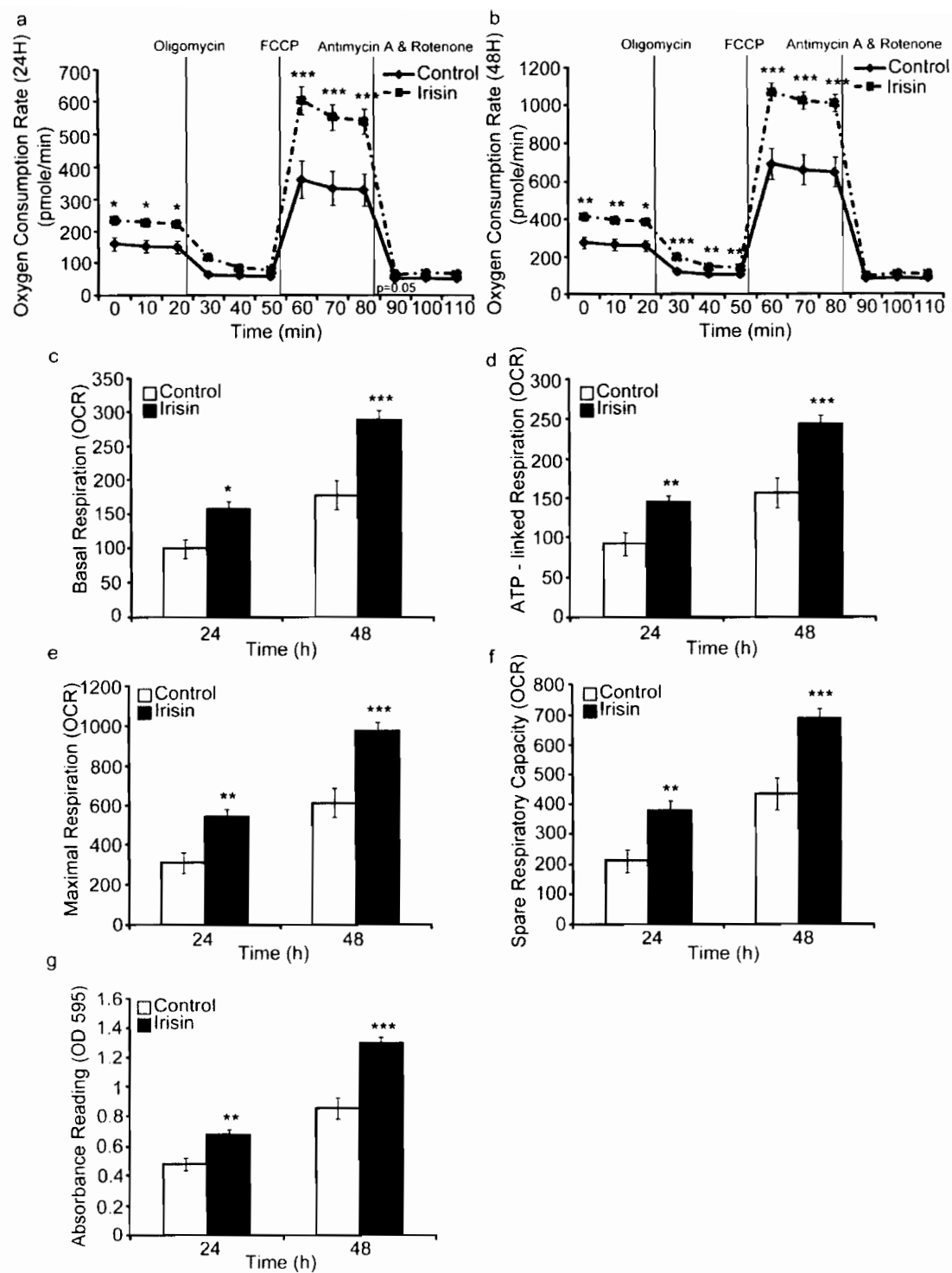
Figure 3.9: Irisin treatment improves mitochondrial function in myotube cultures

(a-b) Graphs displaying mitochondrial oxygen consumption rate (OCR) (pmole/min). OCR was measured at the basal state and in response sequential injection of Oligomycin, FCCP and Antimycin A/Rotenone in 72h differentiated myotubes treated with either DB (Control) or Irisin (1000ng/ml) for a further 24h (a) and 48h (b). Mitochondrial respiration was measured by the XF^e24 Extracellular Flux Analyzer (Seahorse Bioscience). Graphs showing (c) Basal respiration, (d) ATP-linked respiration, (e) Maximal respiration and (f) Spare respiratory capacity are shown. (g) Graph displaying the average total protein content of DB (Control) and Irisin treated 72h differentiated myotube samples used for the OCR assessment above (n=10 biological replicates for all figure panels above). Error bars represent mean ± SEM. For all relevant figures, two-way ANOVA was performed. Significance is indicated with * ($p < 0.05$), ** ($p < 0.01$) and *** ($p < 0.001$).

3.6 Irisin Treatment Results in Improved Mitochondrial Oxygen Consumption, Primarily Due to Increased Myogenic Differentiation

It is known that exercise improves respiratory capacity and increases the production of adenosine triphosphate (ATP). Hence, we treated myotubes with either DB or Irisin and assessed mitochondrial oxygen consumption rate (OCR). Measurement of OCR was measured at the basal state and over time in response to sequential injection of Oligomycin, FCCP and Antimycin A/Rotenone, which allows us to measure ATP-linked respiration, maximum respiration and non-mitochondrial respiration, respectively. Results revealed that Irisin treatment led to increased OCR at both 24h (Figure 3.9a) and 48h (Figure 3.9b) treatment time points. Specifically, our results reveal that Irisin treatment significantly improved Basal respiration (Figure 3.9c), ATP-linked respiration (Figure 3.9d), Maximal respiration (Figure 3.9e) and Spare respiratory capacity (Figure 3.9f), which measures the ability of the cell to respond when there is increased demand for energy. It is important to mention that, consistent with increased myogenic differentiation and hypertrophy, we observed increased total protein content in Irisin treated myotube cultures, when compared to DB treated controls (Figure 3.9g). As such, upon normalization of OCR to total cell protein content, although a trend to enhanced mitochondrial OCR was maintained, the increase was no longer statistically significant. Taken together these data suggest that the enhanced mitochondrial OCR noted upon Irisin treatment may be secondary to the enhanced myogenic differentiation and hypertrophy observed.

3.7 Irisin Signals via the IL6 Pathway during Myogenesis

Treatment with recombinant Irisin induced *IL6* expression in myotubes (Table 3.1 and Figure 3.2d), increased myoblast proliferation (Figure 3.3a) and enhanced myogenic differentiation (Figure 3.3b-3.3d). Since it has been previously reported that IL6 expression is induced during myogenic differentiation[112] and that IL6 regulates myoblast proliferation[111], we proposed that Irisin may signal via IL6 to promote increased myoblast proliferation and differentiation. In order to investigate this hypothesis, we treated proliferating myoblasts with either DB (Control) or Irisin for 24h, 48h and 72h. Gene expression analysis revealed that Irisin treatment resulted in a significant increase in *IL6*, after 24h of treatment (Figure 3.10a). Consistent with this result, we also observed a significant increase in the expression of *Stat3*, a downstream target of IL6, after 24h of Irisin treatment (Figure 3.10b). Socs3, a negative regulator of the IL6 pathway, is known to be upregulated after IL6 activation[176]. Consistent with this, we observed increased *Socs3* expression at 24h, 48h and 72h of proliferation in response to Irisin treatment (Figure 3.10c).

In order to investigate if Irisin induces the IL6 pathway during myogenic differentiation, differentiating myotubes were treated with either DB (Control) or Irisin and gene expression was analyzed. Subsequent qPCR analysis confirmed Irisin regulation of *IL6*, with increased *IL6* expression noted over a treatment time course (Figure 3.10d). Interestingly, we observed no distinct increase in the expression of *Stat3* during differentiation although a trend of increased *Stat3* expression was noted (Figure 3.10e). However, we did observe a marked increase in *Socs3* expression in response to 24h of Irisin treatment (Figure 3.10f).
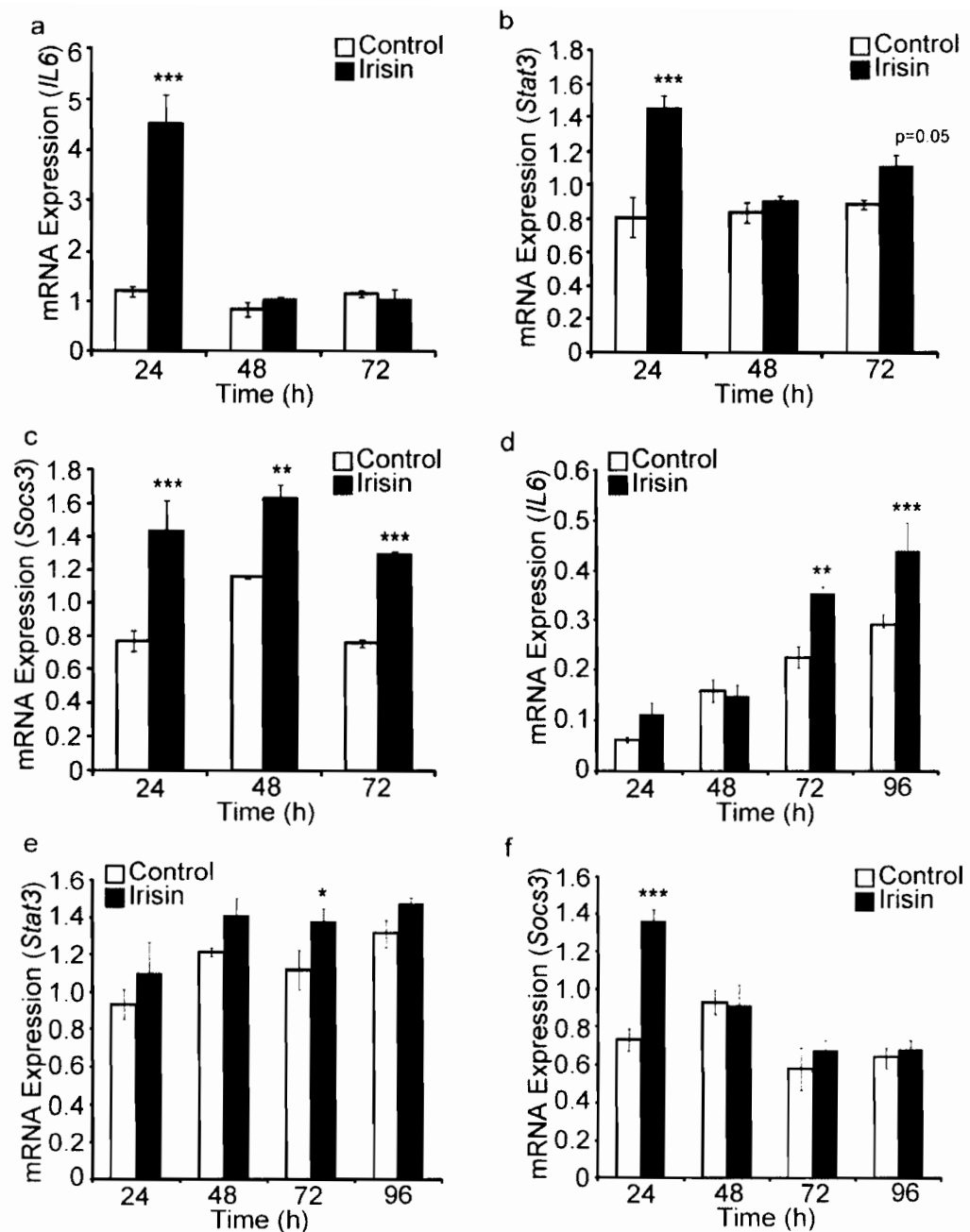
Figure 3.10: Irisin treatment activates the IL6 pathway

Graphs displaying qPCR analysis of *IL6* (a), *Stat3* (b) and *Socs3* (c) in 24h, 48h and 72h proliferating myoblasts treated with either DB (Control) or Irisin (1000ng/ml). Graphs displaying qPCR analysis of *IL6* (d), *Stat3* (e) and *Socs3* (f) in 24h, 48h, 72h and 96h differentiating myoblasts treated with either DB (Control) or Irisin (n=3 biological replicates for all figure panels above). Error bars represent mean ± SEM. Two-way ANOVA was performed for all figure panels. Significance is indicated with * ($p<0.05$), ** ($p<0.01$) and *** ($p<0.001$).

To further probe the involvement of IL6 in Irisin signaling, we knocked down *IL6* in differentiating myoblasts and queried if Irisin is effective in enhancing myogenesis in the absence of *IL6*. Treatment with *IL6* specific siRNA (*IL6-siRNA*), but not control scrambled siRNA (scramb-siRNA) was indeed very effective in reducing (~80% down regulation) *IL6* mRNA expression at 48h differentiation (Figure 3.11a). While Irisin treatment induced significant expression of *IL6* in scramb-siRNA transfected myotubes at 48h differentiation, a significant inhibition in Irisin-mediated induction of *IL6* was observed in the presence of *IL6*-specific siRNA (Figure 3.11a).

To further validate the role of IL6 in the Irisin signaling pathway, we performed histological analysis (Figure 3.11b) and assessed the differentiation potential of myoblasts transfected with either control scramb-siRNA or *IL6*-siRNA and treated with either DB (Control) or Irisin for 72h. Both myotube fusion index and myotube number was significantly increased in scramb-siRNA transfected myotubes treated with Irisin, when compared to DB treated, scramb-siRNA transfected, myotubes (Figure 3.11c and 3.11d) which is consistent with results presented earlier (see Figure 3.3c and 3.3d). In contrast, knockdown of *IL6* in myotubes resulted in impaired differentiation and hence, a reduction in fusion index (Figure 3.11c) and myotube number (Figure 3.11d) was noted in DB treated, *IL6*-siRNA transfected, myotubes. Importantly, a significant reduction in myotube fusion index (Figure 3.11c) and myotube number (Figure 3.11d) was also observed in Irisin treated, *IL6*-siRNA transfected, myotubes, which was comparable to the reduction noted in DB treated, *IL6*-siRNA transfected, myotubes. Thus, these data suggest that Irisin may, at least in part, signal through IL6 to enhance myoblast proliferation and differentiation and resulting skeletal muscle hypertrophy.
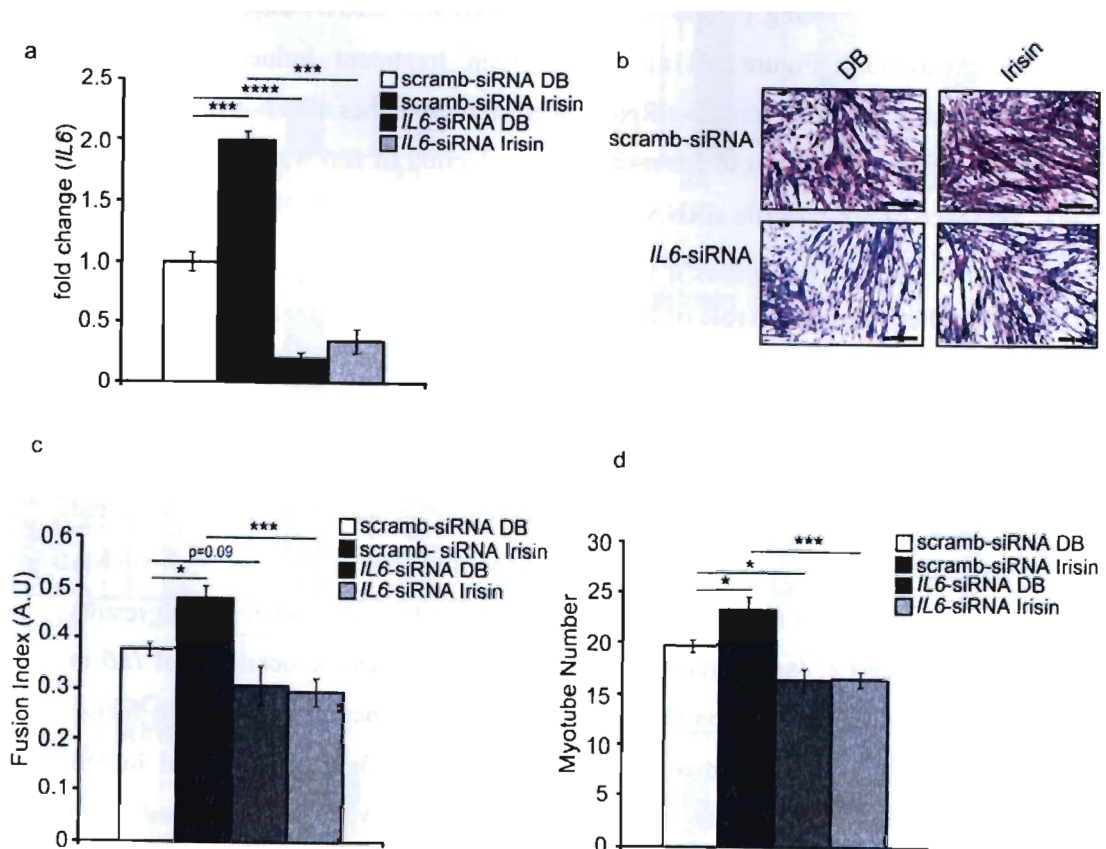
Figure 3.11: Irisin signals through IL6 to regulate myogenesis
(a) Graph displaying qPCR analysis of *IL6* in 48h differentiated DB (Control) or Irisin treated myoblasts transfected with either scrambled siRNA (scramb-siRNA) or *IL6*-specific siRNA (*IL6*-siRNA). All qPCR gene expression results were normalized to *gapdh*. (b) Representative images of H&E stained scramb-siRNA and *IL6* knockdown (*IL6*-siRNA) transfected myoblasts differentiated for 72h in the presence of either DB (Control) or Irisin (1000ng/ml). Graphs showing quantification of myotube fusion index (c) and myotube number (d) in scramb-siRNA and *IL6*-siRNA transfected myoblasts differentiated for 72h in the presence of either DB (Control) or Irisin (1000ng/ml) (n=3 biological replicates for all figure panels above). Error bars represent mean ± SEM. For all relevant figures, two-way ANOVA was performed. Significance is indicated with * (p<0.05) and *** (p<0.001).

3.8 Irisin Promotes Satellite Cell Activation and Expansion during Skeletal Muscle Regeneration

We next tested the efficacy of Irisin in improving skeletal muscle regeneration. Wild type mice were injected with either DB or recombinant Irisin protein one week prior to Notexin-induced injury and three times-a-week for a further period of 1, 2, 3 and 10 days post-injury. Subsequent immunohistochemical analysis of MyoD (a marker of activated satellite cells) revealed increased percentage of MyoD positive cells on Day 2 (Figure 3.12a and 3.12b) and Day 3 (Figure 3.12c and 3.12d) post-Notexin-induced injury in mice injected with Irisin, when compared to DB-injected controls. These data suggest that Irisin treatment resulted in greater influx and/or activation of Satellite cells, which would result in higher numbers of proliferating MyoD positive myoblasts.

To assess if Irisin directly activates satellite cells, primary murine satellite cells were cultured, treated with recombinant Irisin protein and subjected to immunocytochemistry to assess the populations of cells positive for Pax7 and MyoD (Figure 3.13a). The percentages of Pax7$^+$/MyoD$^-$ (quiescent Satellite cells), Pax7$^+$/MyoD$^+$ (proliferating myoblasts) and Pax7$^-$/MyoD$^+$ (committed myoblasts) cells were assessed in cultures treated with either DB or recombinant Irisin protein (Figure 3.13a). Treatment with Irisin resulted in a marked reduction in the percentage of quiescent Satellite cells (Pax7$^+$/MyoD$^-$) (Figure 3.13b), concomitant with an increase in the percentages of proliferating (Pax7$^+$/MyoD$^+$) (Figure 3.13c) and committed myoblasts (Pax7$^-$/MyoD$^+$) (Figure 3.13d). These data suggest that Irisin treatment leads to increased Satellite cell activation and proliferation.
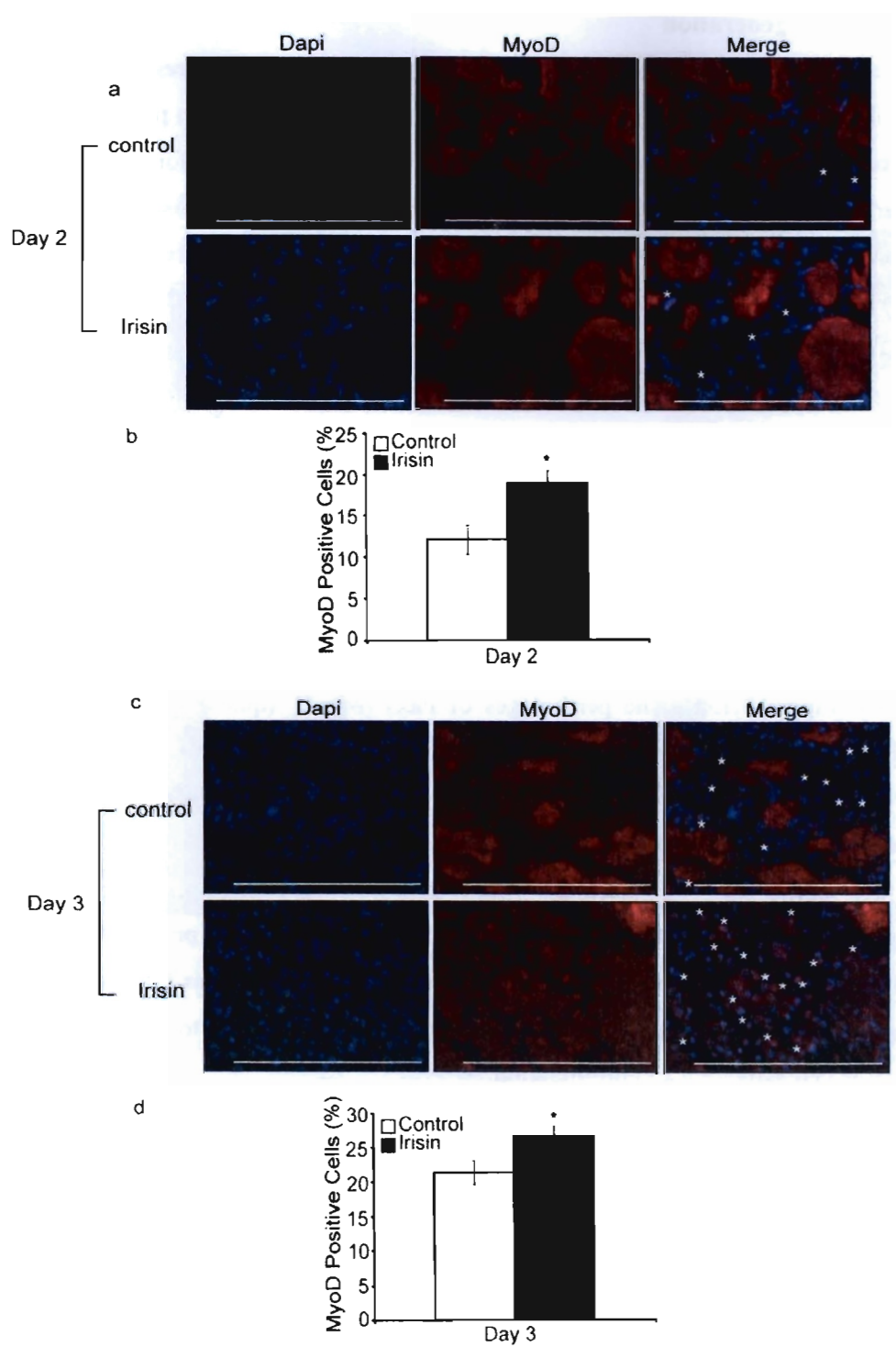
Figure 3.12: Irisin promotes activation of satellite cells in regenerating skeletal muscle

(a) Representative images of MyoD immunostaining of TA muscle sections from DB (Control) or Irisin injected mice at day 2 post-Notexin injury. Images were captured using a 40x objective. Scale bar represents 100μm. Nuclei were counterstained with DAPI. White asterisks denote representative MyoD positive cells. Linear brightness and contrast of the 'Merge' panel was adjusted to visualize MyoD$^+$ cells. This linear adjustment did not in any way alter interpretation of the results. (b) Graph displaying the percentage of MyoD positive cells in TA muscle sections from DB (Control) or Irisin injected mice at day 2 (n=3 mice for both groups) post-Notexin injury. (c) Representative images of MyoD immunostaining of TA muscle sections from DB (Control) or Irisin injected mice at day 3 post-Notexin injury. Images were captured using a 40x objective. Scale bar represents 100μm. Nuclei were counterstained with DAPI. White asterisks denote representative MyoD positive cells. Linear brightness and contrast of the 'Merge' panel was adjusted to visualize MyoD$^+$ cells. This linear adjustment did not in any way alter interpretation of the results. (b) Graph displaying the percentage of MyoD positive cells in TA muscle sections from DB (Control) or Irisin injected mice at day 3 (n=2 mice for control group and n=3 mice for Irisin injected group) post-Notexin injury. Error bars represent mean ± SEM. For all relevant figure panels, Student's T-test was performed. Significance is indicated with * ($p < 0.05$).
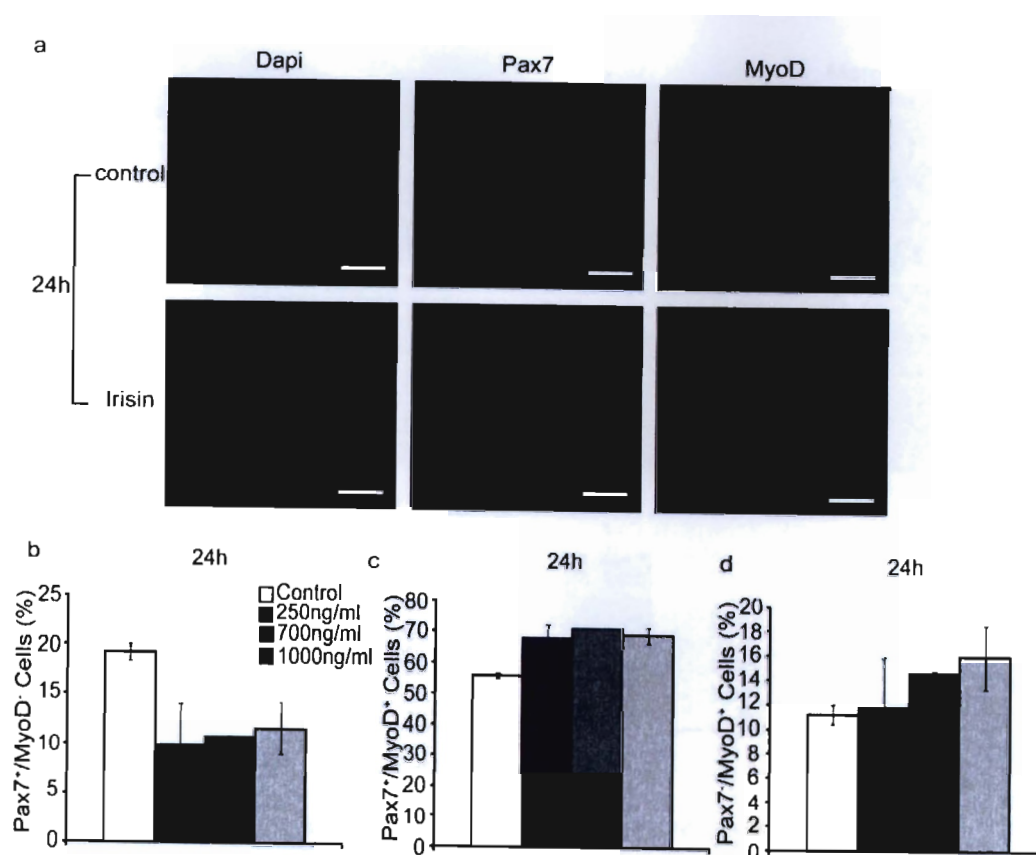
Figure 3.13: Irisin treatment activates satellite cells *in vitro*

(a) Representative images of MyoD and Pax7 immunostaining of primary satellite cell cultures treated with either DB (Control) or Irisin (1000ng/ml) for 24h. Linear brightness and contrast of 'Dapi', 'Pax7' and 'MyoD' panels was adjusted to visualize the positively stained nuclei. This linear adjustment did not in any way alter interpretation of the results. Images were captured using a 10x objective. Scale bar represents 100μm. Graphs displaying the percentage of (b) quiescent (Pax7^{+}/MyoD^{-}), (c) proliferating (Pax7^{+}/MyoD^{+}) and (d) committed (/Pax7^{-}/MyoD^{+}) satellite cells present following treatment with either DB (Control) or increasing concentrations of Irisin (250ng/ml, 700ng/ml and 1000ng/ml) for 24h (n=2 biological replicates for all figure panels above). Error bars represent mean ± SEM. For all relevant figures, one-way ANOVA was performed.

3.9 Irisin Injection Leads to Hypertrophy and Increased Fusion during Skeletal Muscle Regeneration

Next we assessed the effect of Irisin treatment on resulting muscle fibre size and centrally formed nuclei in regenerated skeletal muscle. Subsequent analysis of muscle fiber CSA revealed more myofibers with larger ($>1500\mu m^2$) CSA, concomitant with a reduction in myofibers with smaller ($<1500\mu m^2$) CSA in regenerated muscle subjected to Irisin injection, when compared to DB-injected controls (Figure 3.14a and 3.14b), thus confirming that Irisin injection leads to hypertrophy of skeletal muscle. Consistent with the hypertrophy phenotype seen in the regenerated skeletal muscle, and with the enhanced fusion noted previously (Figure 3.3b and 3.3d), we observed an increase in the percentage of regenerated myofibers that contained two centrally formed nuclei, with a concomitant decrease in the percentage of myofibers with one centrally formed nuclei, in mice injected with recombinant Irisin protein (Figure 3.14c). Centrally placed nuclei is a hallmark of regenerated muscle fibers and indicative of activated myoblast fusion. Hence, these data suggest that Irisin treatment leads to enhanced fusion of satellite cells to myofibers during skeletal muscle regeneration *in vivo*.
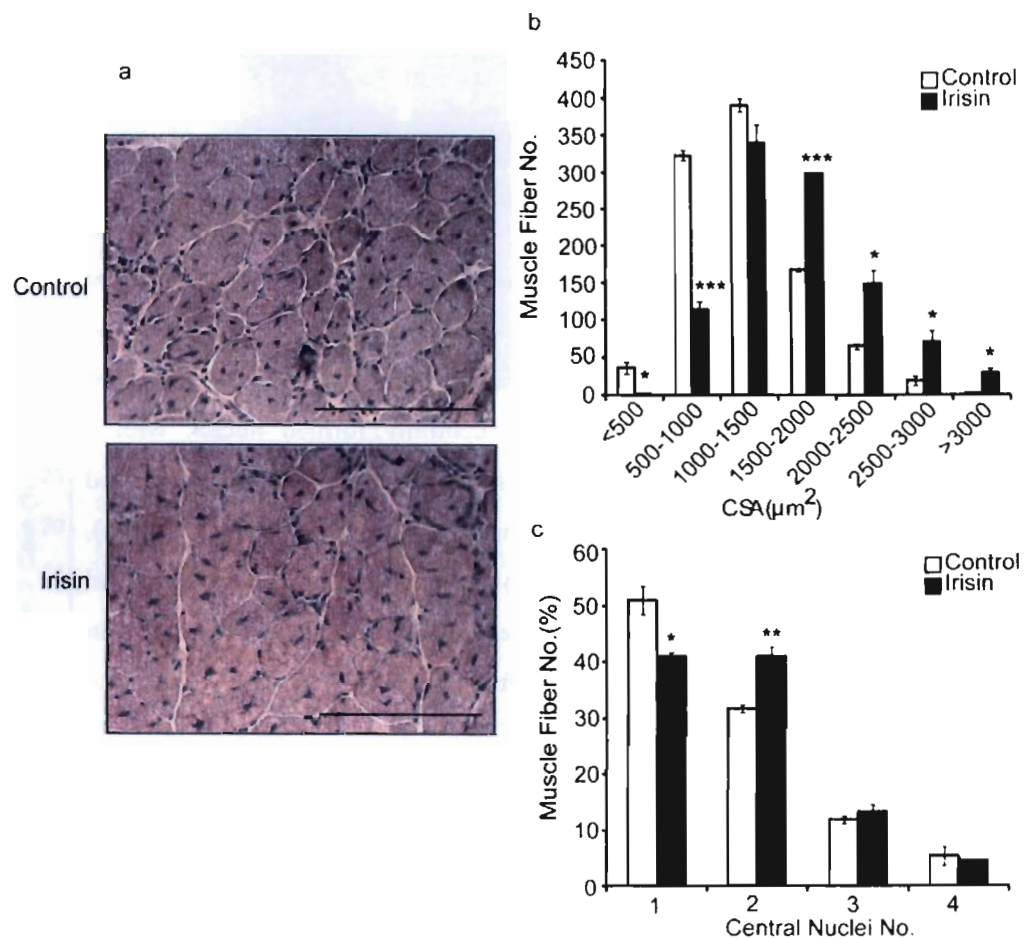
Figure 3.14: Irisin improves regeneration of Notexin-injured skeletal muscle
(a) Representative images of H&E stained TA muscle at day 10 post Notexin-injury from mice injected with either DB (Control) or Irisin (2.5µg/g of body weight). Images were captured using a 20x objective. Scale bar represents 100µm. Graphs showing the distribution of TA myofiber cross-sectional area (CSA) (b) and the percentage of myofibers with 1, 2, 3, or 4 centrally placed nuclei (c), at day 10 post Notexin-injury from mice injected with either DB (Control) or Irisin (2.5µg/g of body weight) (n=3 mice for both groups). Error bars represent mean ± SEM. For all relevant figure panels, Student's T-test was performed. Significance is indicated with * (p<0.05) and *** (p<0.001).

3.10 Irisin Rescues Denervation-induced Atrophy

To investigate the role of Irisin during skeletal muscle atrophy, we utilized a model of denervation-induced atrophy. Mice were pre-injected for one week with DB or Irisin prior to sciatic nerve transection. Mice were further injected with either DB or Irisin for an additional two weeks post-injury. We observed a significant increase in the average body weight of Irisin injected mice at the initial stage (Figure 3.15a). Overall, mice injected with Irisin showed a greater percentage increase in body weight (~13.7%), when compared to DB-injected mice (~12.2%) during the trial (Figure 3.15b). However, this difference was not statistically significant. Comparison of muscle weights revealed a significant increase in denervated Gas ($p<0.01$) and Sol ($p<0.05$) muscle weights (Figure 3.15c) upon Irisin injection. We also noted an increase in denervated TA muscle weights after Irisin injection, although the increase was not statistically significant. A significant increase in denervated skeletal muscle mass following Irisin injection suggests that Irisin may have an important role in rescuing skeletal muscle atrophy.

We next performed histological analysis to quantify myofiber CSA in non-denervated and denervated TA muscle from Control (DB) and Irisin-injected mice (Figure 3.15d). Subsequent analysis of myofiber CSA confirmed that Irisin injection leads to hypertrophy of skeletal muscle fibers (Figure 3.15e and 3.15f). Consistent with induction of atrophy, denervation leads to reduced myofiber CSA (Figure 3.15e and 3.15f). Due to sciatic nerve transection a considerable increase in the number of smaller muscle fibres ($<1000\mu m^2$), concomitant with a decrease in larger muscle fibres ($>1500\mu m^2$) was observed in TA muscles of denervated DB-injected control mice (Figure 3.15e and 3.15f). Consistent with the increase in muscle weights observed in Irisin injected mice (Figure 3.15c), we noted an increase in the numbers of larger muscle fibres ($>1000\mu m^2$), with a concomitant decrease in smaller fibres ($<1000\mu m^2$), in Irisin injected denervated mice, when compared to denervated DB-injected controls (Figure 3.15e and 3.15f). In agreement with this, the average TA muscle CSA of Irisin injected denervated mice was significantly ($p<0.01$) increased, when compared to DB injected denervated control mice (Figure 3.15g).

120
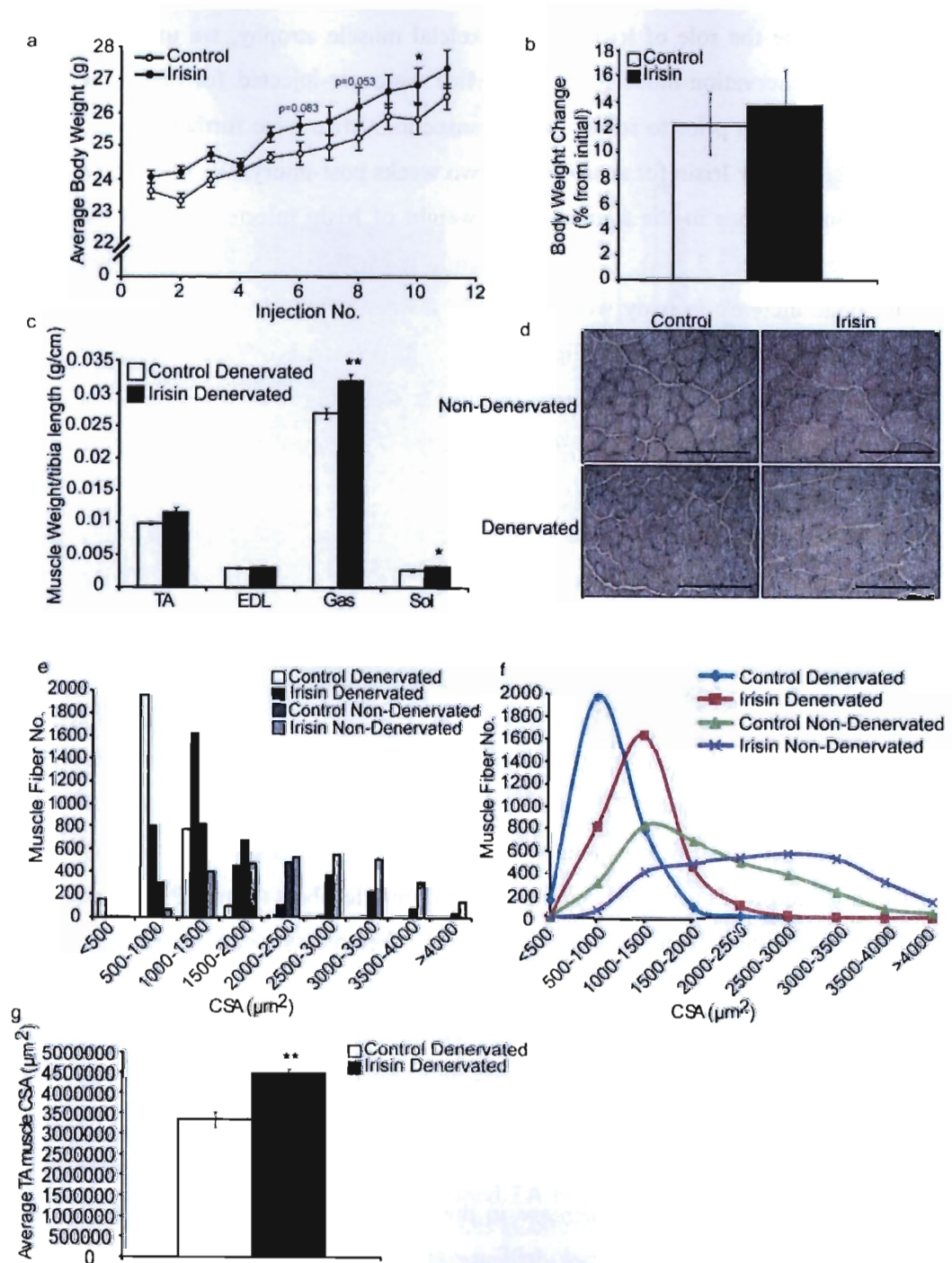
Figure 3.15: Irisin rescues denervation-induced loss of muscle mass
(a) Graph showing average body weight (g) of mice injected with either DB (Control) or Irisin (2.5µg/g body weight) three times-a-week, 1 week prior to, and 2 weeks post-transection of the sciatic nerve. Body weights were measured prior to each injection. (b) Graph showing the percentage change in body weight (from initial) in mice injected with either DB (Control) or Irisin pre- and post-sciatic nerve transection (n=6 mice for both groups for all figure panels above) (c) Graph displaying average weights of denervated TA, EDL, Gas and Sol muscles of mice injected with either DB (Control) or recombinant Irisin protein pre- and post-sciatic nerve transection. All hind limb muscle weights were normalized to tibia length (n=5 mice for DB injected group and n=6 mice for Irisin injected group). (d) Representative images of H&E stained non-denervated and denervated TA muscle from mice injected with either DB (Control) or Irisin. Images were captured using a 20X objective. Scale bar represents 100µm. (e) Histogram and (f) line graph showing the distribution of non-denervated and denervated TA myofiber CSA in mice injected with either DB (Control) or Irisin. (g) Graph displaying the average total CSA of denervated TA muscles from mice injected with either DB (Control) or Irisin (n=3 mice for both groups). Error bars represent mean ± SEM. Two-way ANOVA was performed for Figure 3.15a and Student's T-test was performed for Figures 3.15b, 3.15c and 3.15g. Significance is indicated with * ($p<0.05$) and ** ($p<0.01$).
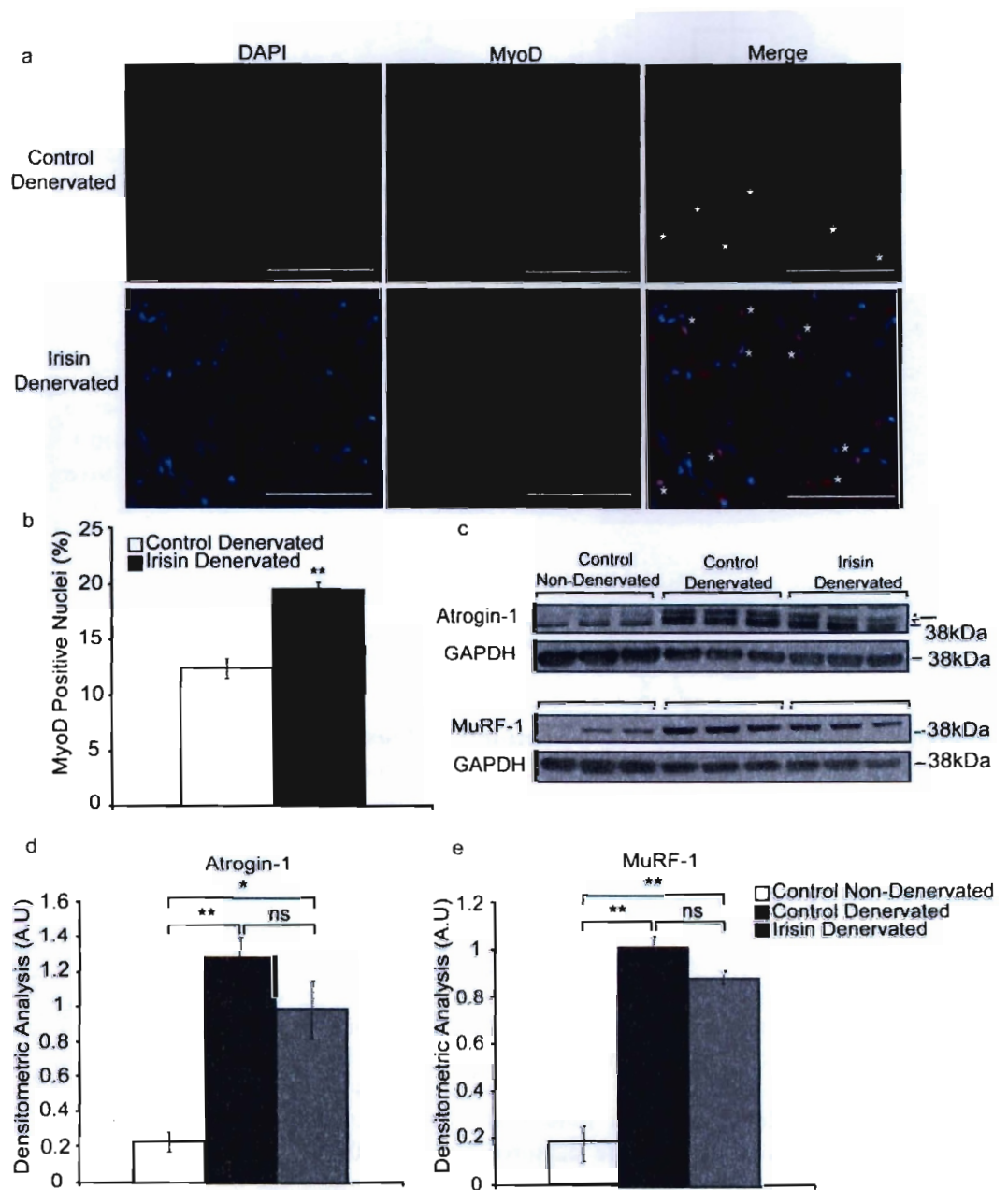
Figure 3.16: Irisin rescues denervation-induced muscle atrophy through activating satellite cells and reducing protein degradation

(a) Representative images of MyoD immunostaining of denervated TA muscles sections from mice injected with either DB (Control) or Irisin. Images were captured using a 20x objective. Scale bar represents 100μm. Nuclei were counterstained with DAPI. White asterisks denote representative MyoD positive cells. Linear brightness and contrast of the 'Merge' panel was adjusted to visualize MyoD$^+$ nuclei. This linear adjustment did not in any way alter interpretation of the results. (b) Graph displaying the percentage of MyoD positive cells in denervated TA muscle sections from mice injected with either DB (Control) or Irisin. (c) IB analysis of Atrogin-1and MuRF-1 protein levels in non-denervated Gas muscle from mice injected with DB (control) and denervated Gas muscle from mice injected with either DB (Control) or Irisin. The levels of GAPDH were assessed as a loading control. Arrow indicates Atrogin-1 band. (d) Graph shows densitometric analysis of Atrogin-1 levels in arbitrary units (A.U), normalized to GAPDH. (e) Graph shows densitometric analysis of MuRF-1 levels in arbitrary units (A.U), normalized to GAPDH (n=3 mice per group for all figure panels above). Error bars represent mean ± SEM. Student's T-test was performed for Figure 3.16b and one-way ANOVA was performed for Figures 3.16d and 3.16e. Significance is indicated with * (p<0.05) and ** (p<0.01).

3.11 Treatment with Irisin Leads to Increased Satellite Cell Activation and Reduced Markers of Protein Degradation during Denervation-Induced Muscle Atrophy

Skeletal muscle injury leads to activation of Satellite cells, which function to repair and regenerate skeletal muscle tissue. As such, we next performed immunocytochemistry on TA muscle sections to determine the numbers of nuclei positive for MyoD (a marker of activated satellite cells) (Figure 3.16a). Subsequent quantification revealed a significant increase in the numbers of MyoD positive nuclei, consistent with increased Satellite cell activation, in Irisin injected denervated TA muscle, when compared to respective DB-injected controls (Figure 3.16b). These data suggest that Irisin treatment results in increased activation of Satellite cells during denervation-induced skeletal muscle atrophy.

Atrogin-1 and MuRF-1 are two E3 ubiquitin ligases that are used as reliable markers for protein degradation during atrophic conditions, including denervation[104]. Therefore, we next measured the protein levels of both Atrogin-1 and MuRF-1 in non-denervated and denervated Gas muscle isolated from DB-injected mice and denervated Gas muscle from Irisin injected mice. As expected, we observed a significant increase in Atrogin-1 (Figure 3.16c and 3.16d) and MuRF-1 (Figure 3.16c and 3.16e) protein levels in response to denervation-induced skeletal muscle atrophy. However, injection of Irisin resulted in a notable reduction in Atrogin-1 (Figure 3.16c and 3.16d) MuRF-1 (Figure 3.16c and 3.16e) protein levels in denervated muscle, when compared to denervated muscle isolated from DB-injected control mice. These data suggest that Irisin treatment leads to reduced expression of key markers of skeletal muscle wasting during denervation-induced muscle atrophy.

The results in this section has been communicated to Oncotarget

3.12 Irisin Injection Promotes Muscular Hypertrophy in Young *mdx* Mice
Histidine-tagged Irisin protein was expressed and purified from *E. coli* using Ni-Agarose resin and resolved on SDS-PAGE. The results confirmed that recombinant Irisin used for the following trials is a homogenous, purified protein (Figure 3.17a). To assess the effect of Irisin on dystrophic muscle loss, young (3-week-old) *mdx* mice were injected with either DB or Irisin three-times-a-week for two weeks. Irisin injected mice showed a significant increase in body weight in the second week of Irisin injection (Figure 3.17b), which was maintained until completion of the trial (Figure 3.17b). No distinct difference in food intake was noted between DB and Irisin injected mice (Figure 3.17c). Analysis of hind limb muscle tissue weights revealed an increase in the weights of all muscles analyzed (Figure 3.17d and 3.17e). However, only Sol muscle showed a significant increase in weight in Irisin injected mice (Figure 3.17d and 3.17e). Histological analysis on transverse sections of the *M. tibialis anterior* (TA) muscle revealed hypertrophy of muscle fibers (Figure 3.17f); with an increased proportion of fibers with larger cross sectional area ($>2500\mu m^2$) and a reduced proportion of fibers with smaller cross sectional area ($<2500\mu m^2$) (Figure 3.17g and 3.17h).
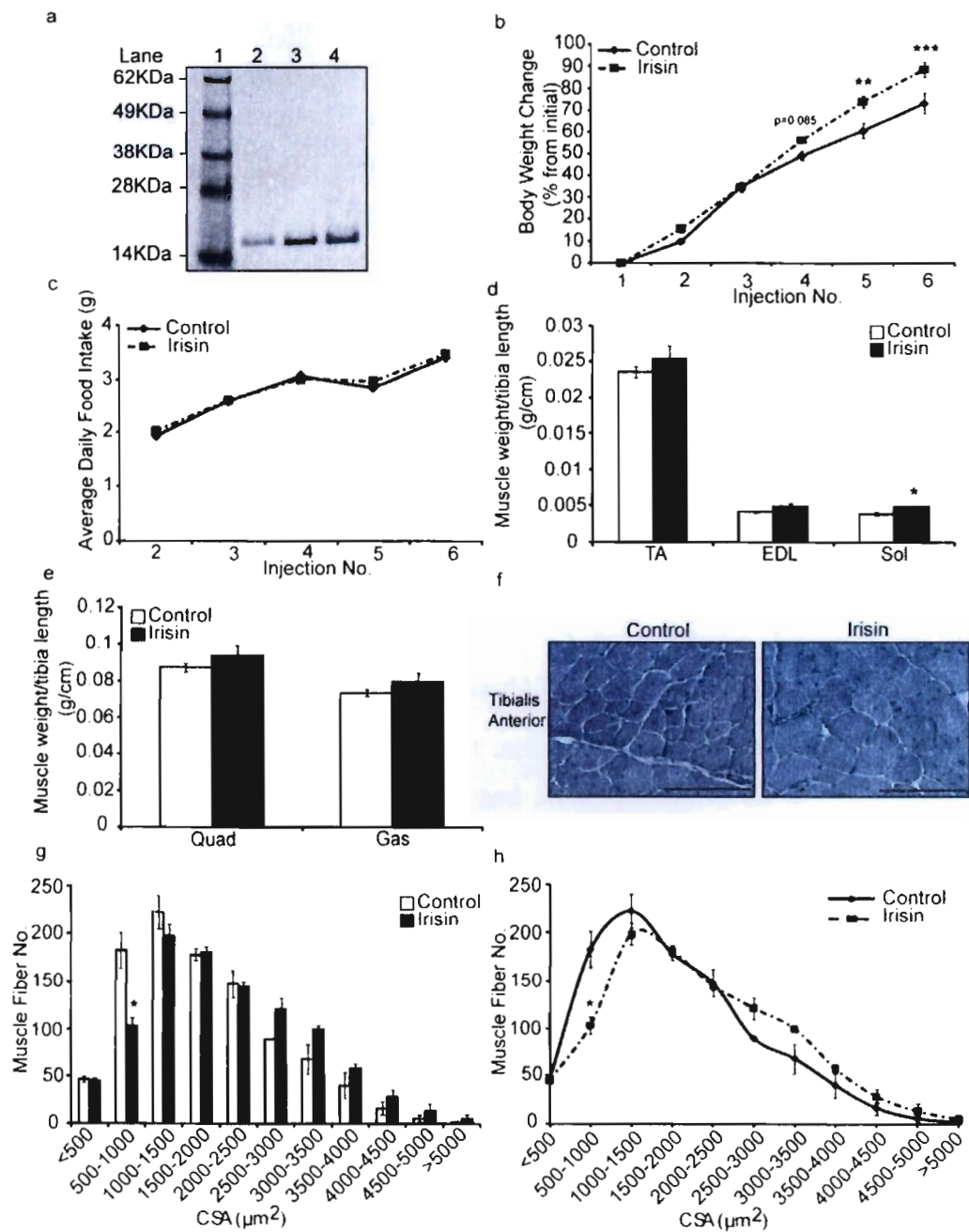
Figure 3.17: Irisin injection increases muscle mass and promotes hypertrophy in young *mdx* mice

(a) Representative image of Coomassie stained protein gel displaying purified recombinant His-tagged Irisin protein. A single band at ~15kDa was detected for recombinant Irisin protein. Lane 1 shows the SeeBlue Plus 2 Pre-Stained ladder. Lanes 2, 3 and 4 show 1μg, 2μg and 3μg of the purified His-tagged Irisin protein, respectively. (b) Graph showing percentage change in body weight (from initial) of young (3-week-old) male *mdx* mice injected three times-a-week with either DB (vehicle control) or Irisin (2.5μg/g body weight) for two weeks. Body weights were measured prior to each injection. (c) Graph showing average daily food intake per mouse. Food intake was measured prior to each injection over the two-week trial. (d) Graph showing the average weight of TA, EDL and Sol skeletal muscle tissue from young *mdx* mice injected with either DB or Irisin for two weeks. (e) Graph showing the average weight of Quad and Gas skeletal muscle tissue from young *mdx* mice injected with either DB or Irisin for two weeks. All hind limb muscle weights were normalized to tibia length (n=5 mice per group for all figure panels above). (f) Representative images of Haematoxylin and Eosin (H&E) stained TA muscle cross sections obtained from young *mdx* mice injected with either DB or Irisin for two weeks. Images were captured using a 20x objective. Scale bar represents 100μm. (g-h) Graphs showing the distribution of TA myofiber CSA from young *mdx* mice injected with either DB or Irisin for two weeks. (n=3 mice per group). Error bars represent mean ± SEM. Two-way ANOVA was performed for Figure 3.17b and Student's T-test was performed for Figures 3.17d, 3.17e, 3.17g and 3.17h. Significance is indicated with * ($p < 0.05$), ** ($p < 0.01$) and *** ($p < 0.001$).
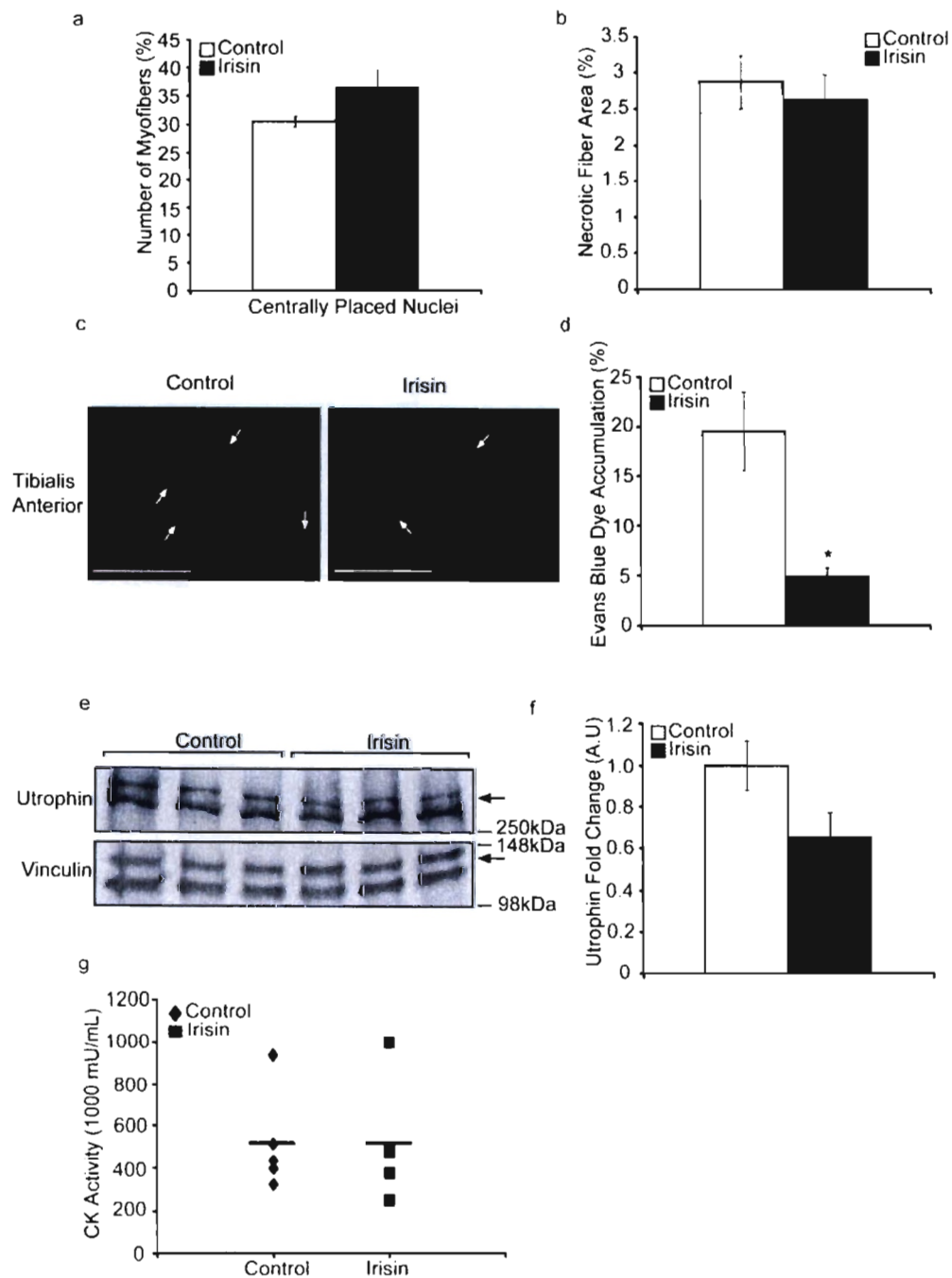
Figure 3.18: Irisin injection protects young *mdx* mice from dystrophic-associated skeletal muscle degeneration

(a) Graph showing the percentage of myofibers with centrally placed nuclei in TA muscle from young *mdx* mice injected with either DB or Irisin for two weeks. (b) Graph showing the percentage necrotic fiber area in TA muscle from young *mdx* mice injected with either DB or Irisin for two weeks. (c) Representative images of Evans blue dye (EBD) stained TA muscle cross sections obtained from young *mdx* mice injected with either DB or Irisin for two weeks. White arrows indicate representative EBD positive myofibers. EBD positive myofibers were visualized using fluorescent microscopy under a 20x objective. Scale bar represents 100μm. (d) Graph showing the percentage of EBD incorporation in TA muscle of young *mdx* mice injected with either DB or Irisin for two weeks. (e) Western Blot analysis of Utrophin protein levels in Gas muscle isolated from young *mdx* mice injected with either DB or Irisin for two weeks. The levels of Vinculin were assessed as a loading control. (f) Graph showing densitometric analysis of Utrophin protein levels in arbitrary units (A.U), normalized to Vinculin (n=3 mice for per group for all figure panels above). (g) Graph showing creatine kinase activity in the serum of young *mdx* mice injected with either DB or Irisin (n=5 mice for both groups). Error bars represent mean ± SEM. For all relevant figures, Student's T-test was performed. Significance is indicated with * (p<0.05).

3.13 Irisin Injection Protects Young *mdx* Mice from Dystrophic Myofiber Damage

Skeletal muscle in *mdx* mice undergoes constant cycles of degeneration and regeneration. One of the hallmark features of newly formed (regenerated) muscle fibers is centrally placed nuclei. As such we next quantified the number of myofibers with centrally placed nuclei in DB and Irisin injected mice to assess if Irisin treatment improves postnatal myogenesis in young *mdx* mice. Our analysis revealed a ~20% increase (albeit not statistically significant) in the percentage of myofibers with centrally placed nuclei in mice injected with Irisin, when compared to DB controls (Figure 3.18a). The percentage of necrotic muscle fibres was also quantified between DB and Irisin injected *mdx* mice, as assessed through the presence of infiltrating mono-nucleated cells, myofibres with fragmented sarcoplasm and hyper-contracted myofibers. Subsequent quantification revealed a 9% reduction in necrotic myofibers in *mdx* mice injected with Irisin, when compared to DB treated controls (Figure 3.18b). However, the reduction was found not to be statistically significant (Figure 3.18b). We further injected Evans Blue Dye (EBD) into DB or Irisin injected *mdx* mice (Figure 3.18c) to assess myofibre permeability. Red fluorescent EBD positive myofibres were assessed and the percentage of fluorescent muscle fibers was quantified through microscopy. Results revealed a significant 75% reduction in red fluorescent fibers in the TA muscle of *mdx* mice injected with Irisin, when compared to DB injected mice (Figure 3.18d).

The levels of Utrophin are indicative of the extent of muscular dystrophy, as Utrophin compensates for the absence of Dystrophin in *mdx* mice. As such, we next assessed the levels of Utrophin in *M. Gastrocnemius* (Gas) muscle following two weeks of Irisin injection. Results revealed a 35% reduction (not statistically significant) in the levels of Utrophin in *mdx* mice injected with Irisin, when compared to vehicle-injected controls (Figure 3.18e and 3.18f). We next measured the creatine kinase (CK) activity in the serum of the *mdx* mice, which is used as a marker to identify the extent of muscular dystrophy, since increased CK levels are associated with muscular dystrophy. We did not observe a distinct difference in CK activity in serum collected from *mdx* mice injected with Irisin (Figure 3.18g). Taken together, these data suggest that Irisin

treatment is able to at least in part alleviate the dystrophic phenotype observed in young *mdx* mice.

3.14 Irisin Promotes Skeletal Muscle Hypertrophy in Adult *mdx* Mice

In order to determine the therapeutic potential of Irisin in alleviating the dystrophic phenotype observed in adult *mdx* mice, 6-week-old (adult) *mdx* mice were injected with either DB or Irisin three-times-a-week for two weeks. No significant difference in body weight (Figure 3.19a) or food intake (Figure 3.19b) was noted between DB and Irisin injected adult *mdx* mice, although a slight increase in food intake was noted in Irisin injected mice prior to the last injection (Injection 7). However, consistent with results obtained upon injection of young *mdx* mice with Irisin (Figure 3.17d and 3.17e), a tendency towards increased weights of all hind limb muscles was seen in adult mice injected with Irisin, although the increase in muscle weights observed were not statistically significant (Figure 3.19c and 3.19d). Histological analysis on transverse sections of the TA muscle revealed hypertrophy of muscle fibers (Figure 3.19e). Specifically, an increased proportion of fibers with larger cross sectional area ($>2000\mu m^2$) and a reduced proportion of fibers with smaller cross sectional area ($<2000\mu m^2$) was observed in Irisin injected adult *mdx* mice, when compared to DB injected mice (Figure 3.19f and 3.19g). It is noteworthy to mention that TA muscles from adult *mdx* mice injected with Irisin had a large number of myofibers with very large cross sectional area ($>4000\mu m^2$), when compared to DB injected mice (Figure 3.19f and 3.19g). These data strongly suggest that Irisin promotes significant skeletal muscle hypertrophy in adult *mdx* mice. It is also important to mention that two weeks of Irisin treatment resulted in a more profound hypertrophy of skeletal muscle in adult *mdx* mice, when compared to young *mdx* mice (Compare Figure 3.17g and 3.17h with 3.19f and 3.19g).

132
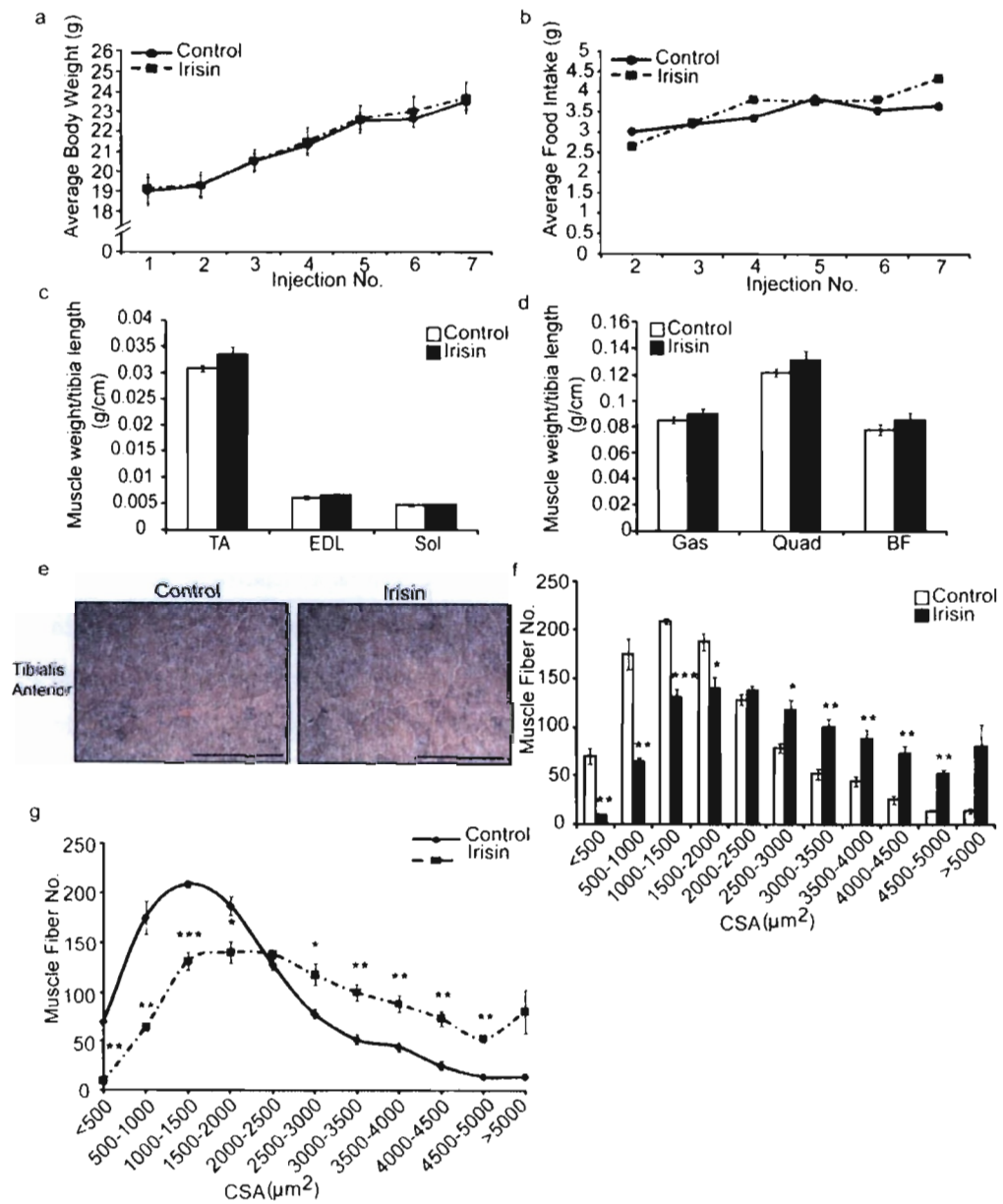
Figure 3.19: Irisin increases muscle weight and promotes muscle hypertrophy in adult *mdx* mice

(a) Graph showing change in body weight of adult (6-week-old) male *mdx* mice injected three times-a-week with either DB (vehicle control) or Irisin (2.5μg/g body weight) for two weeks. Body weights were measured prior to each injection. (b) Graph showing average daily food intake (g) per mouse. Food intake was measured prior to each injection over the two-week trial. (c) Graph showing the average weight of TA, EDL and Sol skeletal muscle tissue from adult *mdx* mice injected with either DB or Irisin for two weeks. (d) Graph showing the average weight of Gas, Quad and BF skeletal muscle tissue from adult *mdx* mice injected with either DB or Irisin for two weeks. All hind limb muscle weights were normalized to tibia length (n=6 mice per group for all experiments above). (e) Representative images of Haematoxylin and Eosin (H&E) stained TA muscle cross sections obtained from adult *mdx* mice injected with either DB or Irisin for two weeks. Images were captured using a 20x objective. Scale bar represents 100μm. (f-g) Graphs showing the distribution of TA myofiber CSA from adult *mdx* mice injected with either DB or Irisin for two weeks. (n=4 mice per group for all figure panels above). Error bars represent mean ± SEM. Two-way ANOVA was performed for Figure 3.19a and Student's T-test was performed for Figures 3.19c, 3.19d, 3.19f and 3.19g. Significance is indicated with * ($p<0.05$), ** ($p<0.01$) and *** ($p<0.001$).

134
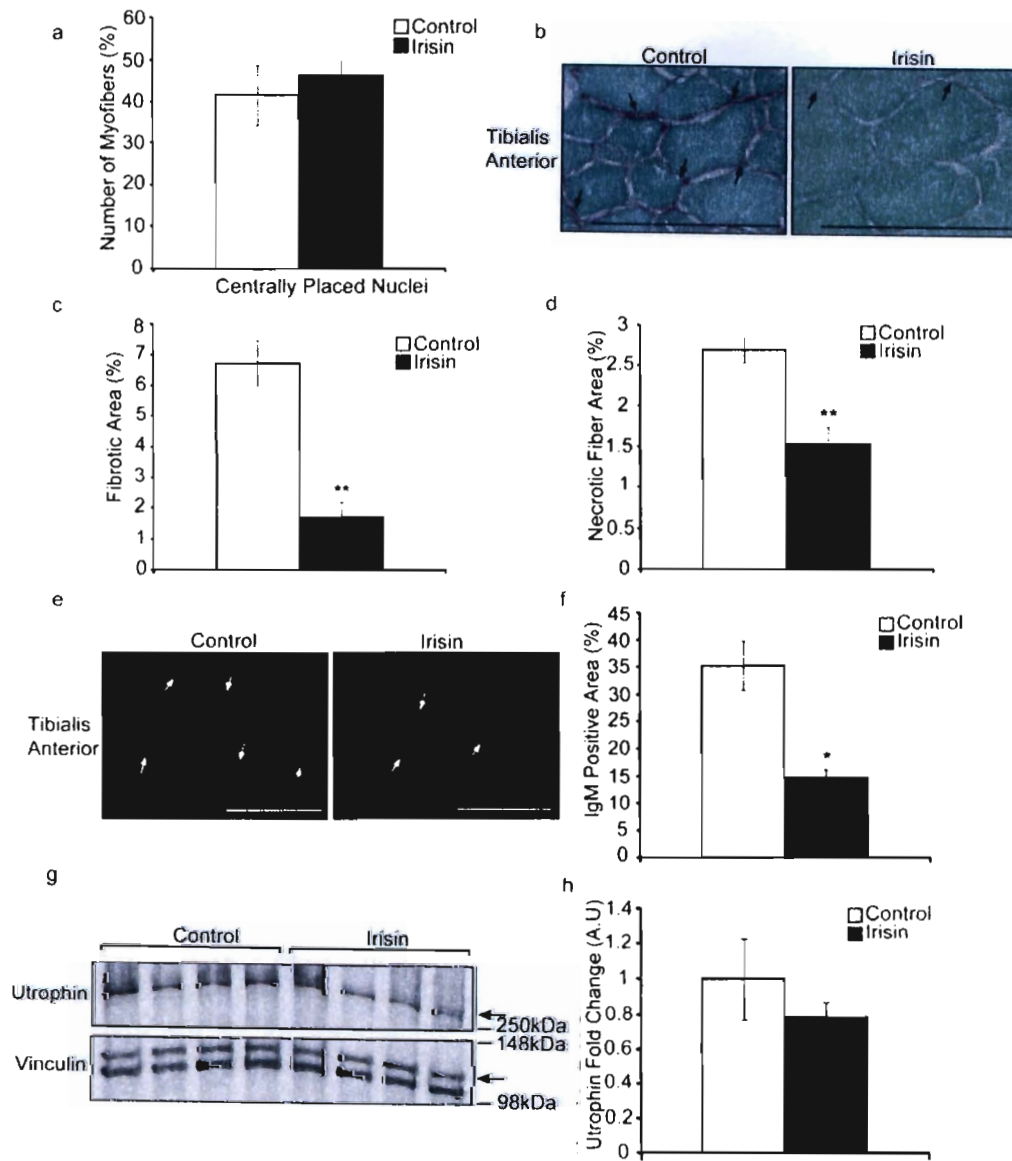
Figure 3.20: Irisin protects adult *mdx* mice from fibrosis and muscle fiber degeneration

(a) Graph showing the percentage of myofibers with centrally placed nuclei in TA muscle from adult *mdx* mice injected with either DB or Irisin for two weeks (n=4 mice for both groups). (b) Representative images of Sirius red and Fast green stained TA muscle cross sections obtained from adult *mdx* mice injected with either DB or Irisin for two weeks. The green stain indicates non-collagenous proteins, while the red stain indicates collagen. Black arrows indicate representative fibrotic areas. Images were captured using a 40x objective. Scale bar represents 100μm. (c) Graph showing the percentage fibrotic area (red stain), expressed as a percentage of total muscle section area, in TA muscle from adult *mdx* mice injected with either DB or Irisin for two weeks, as assessed through Sirius red and fast green staining. (d) Graph showing the percentage necrotic fiber area, expressed as a percentage of total muscle section area, in TA muscles from adult *mdx* mice injected with either DB or Irisin for two weeks (n=3 mice for both groups) (e) Representative images of IgM antibody stained TA muscle sections obtained from adult *mdx* mice injected with either DB or Irisin for two weeks. White arrows indicate representative IgM positive myofibers. Images were captured using a 20x objective. Scale bar represents 100μm. (f) Graph showing IgM positively stained area, expressed as a percentage of total muscle section area, in TA muscle sections from adult *mdx* mice injected with either DB or Irisin for two weeks. (g) Western Blot analysis of Utrophin protein levels in Gas muscle isolated from adult *mdx* mice injected with either DB or Irisin for two weeks. The levels of Vinculin were assessed as a loading control. (h) Graph showing densitometric analysis of Utrophin protein levels in arbitrary units (A.U), normalized to Vinculin (n=4 mice for both groups). Error bars represent mean ± SEM. For all relevant figures, Student's T-test was performed. Significance is indicated with * ($p<0.05$) and ** ($p<0.01$).

136

3.15 Irisin Protects against Fibrosis, Myofiber Necrosis and Sarcolemmal Instability

To further understand the beneficial effects of Irisin on *mdx* muscle, we next analyzed the difference in the proportion of regenerating muscle fibers, as represented by the number of centrally placed nuclei, between adult *mdx* mice injected with either DB or Irisin. It is interesting to note that despite the increase in myofiber cross sectional area noted in the TA muscle from Irisin injected *mdx* mice, the proportion of myofibers with centrally placed nuclei was not significantly different (Figure 3.20a), with ~41% and ~46% of myofibers containing centrally formed nuclei in DB and Irisin injected *mdx* mice, respectively. To confirm that the increase in muscle weights (Figure 3.19c and 3.19d) was not due to increased accumulation of fibrotic tissue and collagen, we performed Sirius Red (collagen) and Fast green (non-collagenous proteins) staining of skeletal muscle sections of TA muscle from DB and Irisin injected *mdx* mice (Figure 3.20b). Subsequent quantification of the fibrotic area (Red) revealed a significant ~4-fold reduction in fibrosis in TA muscle from Irisin injected *mdx* mice, when compared to DB injected mice (Figure 3.20c), suggesting that Irisin treatment protected dystrophic muscle fibers against fibrotic tissue accumulation. We next assessed the numbers of necrotic muscle fibres in muscles isolated from adult *mdx* mice injected with either DB or Irisin. Adult *mdx* mice injected for two weeks with Irisin displayed a dramatic 43% reduction in necrotic muscle fibers, when compared to respective DB controls (Figure 3.20d). Taken together these data reveal a role for Irisin in protecting against myofiber necrosis in adult *mdx* mice.

Myofibers in *mdx* mice have reduced sarcolemmal stability, which allows proteins that are usually found only in circulation to enter and accumulate in the degenerating muscle fibers. To understand the role of Irisin in protecting sarcolemmal integrity of *mdx* mice muscle, we investigated the accumulation of IgM protein in myofibers, which is typically restricted to circulation in healthy mice. Subsequent analysis revealed that a large proportion of the myofibers from *mdx* mice injected with DB stained positively for IgM (Figure 3.20e). However, Irisin injection resulted in a significant 58% reduction in IgM accumulation in myofibers from *mdx* mice (Figure 3.20f). These data suggest

137

that Irisin improves the sarcolemmal stability of dystrophic myofibers. Lastly, we investigated the levels of Utrophin in adult *mdx* mice injected with either DB or Irisin. Similar to the results obtained above (Figure 3.18e and 3.18f), we observed a 22% reduction in Utrophin levels in adult *mdx* Gas muscle (Figure 3.20g and 3.20h). However, the reduction was not statistically significant.

3.16 Prolonged Irisin Treatment Increases Muscle Weights and Enhances Grip Strength of Adult *mdx* Mice

As described above, short-term (2 weeks) injection of Irisin into *mdx* mice tended to increase skeletal muscle weights, although the increase noted in muscle weights were not statistically significant. Given this, we next wanted to investigate whether or not increasing the duration of Irisin treatment of *mdx* mice could improve skeletal muscle weight and function. To study this, 4-week-old *mdx* mice were injected with either DB or Irisin, three-times-a-week for 4 weeks. No significant difference in body weight (Figure 3.21a) or food intake (Figure 3.21b) was noted between *mdx* mice injected with either DB or Irisin for 4 weeks. However, analysis of individual hind limb skeletal muscle weights revealed a significant increase in TA, Sol and Gas muscle weights in Irisin injected *mdx* mice, when compared to DB injected controls (Figure 3.21c and 3.21d). The weights of EDL, Quad and BF skeletal muscles also showed an increase, however, the increase was not statistically significant (Figure 3.21c and 3.21d). Importantly, 4 weeks of Irisin injection further resulted in a significant increase (~2-fold) in the forelimb grip strength of *mdx* mice (Figure 3.21e). These data indicate that prolonging the duration of Irisin treatment could improve both skeletal muscle mass and muscle strength of *mdx* mice.
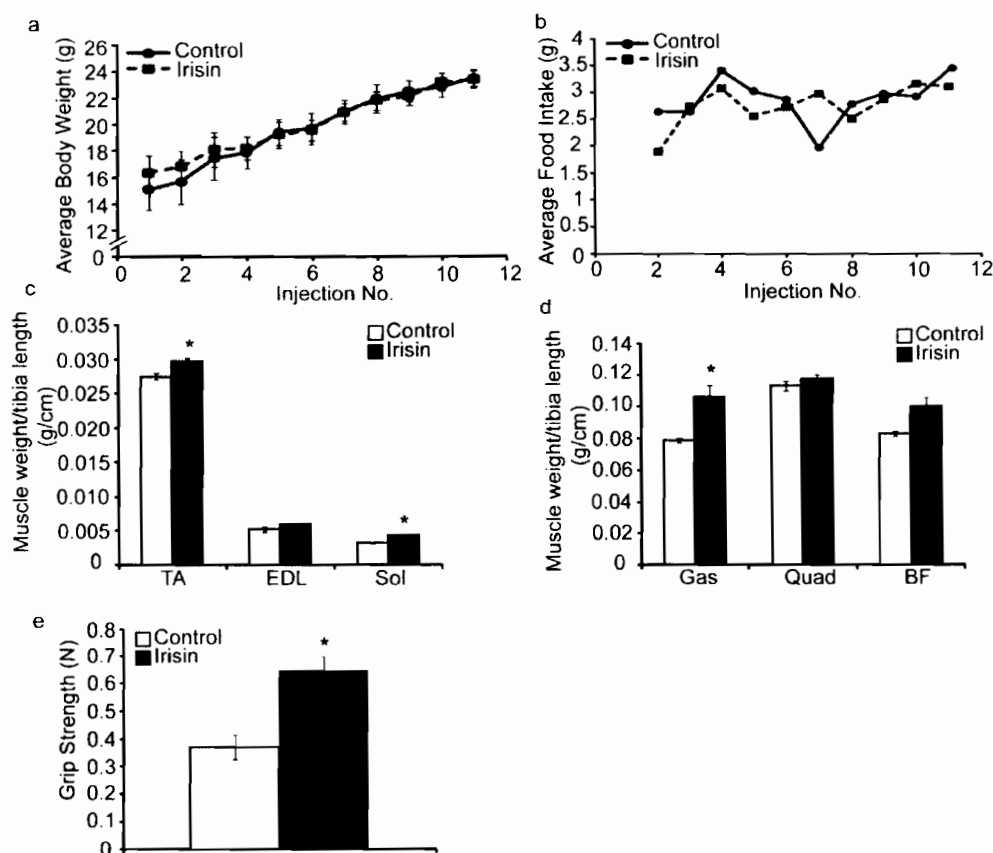
Figure 3.21: Prolonged Irisin injection increases skeletal muscle mass and enhances muscle function in adult *mdx* mice

(a) Graph showing change in average body weight (g) of adult (4-week-old) male *mdx* mice injected three times-a-week with either DB (vehicle control) or Irisin (2.5µg/g body weight) for four weeks. Body weights were measured prior to each injection. (b) Graph showing average daily food intake (g) per mouse. Food intake was measured prior to each injection over the four-week trial. (c) Graph showing the average weight of TA, EDL and Sol skeletal muscle tissue from adult *mdx* mice injected with either DB or Irisin for four weeks. (d) Graph showing the average weight of Gas, Quad and BF skeletal muscle tissue from adult *mdx* mice injected with either DB or Irisin for four weeks. All hind limb muscle weights were normalized to tibia length. (e) Graph showing the forelimb grip strength (N) of adult *mdx* mice injected with either DB or Irisin for four weeks. Grip strength was assessed prior to termination of the mice (n=3 mice for the DB injected control group and n=4 mice for the Irisin injected group). Error bars represent mean ± SEM. Two-way ANOVA was performed for Figure 3.21a and Student's T-test was performed for Figures 3.21c, 3.21d and 3.21e. Significance is indicated with * ($p<0.05$).

139

4. Discussion

Irisin is a novel exercise-induced myokine. Functional studies have revealed that Irisin promotes browning of beige adipose precursor cells in white fat tissue resulting in increased energy expenditure[139, 171, 177, 178, 179, 180]. Since Irisin is an exercise-secreted factor, I reasoned that Irisin may function to enhance skeletal muscle myogenesis and promote hypertrophy, similar to what is noted in response to exercise. Consistent with this, recent studies have revealed a potential role for Irisin in regulating skeletal muscle growth, where Irisin levels positively correlated with biceps circumference in humans[163]. Moreover, Irisin was able to stimulate the expression of muscle growth related genes and reduce Myostatin levels in myocytes by activating the Erk pathway[172]. Improved muscle strength and function was also positively correlated with Irisin levels in serum[154]. However, to date, an in-depth analysis of Irisin regulation of skeletal muscle and for that matter the potential molecular mechanisms through which Irisin may influence skeletal muscle have been largely unexplored. As such, I have undertaken a systematic approach using both *in vitro* and *in vivo* model systems to further define the role of Irisin in regulation of skeletal muscle growth. Results from these studies have revealed that Irisin is a positive regulator of skeletal muscle growth, as such, treatment with Irisin leads to improved myogenesis, skeletal muscle hypertrophy, enhanced muscle strength and improved skeletal muscle regeneration. Moreover, I have shown that exogenous treatment with Irisin not only improves skeletal muscle regeneration but is also able to rescue, at least in part, skeletal muscle atrophy associated with denervation and muscular dystrophy. Taken together, these data reveal that Irisin may have therapeutic potential in improving skeletal muscle growth and overcoming the profound loss of skeletal muscle mass associated with muscle wasting conditions.

The recombinant Irisin protein used in this study was purified using an *E. coli* based system. There are a number of benefits to using *E. coli* bacteria to produce recombinant proteins. *E. coli* has unmatched rapid growth kinetics and in optimal conditions, the doubling time is 20 minutes, which makes this system a convenient one[181]. Moreover, it is easy to transform *E. coli* with exogenous DNA in a very short amount of time[182]. However, recombinant

140

proteins expressed from gram negative *E. coli* may be inadvertently contaminated with endotoxin[183]. Endotoxin is a complex lipopolysaccharide (LPS) found on the cell membrane of *E. coli* and other gram negative bacteria[184], which is shed upon cell death and can result in severe systemic effects[185]. Specifically, endotoxin can induce a severe inflammatory response and result in a sudden increase in inflammatory cytokines such as TNF-α, IL-1β, IL8, IL6, which can result in severe pathological responses[186]. As such, I initially measured the endotoxin levels in the recombinant Irisin protein used in this study and results revealed that endotoxin levels were found to be low [174](1.0 EU/ml). Importantly, treatment with Irisin protein did not result in cell death *in vitro*, as visualized under a light microscope. Furthermore, mice injected with Irisin *in vivo* did not show any adverse change in movement or behavior and there was no notable difference in their food or water consumption. Upon gross pathological examination, mice injected with Irisin did not show any inflammation, toxicity in organs or fluid retention in the body. Therefore, I concluded that the recombinant murine Irisin protein used in this thesis was non-toxic and as such was suitable for my proposed studies.

Another disadvantage of using the bacterial system is that *E. coli* bacteria do not have systems for protein glycosylation[187, 188]. However, circulating Irisin has been previously shown to exist in a glycosylated form[148]. Importantly, production of eukaryotic proteins that normally undergo post translational modification using the prokaryotic system may result in reduced activity of the protein[187, 188]. Hence, it is quite possible that the recombinant Irisin protein used in my studies may have reduced bioactivity. Previous studies have clearly demonstrated that Irisin can increase the levels of Ucp-1 in white adipose tissue. Given this, we further assessed the bioactivity of the recombinant Irisin protein through quantifying changes in *Ucp-1* in adipocyte cultures following Irisin treatment. Treatment with recombinant Irisin protein was able to significantly upregulate the expression of *Ucp-1* in both hADSCs and 3T3L1 cells during adipogenic differentiation (Figure 3.1b and 3.1c), indicating that the Irisin protein used in this thesis is biologically active.

141

Microarray analysis revealed that myotubes treated with Irisin showed gene expression changes similar to that noted in response to exercise (Table 3.1). Notably, genes that inhibit differentiation of Satellite cells were down regulated (*Ogn*, *Sox8*, *Heyl*), while the expression of hypertrophy and growth factors (*IL6* and *Serpina3g*) were increased, supporting that Irisin could be a pro-myogenic growth factor. In agreement with this, treatment with Irisin resulted in enhanced myoblast proliferation (Figure 3.3a), together with increased myoblast fusion and myotube number during myogenic differentiation (Figure 3.3b-3.3d). However, the enhanced differentiation phenotype observed in response to Irisin treatment was not due to increased expression of key myogenic differentiation markers, including MyoD, Myogenin or p21. Despite this, increased levels of MHC were noted following Irisin treatment, which is consistent with the enhanced myotube number observed (Figure 3.4a-3.4e). These data indicated that Irisin may not improve myogenesis through enhancing the expression of myogenic regulatory factors. Further analysis revealed that Irisin upregulates the expression of the primary fusion marker, *Myomaker*, a membrane protein which is necessary and sufficient for the fusion of myoblasts to each other[189] (Figure 3.3e). Therefore, I concluded that Irisin may promote myogenesis thorough enhancing myoblast fusion.

In addition to studies on murine myoblast cultures, I further assessed the function of Irisin on human primary myoblasts. Consistent with results noted in murine myoblasts, treatment with Irisin resulted in a significant increase in myotube number and myoblast fusion in human myoblasts during differentiation (Figure 3.5). These data reveal that human myoblasts are responsive to murine Irisin protein and further suggests the presence of an, as yet unidentified, Irisin-responsive receptor in human myoblasts, which is able to interact and initiate downstream signaling events in response to Irisin treatment. However, further experiments need to be performed to confirm the effect of human Irisin protein on human myoblasts and muscle.

The role of Irisin during myogenesis was further investigated using a mouse model of Notexin-induced muscle injury and regeneration. Consistent with the improved myogenesis noted *in vitro*, Irisin injected into regenerating muscle

resulted in a distinct increase in the numbers of MyoD positive nuclei at Day 2 and Day 3 of regeneration (Figure 3.12a-3.12d). MyoD is a marker of activated and proliferating myoblasts and in fact, Day 2 and Day 3 are key stages during early regeneration where inflammation and Satellite cell recruitment and activation are the dominant processes[48]. Further analysis of the role of Irisin in Satellite cell activation revealed an increase in the proportion of proliferating myoblasts (Pax7$^+$/MyoD$^+$) in primary murine myoblasts upon treatment with Irisin (Figure 3.13a and 3.13c). Irisin treatment also increased the percentage of fusion competent myoblasts (Pax7$^-$/MyoD$^+$) in primary murine cultures (Figure 3.13a and 3.13d). These data suggest that Irisin may directly regulate Satellite cell activation and proliferation, which is further consistent with the enhanced myoblast proliferation noted in C2C12 myoblasts following Irisin treatment (Figure 3.3a). Ten days post-muscle injury, a greater percentage of regenerated myofibers with 2 centrally placed nuclei was noted in Irisin injected mice, indicating greater fusion of activated Satellite cells to repair damaged myofibers (Figure 3.14c). Importantly, this increased fusion of satellite cells is consistent with the hypertrophy noted in Irisin injected regenerated muscle tissue (Figure 3.14b) and moreover, the increase in *Myomaker* and enhanced fusion index and myotube number noted after Irisin treatment *in vitro*. Overall, these data support the hypothesis that Irisin is a pro-myogenic factor and is able to promote muscle hypertrophy by enhancing Satellite cell activation and fusion.

The microarray data and qPCR validation showed that Irisin strongly induces the expression of *IL6* (Table 3.1 and Figure 3.2d). Similar to Irisin, previous publications have revealed that IL6 is secreted during exercise[109] and is also induced during myogenic differentiation[112]. Moreover, loss of IL6 leads to reduced myogenic differentiation, whereas increased levels of IL6 promote myogenic differentiation[112]. IL6 has also been previously shown to also regulate skeletal muscle hypertrophy by activating Satellite cells. Consistent with this, loss of IL6 results in reduced satellite cell proliferation, in a Stat3-dependant manner, which in turn impairs skeletal muscle hypertrophy[111]. Taken together, these studies prompted me to further investigate the Irisin-IL6 axis to understand if Irisin may exert its effects via the IL6 pathway. Irisin was found to distinctly increase the expression of *IL6* in proliferating myoblasts (Figure

143

3.10a) and differentiating myotubes (Figure 3.10d). Importantly, knock down of *IL6* in differentiating myotubes, not only impaired myogenic differentiation and myotube formation, but also interfered with Irisin-mediated enhancement of myogenic differentiation (Figure 3.11c and 3.11d). Therefore, these data reveal that Irisin, at least in part, signals through IL6 to enhance myogenesis (Figure 3.11).

Injection of Irisin into wild type mice resulted in an increase in muscle weights, significant muscle hypertrophy and enhanced forelimb grip strength (Figure 3.6b-3.6f). Importantly, the beneficial effects of Irisin on skeletal muscle mass and function were not observed in mice injected with the control His-tag peptide (Figure 3.7). These data indicate that Irisin-induced hypertrophy and improvement in muscle function are specific. Skeletal muscle hypertrophy can be induced through increasing anabolism (protein synthesis), reducing catabolism (protein degradation)[74, 190, 191] and activating Satellite cells[192]. We have observed in the current study that Irisin is able to activate Satellite cells *in vitro* in primary myoblast cultures and *in vivo* to enhance the activation and function of Satellite cells in damaged muscle. We have further revealed increased levels of p-Akt and p-Erk1/2, together with reduced levels of p-Raptor following Irisin treatment and thus, increased activation of protein synthesis pathways (Figure 3.8a-3.8d). Previous work has revealed that Irisin levels are increased in *myostatin*-null mice through a mechanism involving AMPK (AMPK-PGC1-α-FNDC5). Given that AMPK is increased in situations where energy (ATP) is depleted and moreover, has been previously shown to inhibit mTOR and protein synthesis, AMPK upregulation of Irisin seems to be contradictory to the increased protein synthesis signaling noted upon Irisin treatment in the current thesis. In this thesis I have shown Irisin treatment results in reduced phosphorylation of Raptor. Phosphorylation inactivates raptor, through interfering with the ability of Raptor to act a scaffold protein for mTOR, as such, Irisin-mediated reduction in raptor phosphorylation would potentially lead to activation of the mTOR complex. We speculate that Irisin may work downstream of AMPK to lift AMPK-mediated inhibition of mTOR and protein synthesis, and as such, may form the basis of a feedback loop. Reduced levels of Atrogin-1 and MuRF-1, two muscle-specific E3 ubiquitin ligases responsible

144

for degrading muscle proteins via the ubiquitin proteasome pathway, were also observed in myotubes treated with Irisin (Figure 3.8e-3.8h). The phosphorylation status of FoxO transcription factors has an important role in regulating the expression of Atrogin-1 and MuRF-1. Specifically, reduced phosphorylation of FoxO transcription factors leads to increased expression of Atrogin-1 and MuRF-1 and vice versa[97, 99, 134]. As we observed reduced expression of both Atrogin-1 and MuRF-1 following Irisin treatment we expected to observe increased phosphorylation of FoxO1 in response to Irisin. However, the difference in the levels of phosphorylated FoxO1 noted upon Irisin treatment was not statistically significant (Figure 3.8f). This data suggests that Irisin may signal through alternative pathways to regulate key components of the protein degradation pathway. I speculate that Irisin may influence the expression and/or activity of upstream regulators of Atrogin-1 and MuRF-1, such as NF-κB[193], myostatin/TGF-β[134] and p38 MAPK[194] pathways. However, further work will need to be undertaken to verify this. Microarray results and subsequent qPCR validation revealed a significant upregulation of *Hp* in response to Irisin treatment *in vitro*. Interestingly, previous studies have shown that in the absence of Hp the levels of Atrogin-1 and MuRF-1 are increased and protein synthesis is reduced[195]. Therefore, it is quite possible that Irisin may also signal via Hp to regulate protein synthesis and protein degradation pathways. However, further rescue experiments need to be performed to study if Irisin is able to promote hypertrophy of skeletal muscle in the absence of Hp. Overall, these results suggest that Irisin can promote skeletal muscle hypertrophy by shifting the balance towards increased anabolism and reduced catabolism, coupled with increased Satellite cell activation and fusion.

Since Irisin was able to reduce the levels of enzymes that promote protein degradation, the role of Irisin in denervation-induced atrophy was investigated. Denervation, due to sciatic nerve transection, leads to profound skeletal muscle wasting through activation of Atrogin-1 and MuRF-1 and the ubiquitin proteasome pathway[97, 196]. Previously published results have revealed that exercise can rescue denervation induced skeletal muscle atrophy and in fact promotes re-innervation of muscle fibers[197]. Consistent with this, results in this thesis demonstrated that Irisin partially rescued denervation-induced muscle

145

fiber atrophy through increasing Satellite cell activation and also by reducing Atrogin-1 and MuRF-1 levels (Figure 3.16b-3.16e). Irisin is thus able to reduce protein degradation and enhance the available pool of Satellite cells, which contributes to improved maintenance of muscle mass during denervation-induced muscle atrophy.

Exercise has been shown to upregulate the expression of PGC1-α, which has previously been reported to play an important role in mitochondrial biogenesis[198]. Since Irisin treatment results in similar changes to skeletal muscle as observed in response to exercise, the effect of Irisin on mitochondrial function was studied. We observed a significant improvement in the Basal, ATP-linked, maximal mitochondrial respiration and spare respiratory capacity, indicating that Irisin treatment results in improved mitochondrial oxygen consumption *in vitro*. However, upon normalization of the results to total protein content the differences in mitochondrial oxygen consumption became statistically insignificant, due to the fact that Irisin treatment enhanced myogenic differentiation and as such, total protein content. This suggests that Irisin may not directly enhance mitochondrial function and/or number and that the increased mitochondrial oxygen consumption may be as a consequence of increased myotube number and size.

The results discussed above reveal that Irisin could potentially confer beneficial effects of exercise, including improved muscle strength and functionality, without the need for physical exertion and muscle wear and tear, which could be detrimental for individuals suffering from DMD, where exercise can exacerbate the degenerative process[199].

Young *mdx* mice, a model of DMD, show an acute onset of muscular dystrophy at 3 weeks of age, with distinct muscle fiber necrosis[73, 200]. This acute necrotic pathology appears to decrease in intensity from about 8 weeks of age in *mdx* mice[73, 200]. Importantly, young 3-week-old *mdx* mice injected with Irisin show increased muscle weights and a trend towards increased myofiber size (Figure 3.17f-3.17h). A typical consequence of muscular dystrophy is damage to muscle fibers. Under normal physiological conditions, the muscle membrane is

146

impermeable to circulating proteins, such as albumin. However, during muscular dystrophy, when the sarcolemmal integrity is compromised, muscle fibers become permeable to serum albumin, which binds strongly to Evans blue dye.[201] Albumin-Evans blue dye conjugate permeates across the muscle membrane and accumulates in the damaged fibers. As such, Evans blue dye uptake in muscle can be used as a marker of muscle damage[202, 203]. Consistent with improved muscle structure, Irisin injected *mdx* mice showed a ~75% reduction in Evans blue dye uptake in muscle fibers, which provides evidence to suggest that Irisin may function to protect muscle fibers from sarcolemmal damage in the absence of dystrophin (Figure 3.18 c-3.18d).

Creatine kinase is mainly found in skeletal muscle tissue, heart muscle and in the brain[204]. However, sarcolemmal damage of muscle fibers, such as during muscular dystrophy, causes creatine kinase to leak into circulation[205]. Although we noted a significant reduction in Evans blue dye uptake in *mdx* muscle fibers upon Irisin injection (Figure 3.18c-3.18d), injection of Irisin protein was unable to alter the levels of serum creatine kinase in *mdx* mice (Figure 3.18g). The disparity between Evans blue dye uptake and creatine kinase levels in serum may be due to the increase in muscle mass noted in *mdx* mice upon Irisin injection. Specifically, the increased muscle mass and hypertrophy noted upon Irisin injection could provide the potential for greater amounts of available creatine kinase to leak into circulation. In other words, despite the reduction in Evans blue dye accumulation and protection of sarcolemmal membrane integrity noted in *mdx* mice upon Irisin injection (Figure 3.18c-3.18d), a reduction in serum creatine kinase levels was not observed since there was an overall increase in total muscle tissue. Therefore, creatine kinase levels in this study may not accurately reflect the status of the myofiber damage in Irisin treated *mdx* mice. In agreement with this, a recent publication by Relizani *et al.*, (2014) reported that blockade of Myostatin signaling in *mdx* mice, using a soluble form of the Activin Type II B receptor (sActRIIB), resulted in increased myofiber size in Soleus muscles without altering the overall levels of CK in serum (ref). It could also be possible, that the protective role of Irisin on skeletal muscle structure may not be enough to reduce the levels of creatine

kinase in serum and perhaps a prolonged Irisin treatment regimen may have been required.

Injection of Irisin into adult *mdx* mice resulted in increased muscle tissue weights (Figure 3.19c-3.19d). Moreover, distinct hypertrophy of skeletal muscle fibers was observed in adult *mdx* mice injected with Irisin (3.19e-3.19g). This was notably different from the result observed in young *mdx* mice injected with Irisin for the same duration, where we observed a mild hypertrophy (Figure 3.17f-3.17h). Hypertrophy of adult *mdx* skeletal muscle was accompanied by a remarkable reduction in muscular fibrosis, which is an indication of improved muscle regeneration[206] (Figure 3.20b and 3.20c). The replacement of contractile muscle tissue with non-contractile fibrotic tissue over repeated rounds of degeneration and regeneration reduces the contractile capacity of muscle, leading to a gradual loss in muscle strength[68]. Consistent with improved muscle regeneration, injection with Irisin also resulted in a marked increase in muscle strength in adult *mdx* mice (Figure 3.21e). Moreover, a greater reduction in muscle fiber necrosis was noted in adult *mdx* mice (~43%) (Figure 3.20d), when compared to young *mdx* mice (~9%) (Figure 3.18b) after Irisin injection.

IgM is an antibody secreted by B cells and it is found mainly in the circulation. Similar to albumin entering muscle fibers from circulation due to compromised sarcolemmal integrity, IgM, a 900kDa molecule normally found in the endomyisum or perimysisum, is able to gain entry into the damaged muscle fibers[203]. Distinctly reduced levels of IgM accumulation in muscle fibers of adult *mdx* mice injected with Irisin (Figure 3.20e and 3.20f), served as further validation of Irisin's role in protecting sarcolemmal stability in the absence of dystrophin.

Ubiquitous dystrophin (Utrophin) has similar function and structure as dystrophin, although Utrophin is of a lower molecular mass[207]. The expression of Utrophin was found to be much higher in *mdx* mice lacking dystrophin[208]. Consistent with reversal of dystrophic phenotype, reduced Utrophin levels were observed in both young (Figure 3.18f) and adult mice (Figure 3.20h) in

148

response to Irisin injection, suggesting that Irisin may be able to signal to, at least in part, compensate for the loss of Dystrophin in *mdx* mice.

A much stronger protective response was elicited in adult *mdx* mice injected with Irisin as compared to young *mdx* mice, with a greater increase in muscle fiber cross sectional area and a more pronounced reduction in myofiber necrosis. I propose that this difference in Irisin effect between young and adult *mdx* mice may be due to the natural stabilization of the phenotype exhibited in adult *mdx* mice as they reach 8 weeks of age[73, 200]. As a result of this, injection of Irisin may result in a more pronounced protective effect in adult *mdx* mice, as opposed to young *mdx* mice, which display a more acute muscle damage phenotype[73, 200]. Interestingly, prolonging the duration of the Irisin injection trial to 4 weeks resulted a clear increase in skeletal muscle mass and muscle strength in adult *mdx* mice, which further validates the pro-myogenic capacity of Irisin to improve muscle mass and functionality.

It is possible that Irisin may influence the levels and function of additional growth factors to improve the dystrophic phenotype in *mdx* mice. It has previously been reported that inhibition of myostatin upregulates FNDC5 expression and hence, circulating Irisin levels[171]. Interestingly, Myostatin inhibition has been shown to reverse fibrotic tissue accumulation in dystrophic mice[209] and reduce the severity of dystrophy, thereby enhancing muscle strength[210]. Given that Irisin has the ability to exert pro-myogenic effects on muscle, it is possible that Irisin could play a role in reduced fibrosis noted in response to lack of myostatin. Consistent with this, *mdx* mice injected with Irisin display a significant reduction in fibrotic tissue accumulation in muscle (Figure 3.20b & 3.20c). Moreover, *mdx* mice injected with Irisin showed a significant improvement in grip strength (Figure 3.21e) and distinct hypertrophy of skeletal muscle (Figure 3.19e-3.19g). Irisin treatment has been previously shown to significantly increase IGF-1 expression in human myocytes[172]. Importantly, IGF-1 has been reported to aid in the rescue of muscle loss and reduce fibrosis in *mdx* mice[68]. Thus, Irisin regulation of IGF-1 may be a further mechanism through which Irisin functions to partially prevent/reverse dystrophic muscle loss in *mdx* mice[68]. Overall, results in this

149

thesis show that Irisin may be a promising therapeutic target for treating muscular dystrophy.

In this thesis, the function of Irisin in regulating muscle growth was systematically studied using *in vitro* and *in vivo* murine models. Results have revealed that Irisin is a pro-myogenic factor, which promotes skeletal muscle hypertrophy in mice. Irisin further enhances muscle regeneration and is able to rescue denervation-induced atrophy of muscle mass. Moreover, Irisin may play an important role in preventing, or reversing, dystrophic muscle loss. Taken together, these data reveal that treatment with Irisin, or situations that lead to increased Irisin levels, may have therapeutic potential in enhancing skeletal muscle growth and preventing skeletal muscle atrophy.

Based on the four different mouse trials, Irisin injection has consistently resulted in skeletal muscle hypertrophy. These data are important as they suggest that Irisin may have therapeutic potential in alleviating conditions that result in loss of skeletal muscle mass. Moreover, human and mouse Irisin share 100% sequence homology, which suggests that the Irisin receptor binding site in the Irisin protein may be the same between mice and humans. As such, Irisin could also confer positive effects on skeletal muscle of humans. As a therapeutic, Irisin protein could be injected into skeletal muscle of humans suffering from muscle loss or muscle wasting during conditions, such as prolonged periods of bed rest that result in disuse atrophy. Irisin could also be beneficial in enabling the rebuilding of muscle mass when an individual is unable to exercise, such as conditions when an individual has a limb in a cast. Irisin could also complement physiotherapy to accelerate the recovery of muscle mass and strength of patients. In conditions of muscular dystrophy, Irisin could also enhance muscle strength and mass, which could significantly reduce morbidity of the disease as well as mortality.

Although, Irisin mimics the phenotype of exercise in promoting muscle hypertrophy and myogenesis, there is insufficient evidence to show that Irisin has the potential to replace exercise entirely. Exercise results in a multitude of physiological effects on the body, which has not been assessed in response to

Irisin treatment. For example aerobic exercise increases cardiac output and heart muscle undergoes hypertrophy to enable the heart to pump more blood per stroke and hence, can supply more oxygen throughout the body. In response to exercise skeletal muscle consumes more oxygen and blood capillary density also increases in muscle. Exercise also exerts its effect on the endocrine system, resulting in enhanced levels of catecholamines, growth hormones, adrenocorticotropic (ACTH)-cortisol, testosterone, estradiol-progesterone and glucagon to name just a few. Hence, instead of replacing exercise, treatment with Irisin may act as a supplement to exercise and protect against loss of muscle mass and weakening of muscle.
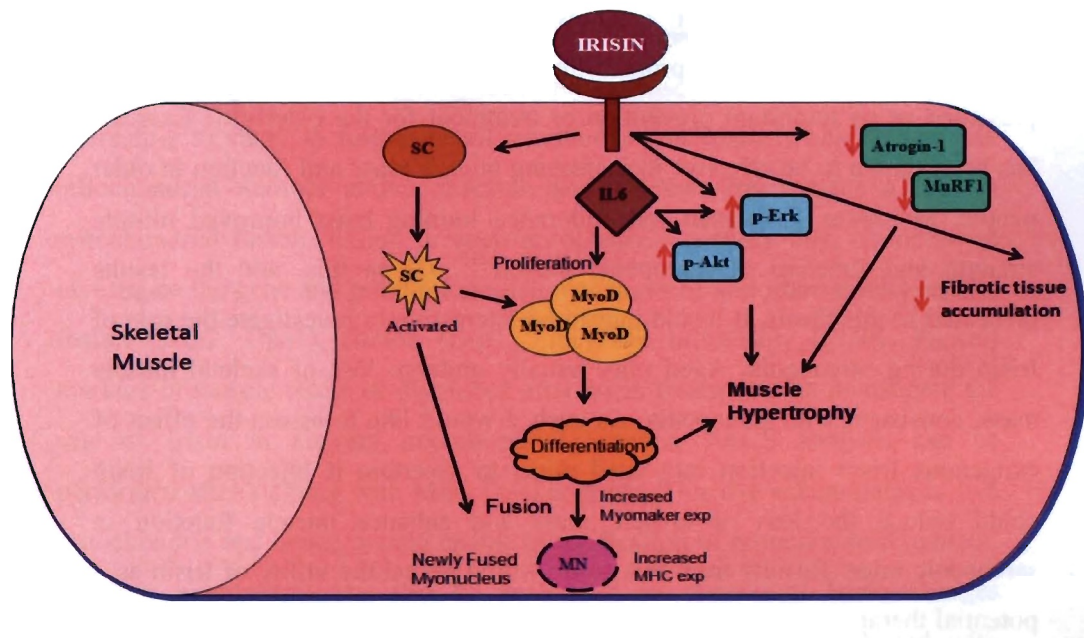
Figure 4.1: Irisin enhances myogenesis and promotes skeletal muscle hypertrophy

(a) Schematic diagram summarizing the role of Irisin in skeletal muscle. Binding of Irisin to an unknown receptor on skeletal muscle activates several pathways. Irisin activates Satellite cells, which can directly fuse to contribute to myonuclear domain expansion. Activated Satellite cells can also undergo repeated rounds of proliferation, differentiation and fusion. Irisin enhances fusion by increasing expression of the primary fusion marker, Myomaker. Enhanced myogenic differentiation can be validated by the increase in MHC expression. Irisin signals through IL6 to positively regulate myogenesis. Irisin also enhances protein synthesis pathways by activating p-Akt and p-Erk as well as by reducing raptor activity (*not shown in this diagram*). p-Akt and p-Erk activation can occur via IL6 signaling as well. Irisin also reduced the expression of key protein degradation markers, such as Atrogin-1 and MuRF1. In dystrophic conditions, Irisin is able to reduce fibrotic tissue accumulation and enhance sarcolemma stability (purple outline on skeletal muscle). These processes subsequently give rise to skeletal muscle hypertrophy. SC: Satellite cells, MN: Myonucleus, MHC: Myosin Heavy Chain.

152

5. Future Prospective

Sarcopenia is defined as the loss of skeletal muscle mass and strength due to ageing and is associated with the increased morbidity and mortality observed with ageing. Sarcopenia is a multi-factorial syndrome, which remains to be fully understood. However, it is known that physical inactivity could be a contributing factor to the progression of sarcopenia. Exercise has been presented as an important prevention or treatment for the elderly[211]. Exercise has been shown to be effective in increasing muscle mass and function in older people. Moreover, resistance and endurance training have improved muscle strength and function in sarcopenic muscle[212]. Given this, and the results presented in this thesis, it would indeed be interesting to investigate the role of Irisin during sarcopenia. Aged mice usually undergo loss of skeletal muscle mass, consistent with sarcopenia. As such, I would like to assess the effect of exogenous Irisin injection into aged mice, to ascertain if injection of Irisin could reduce the loss of muscle mass and enhance muscle function in sarcopenic mice. Results from this study would reveal the utility of Irisin as a potential therapeutic to protect against age-related loss of skeletal muscle mass and function.

Recently, Jedrychowski *et al.*, (2015) have confirmed the presence of circulating Irisin in humans, which is further increased following exercise[160]. Although it has been previously reported that human and mouse mature Irisin protein sequences are 100% identical[139], the biological effect of human Irisin on human skeletal muscle is yet to be fully studied. Results presented in this thesis revealed that human primary myoblasts were able to respond in a similar manner to murine myoblasts treated with murine recombinant Irisin protein, resulting in a significant increase in myotube number and myoblast fusion. These data suggest that human and mouse Irisin may have a similar function, or that the receptor and/or receptor binding domain between human and mouse Irisin may be identical. To identify the Irisin receptor in muscle, I will utilize biotinylated Irisin to isolate interacting proteins, including the potential Irisin receptor, using the affinity trapping method. Interacting proteins will be

153

identified by LC-MALDI-MS/MS[213]. Mutational analysis will then be employed to identify specific protein domains important for Irisin binding.

Results reported in this thesis show that Irisin is able to increase mitochondrial oxygen consumption in myoblast cultures. However, normalization of data to total protein content suggested that this phenomenon may be secondary to the increased myotube number and myoblast fusion observed. As such, it would be interesting to study in further detail whether or not Irisin is able to increase mitochondrial number and/or function and whether Irisin plays a role in mitochondrial fusion, fission or even mitophagy. To study this, I propose to investigate the gene and protein expression changes of important mitochondrial fusion (Mfn2, Opa1), fission (Drp1, Fis1) and mitophagy (PINK, Parkin) markers in muscle tissue or myotubes after Irisin treatment. To investigate the role of Irisin in altering mitochondrial number, FACS analysis can be performed after staining with Mito Tracker green. This dye accumulates in live mitochondria and hence, would enable quantification of mitochondrial number. Electron microscopy can also be performed to observe if Irisin changes mitochondrial morphology or topology. PGC1-α has been associated with increased mitochondrial biogenesis and is also known to increase the expression of FNDC5 in skeletal muscle. In this thesis, I have shown an increase in mitochondrial oxygen consumption after Irisin treatment. It would be interesting to investigate if PGC1-α can promote mitochondrial biogenesis via Irisin. To study this, *FNDC5* can be knocked down using siRNA targeted knockdown in C2C12 myotubes. To assess mitochondrial biogenesis, mitochondrial DNA copy number can be measured against nuclear DNA copy number in *FNDC5* knockdown myotubes using qPCR analysis.

In this thesis, I have shown that Irisin activates components of protein synthesis pathways and reduces markers involved in protein degradation. However, protein synthesis or protein degradation rates have not been directly quantified. Performing these experiments will add value to this study. Protein synthesis assay kits are available where nascent protein synthesis can be measure using L-homopropargylglycine (HPG), which is an analog of methionine and contain a fluorescent moiety. HPG will be incorporated instead of methionine during

154

active protein synthesis and newly formed proteins will contain a fluorescent tag which can then be detected by image based analysis. Protein degradation can also be assessed by measuring the expression levels of enzymes found in the 20s core component in the Proteasome, such as caspase like, trypsin like and chymotrypsin like. This will give an indication of the enzyme activity in the proteasome and whether or not Irisin is able to reduce proteasomal enzyme activity.

Overall, results in this thesis reveal that Irisin is indeed a pro-myogenic myokine, and as such warrants further investigation to unravel potential, as yet undiscovered, benefits.

6. Appendices

Appendix 6.1: Copyright clearance obtained for Figure 1.4

11/30/2016   RightsLink® by Copyright Clearance Center

Copyright Clearance Center — **RightsLink**®   Home | Account Info | Help

SAGE Publishing

Title:	The Skeletal Muscle Satellite Cell: The Stem Cell That Came in From the Cold:
Author:	Peter S. Zammit, Terence A. Partridge, Zipora Yablonka-Reuveni
Publication:	Journal of Histochemistry & Cytochemistry
Publisher:	SAGE Publications
Date:	11/01/2006

Copyright © 2006, © SAGE Publications

Logged in as:
maisha reza
Account #:
3001088599

LOGOUT

Gratis Reuse

Permission is granted at no cost for use of content in a Master's Thesis and/or Doctoral Dissertation. If you intend to distribute or sell your Master's Thesis/Doctoral Dissertation to the general public through print or website publication, please return to the previous page and select 'Republish in a Book/Journal' or 'Post on intranet/password-protected website' to complete your request.

BACK   CLOSE WINDOW

Appendix 6.2: Copyright clearance obtained for Figure 1.6

11/30/2016   Rightslink® by Copyright Clearance Center

Copyright Clearance Center   **RightsLink**   Home   Account Info   Help   ✉

Title:	Intracellular signaling pathways regulating net protein balance following diaphragm muscle denervation	Logged in as: maisha reza
Author:	Heather M. Argadine, Carlos B. Mantilla, Wen-Zhi Zhan, Gary C. Sieck	Account #: 3001088599
Publication:	Am J Physiol-Cell Physiology	LOGOUT
Publisher:	The American Physiological Society	
Date:	Feb 1, 2011	

Copyright © 2011, Copyright © 2011 the American Physiological Society

Permission Not Required

Permission is not required for this type of use.

BACK   CLOSE WINDOW

Appendix 6.3: Copyright clearance obtained for Figure 1.7

Rightslink® by Copyright Clearance Center

RightsLink

Home | Account Info | Help

nature publishing group

Title:	Muscles, exercise and obesity: skeletal muscle as a secretory organ
Author:	Bente K. Pedersen and Mark A. Febbraio
Publication:	Nature Reviews Endocrinology
Publisher:	Nature Publishing Group
Date:	Aug 1, 2012

Copyright © 2012, Rights Managed by Nature Publishing Group

Logged in as:
maisha reza
Account #:
3001088599

LOGOUT

Order Completed

Thank you for your order.

This Agreement between maisha reza ("You") and Nature Publishing Group ("Nature Publishing Group") consists of your license details and the terms and conditions provided by Nature Publishing Group and Copyright Clearance Center.

Your confirmation email will contain your order number for future reference.

Printable details.

License Number	3998621368997
License date	Nov 30, 2016
Licensed Content Publisher	Nature Publishing Group
Licensed Content Publication	Nature Reviews Endocrinology
Licensed Content Title	Muscles, exercise and obesity: skeletal muscle as a secretory organ
Licensed Content Author	Bente K. Pedersen and Mark A. Febbraio
Licensed Content Date	Aug 1, 2012
Licensed Content Volume	8
Licensed Content Issue	8
Type of Use	reuse in a dissertation / thesis
Requestor type	academic/educational
Format	print and electronic
Portion	figures/tables/illustrations
Number of figures/tables/illustrations	1
High-res required	no
Figures	Figure 1.7 Skeletal muscle as a secretory organ.
Author of this NPG article	no
Your reference number	
Title of your thesis / dissertation	CHARACTERIZATION OF THE ROLE OF IRISIN IN SKELETAL MUSCLE GROWTH AND REPAIR
Expected completion date	Dec 2016
Estimated size (number of pages)	120
Requestor Location	maisha reza Brenner Centre for Molecular Medicine 30 medical drive singapore, 117609 Singapore Attn: maisha reza
Billing Type	Invoice
Billing address	maisha reza Brenner Centre for Molecular Medicine 30 medical drive singapore, Singapore 117609 Attn: maisha reza

Appendix 6.4 Copyright clearance obtained for Figure 1.8

Copyright Clearance Center

RightsLink®

Home | Account Info | Help

nature publishing group

Title:	A PGC1-α-dependent myokine that drives brown-fat-like development of white fat and thermogenesis
Author:	Pontus Boström, Jun Wu, Mark P. Jedrychowski, Anisha Korde, Li Ye et al.
Publication:	Nature
Publisher:	Nature Publishing Group
Date:	Jan 11, 2012

Copyright © 2012, Rights Managed by Nature Publishing Group

Logged in as:
maisha reza
Account #:
3001088599

LOGOUT

Order Completed

Thank you for your order.

This Agreement between maisha reza ("You") and Nature Publishing Group ("Nature Publishing Group") consists of your license details and the terms and conditions provided by Nature Publishing Group and Copyright Clearance Center.

Your confirmation email will contain your order number for future reference.

Printable details.

License Number	3998630235904
License date	Nov 30, 2016
Licensed Content Publisher	Nature Publishing Group
Licensed Content Publication	Nature
Licensed Content Title	A PGC1-α-dependent myokine that drives brown-fat-like development of white fat and thermogenesis
Licensed Content Author	Pontus Boström, Jun Wu, Mark P. Jedrychowski, Anisha Korde, Li Ye et al.
Licensed Content Date	Jan 11, 2012
Licensed Content Volume	481
Licensed Content Issue	7382
Type of Use	reuse in a dissertation / thesis
Requestor type	academic/educational
Format	print and electronic
Portion	figures/tables/illustrations
Number of figures/tables/illustrations	1
High-res required	no
Figures	Figure 1.8: FNDC5 is proteolytically cleaved and secreted into circulation
Author of this NPG article	no
Your reference number	
Title of your thesis / dissertation	CHARACTERIZATION OF THE ROLE OF IRISIN IN SKELETAL MUSCLE GROWTH AND REPAIR
Expected completion date	Dec 2016
Estimated size (number of pages)	120
Requestor Location	maisha reza Brenner Centre for Molecular Medicine 30 medical drive singapore, 117609 Singapore Attn: maisha reza
Billing Type	Invoice
Billing address	maisha reza Brenner Centre for Molecular Medicine 30 medical drive singapore, Singapore 117609 Attn: maisha reza
Total	0.00 USD

7. References

1. Ten Broek RW, Grefte S, Von den Hoff JW. Regulatory factors and cell populations involved in skeletal muscle regeneration. *J Cell Physiol* **224**, 7-16 (2010).

2. Huxley AF, Taylor RE. Local activation of striated muscle fibres. *J Physiol* **144**, 426-441 (1958).

3. Jenkins GK, Tortora G. *Anantomy and Physiology: From Science to Life*. John wiley and sons, Inc (2006).

4. Ivy JL, Goforth HW, Jr., Damon BM, McCauley TR, Parsons EC, Price TB. Early postexercise muscle glycogen recovery is enhanced with a carbohydrate-protein supplement. *J Appl Physiol (1985)* **93**, 1337-1344 (2002).

5. Huxley AF. Muscle structure and theories of contraction. *Prog Biophys Biophys Chem* **7**, 255-318 (1957).

6. Zot AS, Potter JD. Structural aspects of troponin-tropomyosin regulation of skeletal muscle contraction. *Annu Rev Biophys Biophys Chem* **16**, 535-559 (1987).

7. Alberts B, Johnson A, Lewis J, Raff M, Roberts K, Walter P. *Molecular Biology of the Cell, 4th edition* (2002).

8. Rayment I, *et al.* Structure of the actin-myosin complex and its implications for muscle contraction. *Science* **261**, 58-65 (1993).

9. Fukunaga T, Ito M, Ichinose Y, Kuno S, Kawakami Y, Fukashiro S. Tendinous movement of a human muscle during voluntary contractions determined by real-time ultrasonography. *J Appl Physiol (1985)* **81**, 1430-1433 (1996).

10. Hall ZW, Sanes JR. Synaptic structure and development: the neuromuscular junction. *Cell* **72 Suppl**, 99-121 (1993).

11. Schneider MF. Control of calcium release in functioning skeletal muscle fibers. *Annu Rev Physiol* **56**, 463-484 (1994).

12. MacIntosh BR, Gardiner PF, McComas AJ. *Skeletal Muscle: Form and Function* (2006).

13. Marieb EN. *Human Anatomy & Physiology*. Pearson Education (2004).

14. Yaffe D, Feldman M. The Formation of Hybrid Multinucleated Muscle Fibers from Myoblasts of Different Genetic Origin. *Dev Biol* **11**, 300-317 (1965).

15.   Parker MH, Seale P, Rudnicki MA. Looking back to the embryo: defining transcriptional networks in adult myogenesis. *Nat Rev Genet* **4**, 497-507 (2003).

16.   Sambasivan R, Tajbakhsh S. Skeletal muscle stem cell birth and properties. *Semin Cell Dev Biol* **18**, 870-882 (2007).

17.   Davis TA, Fiorotto ML. Regulation of muscle growth in neonates. *Curr Opin Clin Nutr Metab Care* **12**, 78-85 (2009).

18.   Aulehla A, Pourquie O. Oscillating signaling pathways during embryonic development. *Curr Opin Cell Biol* **20**, 632-637 (2008).

19.   Yusuf F, Brand-Saberi B. The eventful somite: patterning, fate determination and cell division in the somite. *Anat Embryol (Berl)* **211 Suppl 1**, 21-30 (2006).

20.   Kiefer JC, Hauschka SD. Myf-5 is transiently expressed in nonmuscle mesoderm and exhibits dynamic regional changes within the presegmented mesoderm and somites I-IV. *Dev Biol* **232**, 77-90 (2001).

21.   Bladt F, Riethmacher D, Isenmann S, Aguzzi A, Birchmeier C. Essential role for the c-met receptor in the migration of myogenic precursor cells into the limb bud. *Nature* **376**, 768-771 (1995).

22.   Tajbakhsh S, Rocancourt D, Cossu G, Buckingham M. Redefining the genetic hierarchies controlling skeletal myogenesis: Pax- 3 and Myf-5 act upstream of MyoD. *Cell* **89**, 127-138 (1997).

23.   Gros J, Manceau M, Thome V, Marcelle C. A common somitic origin for embryonic muscle progenitors and satellite cells. *Nature* **435**, 954-958 (2005).

24.   Kassar-Duchossoy L, Giacone E, Gayraud-Morel B, Jory A, Gomes D, Tajbakhsh S. Pax3/Pax7 mark a novel population of primitive myogenic cells during development. *Genes Dev* **19**, 1426-1431 (2005).

25.   Relaix F, Rocancourt D, Mansouri A, Buckingham M. A Pax3/Pax7-dependent population of skeletal muscle progenitor cells. *Nature* **435**, 948-953 (2005).

26.   Kablar B, Krastel K, Ying C, Asakura A, Tapscott SJ, Rudnicki MA. MyoD and Myf-5 differentially regulate the development of limb versus trunk skeletal muscle. *Development* **124**, 4729-4738 (1997).

27.   Rudnicki MA, Schnegelsberg PN, Stead RH, Braun T, Arnold HH, Jaenisch R. MyoD or Myf-5 is required for the formation of skeletal muscle. *Cell* **75**, 1351-1359 (1993).

28.   Montarras D, *et al.* Developmental patterns in the expression of Myf5, MyoD, myogenin, and MRF4 during myogenesis. *New Biol* **3**, 592-600 (1991).

29.   Weintraub H. The MyoD family and myogenesis: redundancy, networks, and thresholds. *Cell* **75**, 1241-1244 (1993).

30.   Zhang W, Behringer RR, Olson EN. Inactivation of the myogenic bHLH gene MRF4 results in up-regulation of myogenin and rib anomalies. *Genes Dev* **9**, 1388-1399 (1995).

31.   Schmalbruch H, Lewis DM. Dynamics of nuclei of muscle fibers and connective tissue cells in normal and denervated rat muscles. *Muscle Nerve* **23**, 617-626 (2000).

32.   Pellettieri J, Sanchez Alvarado A. Cell turnover and adult tissue homeostasis: from humans to planarians. *Annu Rev Genet* **41**, 83-105 (2007).

33.   Katz F. The termination of the afferent nerve fiber in the muslce spindle of the frog. *Phil trans Roy Soc Lond* **243**, 221-225 (1961).

34.   Mauro A. Satellite cell of skeletal fibers. *Journal of Biophysical & Biochemistry Cytology* **9**, 493-498 (1961).

35.   Bischoff R. Analysis of muscle regeneration using single myofibers in culture. *Med Sci Sports Exerc* **21**, S164-172 (1989).

36.   Zammit PS, *et al.* Pax7 and myogenic progression in skeletal muscle satellite cells. *J Cell Sci* **119**, 1824-1832 (2006).

37.   Tatsumi R, Hattori A, Ikeuchi Y, Anderson JE, Allen RE. Release of hepatocyte growth factor from mechanically stretched skeletal muscle satellite cells and role of pH and nitric oxide. *Mol Biol Cell* **13**, 2909-2918 (2002).

38.   Allen RE, Boxhorn LK. Regulation of skeletal muscle satellite cell proliferation and differentiation by transforming growth factor-beta, insulin-like growth factor I, and fibroblast growth factor. *J Cell Physiol* **138**, 311-315 (1989).

39.   Allen RE, Rankin LL. Regulation of satellite cells during skeletal muscle growth and development. *Proc Soc Exp Biol Med* **194**, 81-86 (1990).

40.   Vaz R, Martins GG, Thorsteinsdottir S, Rodrigues G. Fibronectin promotes migration, alignment and fusion in an in vitro myoblast cell model. *Cell Tissue Res* **348**, 569-578 (2012).

41. Menko AS, Boettiger D. Occupation of the extracellular matrix receptor, integrin, is a control point for myogenic differentiation. *Cell* **51**, 51-57 (1987).

42. Yaffe D, Fuchs S. Autoradiographic study of the incorporation of uridine-3H during myogenesis in tissue culture. *Dev Biol* **15**, 33-50 (1967).

43. Kuang S, Gillespie MA, Rudnicki MA. Niche regulation of muscle satellite cell self-renewal and differentiation. *Cell Stem Cell* **2**, 22-31 (2008).

44. Boonen KJ, Post MJ. The muscle stem cell niche: regulation of satellite cells during regeneration. *Tissue Eng Part B Rev* **14**, 419-431 (2008).

45. Conboy MJ, Karasov AO, Rando TA. High incidence of non-random template strand segregation and asymmetric fate determination in dividing stem cells and their progeny. *PLoS Biol* **5**, e102 (2007).

46. Kuang S, Kuroda K, Le Grand F, Rudnicki MA. Asymmetric self-renewal and commitment of satellite stem cells in muscle. *Cell* **129**, 999-1010 (2007).

47. Bentzinger CF, Wang YX, Rudnicki MA. Building muscle: molecular regulation of myogenesis. *Cold Spring Harb Perspect Biol* **4**, (2012).

48. Grounds MD. *Regeneration of Muscle*. John Wiley & Sons, Ltd (2001).

49. Grounds MD. Age-associated changes in the response of skeletal muscle cells to exercise and regeneration. *Ann N Y Acad Sci* **854**, 78-91 (1998).

50. Jarvinen TA, Jarvinen TL, Kaariainen M, Kalimo H, Jarvinen M. Muscle injuries: biology and treatment. *Am J Sports Med* **33**, 745-764 (2005).

51. Smith C, Kruger MJ, Smith RM, Myburgh KH. The inflammatory response to skeletal muscle injury: illuminating complexities. *Sports Med* **38**, 947-969 (2008).

52. Schiaffino S, Partridge T. *Skeletal Muscle Repair and Regeneration* (2008).

53. Brigitte M, *et al.* Muscle resident macrophages control the immune cell reaction in a mouse model of notexin-induced myoinjury. *Arthritis Rheum* **62**, 268-279 (2010).

54. Chazaud B, *et al.* Dual and beneficial roles of macrophages during skeletal muscle regeneration. *Exerc Sport Sci Rev* **37**, 18-22 (2009).

55. Wiedow O, Meyer-Hoffert U. Neutrophil serine proteases: potential key regulators of cell signalling during inflammation. *J Intern Med* **257**, 319-328 (2005).

56. Arnold L, *et al.* Inflammatory monocytes recruited after skeletal muscle injury switch into antiinflammatory macrophages to support myogenesis. *J Exp Med* **204**, 1057-1069 (2007).

57. Mann CJ, *et al.* Aberrant repair and fibrosis development in skeletal muscle. *Skelet Muscle* **1**, 21 (2011).

58. McLennan IS. Degenerating and regenerating skeletal muscles contain several subpopulations of macrophages with distinct spatial and temporal distributions. *J Anat* **188**, 17-28 (1996).

59. Robertson TA, Maley MA, Grounds MD, Papadimitriou JM. The role of macrophages in skeletal muscle regeneration with particular reference to chemotaxis. *Exp Cell Res* **207**, 321-331 (1993).

60. Serrano AL, Munoz-Canoves P. Regulation and dysregulation of fibrosis in skeletal muscle. *Exp Cell Res* **316**, 3050-3058 (2010).

61. Chen X, Li Y. Role of matrix metalloproteinases in skeletal muscle: migration, differentiation, regeneration and fibrosis. *Cell Adh Migr* **3**, 337-341 (2009).

62. Burks TN, Cohn RD. Role of TGF-beta signaling in inherited and acquired myopathies. *Skelet Muscle* **1**, 19 (2011).

63. Li Y, *et al.* Transforming growth factor-beta1 induces the differentiation of myogenic cells into fibrotic cells in injured skeletal muscle: a key event in muscle fibrogenesis. *Am J Pathol* **164**, 1007-1019 (2004).

64. Hudlicka O, Brown M, Egginton S. Angiogenesis in skeletal and cardiac muscle. *Physiol Rev* **72**, 369-417 (1992).

65. Sussman M. Duchenne muscular dystrophy. *J Am Acad Orthop Surg* **10**, 138-151 (2002).

66. Menezes MP, North KN. Inherited neuromuscular disorders: pathway to diagnosis. *J Paediatr Child Health* **48**, 458-465 (2012).

67. Gosselin LE, McCormick KM. Targeting the immune system to improve ventilatory function in muscular dystrophy. *Med Sci Sports Exerc* **36**, 44-51 (2004).

68. Barton ER, Morris L, Musaro A, Rosenthal N, Sweeney HL. Muscle-specific expression of insulin-like growth factor I counters muscle decline in mdx mice. *J Cell Biol* **157**, 137-148 (2002).

69.   Yiu EM, Kornberg AJ. Duchenne muscular dystrophy. *Neurol India* **56**, 236-247 (2008).

70.   Hoffman EP, Brown RH, Jr., Kunkel LM. Dystrophin: the protein product of the Duchenne muscular dystrophy locus. *Cell* **51**, 919-928 (1987).

71.   Whitehead NP, Yeung EW, Allen DG. Muscle damage in mdx (dystrophic) mice: role of calcium and reactive oxygen species. *Clin Exp Pharmacol Physiol* **33**, 657-662 (2006).

72.   Duddy W, *et al.* Muscular dystrophy in the mdx mouse is a severe myopathy compounded by hypotrophy, hypertrophy and hyperplasia. *Skelet Muscle* **5**, 16 (2015).

73.   Tanabe Y, Esaki K, Nomura T. Skeletal muscle pathology in X chromosome-linked muscular dystrophy (mdx) mouse. *Acta Neuropathol* **69**, 91-95 (1986).

74.   Glass DJ. Molecular mechanisms modulating muscle mass. *Trends Mol Med* **9**, 344-350 (2003).

75.   Blaauw B, Reggiani C. The role of satellite cells in muscle hypertrophy. *J Muscle Res Cell Motil* **35**, 3-10 (2014).

76.   Tesch PA. Skeletal muscle adaptations consequent to long-term heavy resistance exercise. *Med Sci Sports Exerc* **20**, S132-134 (1988).

77.   Welle S, Bhatt K, Thornton CA. Stimulation of myofibrillar synthesis by exercise is mediated by more efficient translation of mRNA. *J Appl Physiol (1985)* **86**, 1220-1225 (1999).

78.   Yarasheski KE, Zachwieja JJ, Bier DM. Acute effects of resistance exercise on muscle protein synthesis rate in young and elderly men and women. *Am J Physiol* **265**, E210-214 (1993).

79.   Bodine SC, *et al.* Akt/mTOR pathway is a crucial regulator of skeletal muscle hypertrophy and can prevent muscle atrophy in vivo. *Nat Cell Biol* **3**, 1014-1019 (2001).

80.   Argadine HM, Mantilla CB, Zhan WZ, Sieck GC. Intracellular signaling pathways regulating net protein balance following diaphragm muscle denervation. *Am J Physiol Cell Physiol* **300**, C318-327 (2011).

81.   Widegren U, Wretman C, Lionikas A, Hedin G, Henriksson J. Influence of exercise intensity on ERK/MAP kinase signalling in human skeletal muscle. *Pflugers Arch* **441**, 317-322 (2000).

82.   Yu M, Blomstrand E, Chibalin AV, Krook A, Zierath JR. Marathon running increases ERK1/2 and p38 MAP kinase signalling to

downstream targets in human skeletal muscle. *J Physiol* **536**, 273-282 (2001).

83.   Creer A, Gallagher P, Slivka D, Jemiolo B, Fink W, Trappe S. Influence of muscle glycogen availability on ERK1/2 and Akt signaling after resistance exercise in human skeletal muscle. *J Appl Physiol (1985)* **99**, 950-956 (2005).

84.   Aronson D, Violan MA, Dufresne SD, Zangen D, Fielding RA, Goodyear LJ. Exercise stimulates the mitogen-activated protein kinase pathway in human skeletal muscle. *J Clin Invest* **99**, 1251-1257 (1997).

85.   Waskiewicz AJ, Flynn A, Proud CG, Cooper JA. Mitogen-activated protein kinases activate the serine/threonine kinases Mnk1 and Mnk2. *EMBO J* **16**, 1909-1920 (1997).

86.   Williamson D, Gallagher P, Harber M, Hollon C, Trappe S. Mitogen-activated protein kinase (MAPK) pathway activation: effects of age and acute exercise on human skeletal muscle. *J Physiol* **547**, 977-987 (2003).

87.   McKoy G, *et al.* Expression of insulin growth factor-1 splice variants and structural genes in rabbit skeletal muscle induced by stretch and stimulation. *J Physiol* **516 (Pt 2)**, 583-592 (1999).

88.   Semsarian C, Sutrave P, Richmond DR, Graham RM. Insulin-like growth factor (IGF-I) induces myotube hypertrophy associated with an increase in anaerobic glycolysis in a clonal skeletal-muscle cell model. *Biochem J* **339 (Pt 2)**, 443-451 (1999).

89.   Nojima H, *et al.* The mammalian target of rapamycin (mTOR) partner, raptor, binds the mTOR substrates p70 S6 kinase and 4E-BP1 through their TOR signaling (TOS) motif. *J Biol Chem* **278**, 15461-15464 (2003).

90.   Schalm SS, Fingar DC, Sabatini DM, Blenis J. TOS motif-mediated raptor binding regulates 4E-BP1 multisite phosphorylation and function. *Curr Biol* **13**, 797-806 (2003).

91.   Gwinn DM, *et al.* AMPK phosphorylation of raptor mediates a metabolic checkpoint. *Mol Cell* **30**, 214-226 (2008).

92.   Goberdhan DC, Paricio N, Goodman EC, Mlodzik M, Wilson C. Drosophila tumor suppressor PTEN controls cell size and number by antagonizing the Chico/PI3-kinase signaling pathway. *Genes Dev* **13**, 3244-3258 (1999).

93.   Huang H, *et al.* PTEN affects cell size, cell proliferation and apoptosis during Drosophila eye development. *Development* **126**, 5365-5372 (1999).

94.   Xu Z, Stokoe D, Kane LP, Weiss A. The inducible expression of the tumor suppressor gene PTEN promotes apoptosis and decreases cell size by inhibiting the PI3K/Akt pathway in Jurkat T cells. *Cell Growth Differ* **13**, 285-296 (2002).

95.   Rommel C, *et al.* Mediation of IGF-1-induced skeletal myotube hypertrophy by PI(3)K/Akt/mTOR and PI(3)K/Akt/GSK3 pathways. *Nat Cell Biol* **3**, 1009-1013 (2001).

96.   Dupont-Versteegden EE, *et al.* Exercise-induced gene expression in soleus muscle is dependent on time after spinal cord injury in rats. *Muscle Nerve* **29**, 73-81 (2004).

97.   Sandri M, *et al.* PGC-1alpha protects skeletal muscle from atrophy by suppressing FoxO3 action and atrophy-specific gene transcription. *Proc Natl Acad Sci U S A* **103**, 16260-16265 (2006).

98.   Lecker SH, Solomon V, Mitch WE, Goldberg AL. Muscle protein breakdown and the critical role of the ubiquitin-proteasome pathway in normal and disease states. *J Nutr* **129**, 227S-237S (1999).

99.   Sandri M, *et al.* Foxo transcription factors induce the atrophy-related ubiquitin ligase atrogin-1 and cause skeletal muscle atrophy. *Cell* **117**, 399-412 (2004).

100.   Bailey JL, Wang X, England BK, Price SR, Ding X, Mitch WE. The acidosis of chronic renal failure activates muscle proteolysis in rats by augmenting transcription of genes encoding proteins of the ATP-dependent ubiquitin-proteasome pathway. *J Clin Invest* **97**, 1447-1453 (1996).

101.   Pickering WP, Price SR, Bircher G, Marinovic AC, Mitch WE, Walls J. Nutrition in CAPD: serum bicarbonate and the ubiquitin-proteasome system in muscle. *Kidney Int* **61**, 1286-1292 (2002).

102.   Thomason DB, Herrick RE, Surdyka D, Baldwin KM. Time course of soleus muscle myosin expression during hindlimb suspension and recovery. *J Appl Physiol (1985)* **63**, 130-137 (1987).

103.   Castillero E, Alamdari N, Lecker SH, Hasselgren PO. Suppression of atrogin-1 and MuRF1 prevents dexamethasone-induced atrophy of cultured myotubes. *Metabolism* **62**, 1495-1502 (2013).

104.   Bodine SC, *et al.* Identification of ubiquitin ligases required for skeletal muscle atrophy. *Science* **294**, 1704-1708 (2001).

105.   Hoffman EP, Nader GA. Balancing muscle hypertrophy and atrophy. *Nat Med* **10**, 584-585 (2004).

106. Sacheck JM, Ohtsuka A, McLary SC, Goldberg AL. IGF-1 stimulates muscle growth by suppressing protein breakdown and expression of atrophy-related ubiquitin-ligases, atrogin-1 and MuRF1. *Am J Physiol Endocrinol Metab*, (2004).

107. Li YP, Reid MB. NF-kappaB mediates the protein loss induced by TNF-alpha in differentiated skeletal muscle myotubes. *Am J Physiol Regul Integr Comp Physiol* **279**, R1165-1170 (2000).

108. Pedersen BK, Febbraio MA. Muscles, exercise and obesity: skeletal muscle as a secretory organ. *Nat Rev Endocrinol* **8**, 457-465 (2012).

109. Pedersen BK, Steensberg A, Schjerling P. Muscle-derived interleukin-6: possible biological effects. *J Physiol* **536**, 329-337 (2001).

110. Jonsdottir IH, Schjerling P, Ostrowski K, Asp S, Richter EA, Pedersen BK. Muscle contractions induce interleukin-6 mRNA production in rat skeletal muscles. *J Physiol* **528 Pt 1**, 157-163 (2000).

111. Serrano AL, Baeza-Raja B, Perdiguero E, Jardi M, Munoz-Canoves P. Interleukin-6 is an essential regulator of satellite cell-mediated skeletal muscle hypertrophy. *Cell Metab* **7**, 33-44 (2008).

112. Baeza-Raja B, Munoz-Canoves P. p38 MAPK-induced nuclear factor-kappaB activity is required for skeletal muscle differentiation: role of interleukin-6. *Mol Biol Cell* **15**, 2013-2026 (2004).

113. Taga T, *et al.* Interleukin-6 triggers the association of its receptor with a possible signal transducer, gp130. *Cell* **58**, 573-581 (1989).

114. Heinrich PC, Behrmann I, Muller-Newen G, Schaper F, Graeve L. Interleukin-6-type cytokine signalling through the gp130/Jak/STAT pathway. *Biochem J* **334 (Pt 2)**, 297-314 (1998).

115. Begue G, *et al.* Early activation of rat skeletal muscle IL-6/STAT1/STAT3 dependent gene expression in resistance exercise linked to hypertrophy. *PLoS One* **8**, e57141 (2013).

116. Glund S, *et al.* Interleukin-6 directly increases glucose metabolism in resting human skeletal muscle. *Diabetes* **56**, 1630-1637 (2007).

117. Kim TH, *et al.* IL-6 induction of TLR-4 gene expression via STAT3 has an effect on insulin resistance in human skeletal muscle. *Acta Diabetol* **50**, 189-200 (2013).

118. Starr R, *et al.* A family of cytokine-inducible inhibitors of signalling. *Nature* **387**, 917-921 (1997).

119. Endo TA, *et al.* A new protein containing an SH2 domain that inhibits JAK kinases. *Nature* **387**, 921-924 (1997).

120. Naka T, et al. Structure and function of a new STAT-induced STAT inhibitor. Nature 387, 924-929 (1997).

121. Carey AL, et al. Interleukin-6 increases insulin-stimulated glucose disposal in humans and glucose uptake and fatty acid oxidation in vitro via AMP-activated protein kinase. Diabetes 55, 2688-2697 (2006).

122. Rieusset J, et al. Suppressor of cytokine signaling 3 expression and insulin resistance in skeletal muscle of obese and type 2 diabetic patients. Diabetes 53, 2232-2241 (2004).

123. Hoene M, Runge H, Haring HU, Schleicher ED, Weigert C. Interleukin-6 promotes myogenic differentiation of mouse skeletal muscle cells: role of the STAT3 pathway. Am J Physiol Cell Physiol 304, C128-136 (2013).

124. Wang K, Wang C, Xiao F, Wang H, Wu Z. JAK2/STAT2/STAT3 are required for myogenic differentiation. J Biol Chem 283, 34029-34036 (2008).

125. Kambadur R, Sharma M, Smith TP, Bass JJ. Mutations in myostatin (GDF8) in double-muscled Belgian Blue and Piedmontese cattle. Genome Res 7, 910-916 (1997).

126. McPherron AC, Lawler AM, Lee SJ. Regulation of skeletal muscle mass in mice by a new TGF-beta superfamily member. Nature 387, 83-90 (1997).

127. Lee SJ, McPherron AC. Regulation of myostatin activity and muscle growth. Proc Natl Acad Sci U S A 98, 9306-9311 (2001).

128. Zhu X, Topouzis S, Liang LF, Stotish RL. Myostatin signaling through Smad2, Smad3 and Smad4 is regulated by the inhibitory Smad7 by a negative feedback mechanism. Cytokine 26, 262-272 (2004).

129. McFarlane C, et al. Human myostatin negatively regulates human myoblast growth and differentiation. Am J Physiol Cell Physiol 301, C195-203 (2011).

130. Thomas M, et al. Myostatin, a negative regulator of muscle growth, functions by inhibiting myoblast proliferation. J Biol Chem 275, 40235-40243 (2000).

131. Langley B, Thomas M, Bishop A, Sharma M, Gilmour S, Kambadur R. Myostatin inhibits myoblast differentiation by down-regulating MyoD expression. J Biol Chem 277, 49831-49840 (2002).

132. Trendelenburg AU, Meyer A, Rohner D, Boyle J, Hatakeyama S, Glass DJ. Myostatin reduces Akt/TORC1/p70S6K signaling, inhibiting

myoblast differentiation and myotube size. *Am J Physiol Cell Physiol* **296**, C1258-1270 (2009).

133.   Amirouche A, *et al.* Down-regulation of Akt/mammalian target of rapamycin signaling pathway in response to myostatin overexpression in skeletal muscle. *Endocrinology* **150**, 286-294 (2009).

134.   McFarlane C, *et al.* Myostatin induces cachexia by activating the ubiquitin proteolytic system through an NF-kappaB-independent, FoxO1-dependent mechanism. *J Cell Physiol* **209**, 501-514 (2006).

135.   McCroskery S, Thomas M, Maxwell L, Sharma M, Kambadur R. Myostatin negatively regulates satellite cell activation and self-renewal. *J Cell Biol* **162**, 1135-1147 (2003).

136.   McCroskery S, *et al.* Improved muscle healing through enhanced regeneration and reduced fibrosis in myostatin-null mice. *J Cell Sci* **118**, 3531-3541 (2005).

137.   Li ZB, Kollias HD, Wagner KR. Myostatin directly regulates skeletal muscle fibrosis. *J Biol Chem* **283**, 19371-19378 (2008).

138.   Zhu J, *et al.* Relationships between transforming growth factor-beta1, myostatin, and decorin: implications for skeletal muscle fibrosis. *J Biol Chem* **282**, 25852-25863 (2007).

139.   Bostrom P, *et al.* A PGC1-alpha-dependent myokine that drives brown-fat-like development of white fat and thermogenesis. *Nature* **481**, 463-468 (2012).

140.   Handschin C, Spiegelman BM. The role of exercise and PGC1alpha in inflammation and chronic disease. *Nature* **454**, 463-469 (2008).

141.   Wenz T, Rossi SG, Rotundo RL, Spiegelman BM, Moraes CT. Increased muscle PGC-1alpha expression protects from sarcopenia and metabolic disease during aging. *Proc Natl Acad Sci U S A* **106**, 20405-20410 (2009).

142.   Ibrahim MM. Subcutaneous and visceral adipose tissue: structural and functional differences. *Obes Rev* **11**, 11-18 (2010).

143.   Bartelt A, *et al.* Brown adipose tissue activity controls triglyceride clearance. *Nat Med* **17**, 200-205 (2011).

144.   Cannon B, Nedergaard J. Brown adipose tissue: function and physiological significance. *Physiol Rev* **84**, 277-359 (2004).

145.   Wu J, *et al.* Beige adipocytes are a distinct type of thermogenic fat cell in mouse and human. *Cell* **150**, 366-376 (2012).

146. Lidell ME, Enerback S. Brown adipose tissue--a new role in humans? *Nat Rev Endocrinol* **6**, 319-325 (2010).

147. Ravussin E, Galgani JE. The implication of brown adipose tissue for humans. *Annu Rev Nutr* **31**, 33-47 (2011).

148. Zhang Y, *et al.* Irisin stimulates browning of white adipocytes through mitogen-activated protein kinase p38 MAP kinase and ERK MAP kinase signaling. *Diabetes* **63**, 514-525 (2014).

149. Assyov Y, Gateva A, Tsakova A, Kamenov Z. Irisin in the Glucose Continuum. *Exp Clin Endocrinol Diabetes* **124**, 22-27 (2016).

150. Choi YK, *et al.* Serum irisin levels in new-onset type 2 diabetes. *Diabetes Res Clin Pract* **100**, 96-101 (2013).

151. Xin C, *et al.* Irisin improves fatty acid oxidation and glucose utilization in type 2 diabetes by regulating the AMPK signaling pathway. *Int J Obes (Lond)* **40**, 443-451 (2016).

152. Lu Y, *et al.* Swimming exercise increases serum irisin level and reduces body fat mass in high-fat-diet fed Wistar rats. *Lipids Health Dis* **15**, 93 (2016).

153. Kim HJ, Lee HJ, So B, Son JS, Yoon D, Song W. Effect of aerobic training and resistance training on circulating irisin level and their association with change of body composition in overweight/obese adults: a pilot study. *Physiol Res* **65**, 271-279 (2016).

154. Kim HJ, So B, Choi M, Kang D, Song W. Resistance exercise training increases the expression of irisin concomitant with improvement of muscle function in aging mice and humans. *Exp Gerontol* **70**, 11-17 (2015).

155. Tsuchiya Y, Ando D, Takamatsu K, Goto K. Resistance exercise induces a greater irisin response than endurance exercise. *Metabolism* **64**, 1042-1050 (2015).

156. Raschke S, *et al.* Evidence against a beneficial effect of irisin in humans. *PLoS One* **8**, e73680 (2013).

157. Albrecht E, *et al.* Irisin - a myth rather than an exercise-inducible myokine. *Sci Rep* **5**, 8889 (2015).

158. Pekkala S, *et al.* Are skeletal muscle FNDC5 gene expression and irisin release regulated by exercise and related to health? *J Physiol* **591**, 5393-5400 (2013).

159. Kurdiova T, *et al.* Exercise-mimicking treatment fails to increase Fndc5 mRNA & irisin secretion in primary human myotubes. *Peptides* **56**, 1-7 (2014).

160. Jedrychowski MP, *et al.* Detection and Quantitation of Circulating Human Irisin by Tandem Mass Spectrometry. *Cell Metab* **22**, 734-740 (2015).

161. Lee P, *et al.* Irisin and FGF21 are cold-induced endocrine activators of brown fat function in humans. *Cell Metab* **19**, 302-309 (2014).

162. Roca-Rivada A, *et al.* FNDC5/irisin is not only a myokine but also an adipokine. *PLoS One* **8**, e60563 (2013).

163. Huh JY, *et al.* FNDC5 and irisin in humans: I. Predictors of circulating concentrations in serum and plasma and II. mRNA expression and circulating concentrations in response to weight loss and exercise. *Metabolism* **61**, 1725-1738 (2012).

164. Liu TY, *et al.* Irisin inhibits hepatic gluconeogenesis and increases glycogen synthesis via the PI3K/Akt pathway in type 2 diabetic mice and hepatocytes. *Clin Sci (Lond)* **129**, 839-850 (2015).

165. Park MJ, Kim DI, Choi JH, Heo YR, Park SH. New role of irisin in hepatocytes: The protective effect of hepatic steatosis in vitro. *Cell Signal* **27**, 1831-1839 (2015).

166. Wrann CD, *et al.* Exercise induces hippocampal BDNF through a PGC-1alpha/FNDC5 pathway. *Cell Metab* **18**, 649-659 (2013).

167. Rodriguez-Carmona A, *et al.* Serum levels of the adipomyokine irisin in patients with chronic kidney disease. *Nefrologia* **36**, 496-502 (2016).

168. Ebert T, *et al.* Serum levels of the myokine irisin in relation to metabolic and renal function. *Eur J Endocrinol* **170**, 501-506 (2014).

169. Wen MS, Wang CY, Lin SL, Hung KC. Decrease in irisin in patients with chronic kidney disease. *PLoS One* **8**, e64025 (2013).

170. Vaughan RA, *et al.* Characterization of the metabolic effects of irisin on skeletal muscle in vitro. *Diabetes Obes Metab* **16**, 711-718 (2014).

171. Shan T, Liang X, Bi P, Kuang S. Myostatin knockout drives browning of white adipose tissue through activating the AMPK-PGC1alpha-Fndc5 pathway in muscle. *FASEB J*, (2013).

172. Huh JY, Dincer F, Mesfum E, Mantzoros CS. Irisin stimulates muscle growth-related genes and regulates adipocyte differentiation and metabolism in humans. *Int J Obes (Lond)* **38**, 1538-1544 (2014).

173. Yaffe D, Saxel O. Serial passaging and differentiation of myogenic cells isolated from dystrophic mouse muscle. *Nature* **270**, 725-727 (1977).

174. Wang H, *et al.* High-level expression and purification of soluble recombinant FGF21 protein by SUMO fusion in Escherichia coli. *BMC Biotechnology* **10**, 14-14 (2010).

175. Vasudevan KM, *et al.* AKT-independent signaling downstream of oncogenic PIK3CA mutations in human cancer. *Cancer Cell* **16**, 21-32 (2009).

176. Sarvas JL, Khaper N, Lees SJ. The IL-6 Paradox: Context Dependent Interplay of SOCS3 and AMPK. *Journal of diabetes & metabolism* **Suppl 13**, 10.4172/2155-6156.S4113-4003 (2013).

177. Mahajan RD, Patra SK. Irisin, a novel myokine responsible for exercise induced browning of white adipose tissue. *Indian J Clin Biochem* **28**, 102-103 (2013).

178. Pyrzak B, Demkow U, Kucharska AM. Brown Adipose Tissue and Browning Agents: Irisin and FGF21 in the Development of Obesity in Children and Adolescents. *Adv Exp Med Biol* **866**, 25-34 (2015).

179. Zhang Y, *et al.* Irisin exerts dual effects on browning and adipogenesis of human white adipocytes. *Am J Physiol Endocrinol Metab* **311**, E530-541 (2016).

180. Zhou X, *et al.* ROCK1 reduces mitochondrial content and irisin production in muscle suppressing adipocyte browning and impairing insulin sensitivity. *Sci Rep* **6**, 29669 (2016).

181. Sezonov G, Joseleau-Petit D, D'Ari R. Escherichia coli physiology in Luria-Bertani broth. *J Bacteriol* **189**, 8746-8749 (2007).

182. Pope B, Kent HM. High efficiency 5 min transformation of Escherichia coli. *Nucleic Acids Res* **24**, 536-537 (1996).

183. Rietschel ET, *et al.* Bacterial endotoxin: Chemical constitution, biological recognition, host response, and immunological detoxification. *Curr Top Microbiol Immunol* **216**, 39-81 (1996).

184. Raetz CR, Whitfield C. Lipopolysaccharide endotoxins. *Annu Rev Biochem* **71**, 635-700 (2002).

185. Suffredini AF, Hochstein HD, McMahon FG. Dose-related inflammatory effects of intravenous endotoxin in humans: evaluation of a new clinical lot of Escherichia coli O:113 endotoxin. *J Infect Dis* **179**, 1278-1282 (1999).

186. Werling D, *et al.* Characterisation of the acute phase response of heifers to a prolonged low dose infusion of lipopolysaccharide. *Res Vet Sci* **61**, 252-257 (1996).

187. Sahdev S, Khattar SK, Saini KS. Production of active eukaryotic proteins through bacterial expression systems: a review of the existing biotechnology strategies. *Mol Cell Biochem* **307**, 249-264 (2008).

188. Khow O, Suntrarachun S. Strategies for production of active eukaryotic proteins in bacterial expression system. *Asian Pac J Trop Biomed* **2**, 159-162 (2012).

189. Millay DP, *et al.* Myomaker is a membrane activator of myoblast fusion and muscle formation. *Nature* **499**, 301-305 (2013).

190. Glass DJ. Signalling pathways that mediate skeletal muscle hypertrophy and atrophy. *Nat Cell Biol* **5**, 87-90 (2003).

191. Glass DJ. Skeletal muscle hypertrophy and atrophy signaling pathways. *Int J Biochem Cell Biol* **37**, 1974-1984 (2005).

192. Rosenblatt JD, Yong D, Parry DJ. Satellite cell activity is required for hypertrophy of overloaded adult rat muscle. *Muscle Nerve* **17**, 608-613 (1994).

193. Jackman RW, Kandarian SC. The molecular basis of skeletal muscle atrophy. *Am J Physiol Cell Physiol* **287**, C834-843 (2004).

194. McClung JM, Judge AR, Powers SK, Yan Z. p38 MAPK links oxidative stress to autophagy-related gene expression in cachectic muscle wasting. *Am J Physiol Cell Physiol* **298**, C542-549 (2010).

195. Bertaggia E, *et al.* Haptoglobin is required to prevent oxidative stress and muscle atrophy. *PLoS One* **9**, e100745 (2014).

196. Medina R, Wing SS, Haas A, Goldberg AL. Activation of the ubiquitin-ATP-dependent proteolytic system in skeletal muscle during fasting and denervation atrophy. *Biomed Biochim Acta* **50**, 347-356 (1991).

197. Mosole S, *et al.* Long-term high-level exercise promotes muscle reinnervation with age. *J Neuropathol Exp Neurol* **73**, 284-294 (2014).

198. Wu Z, *et al.* Mechanisms controlling mitochondrial biogenesis and respiration through the thermogenic coactivator PGC-1. *Cell* **98**, 115-124 (1999).

199. Brussee V, Tardif F, Tremblay JP. Muscle fibers of mdx mice are more vulnerable to exercise than those of normal mice. *Neuromuscul Disord* **7**, 487-492 (1997).

200. McGeachie JK, Grounds MD, Partridge TA, Morgan JE. Age-related changes in replication of myogenic cells in mdx mice: quantitative autoradiographic studies. *J Neurol Sci* **119**, 169-179 (1993).

201. Radu M, Chernoff J. An in vivo assay to test blood vessel permeability. *J Vis Exp*, e50062 (2013).

202. Hamer PW, McGeachie JM, Davies MJ, Grounds MD. Evans Blue Dye as an in vivo marker of myofibre damage: optimising parameters for detecting initial myofibre membrane permeability. *J Anat* **200**, 69-79 (2002).

203. Straub V, Rafael JA, Chamberlain JS, Campbell KP. Animal models for muscular dystrophy show different patterns of sarcolemmal disruption. *J Cell Biol* **139**, 375-385 (1997).

204. Walker H, Hall W, Hurst J. *Clinical Methods: The History, Physical, and Laboratory Examinations*. Butterworths (1990).

205. Bulfield G, Siller WG, Wight PA, Moore KJ. X chromosome-linked muscular dystrophy (mdx) in the mouse. *Proc Natl Acad Sci U S A* **81**, 1189-1192 (1984).

206. Grounds MD. *Skeletal Muscle Repair and Regeneration* (2008).

207. Clerk A, Morris GE, Dubowitz V, Davies KE, Sewry CA. Dystrophin-related protein, utrophin, in normal and dystrophic human fetal skeletal muscle. *Histochem J* **25**, 554-561 (1993).

208. Baban D, Davies KE. Microarray analysis of mdx mice expressing high levels of utrophin: therapeutic implications for dystrophin deficiency. *Neuromuscul Disord* **18**, 239-247 (2008).

209. Bo Li Z, Zhang J, Wagner KR. Inhibition of myostatin reverses muscle fibrosis through apoptosis. *J Cell Sci* **125**, 3957-3965 (2012).

210. Wagner KR, McPherron AC, Winik N, Lee SJ. Loss of myostatin attenuates severity of muscular dystrophy in mdx mice. *Ann Neurol* **52**, 832-836 (2002).

211. Montero-Fernandez N, Serra-Rexach JA. Role of exercise on sarcopenia in the elderly. *Eur J Phys Rehabil Med* **49**, 131-143 (2013).

212. Phu S, Boersma D, Duque G. Exercise and Sarcopenia. *J Clin Densitom* **18**, 488-492 (2015).

213. Shinya T, *et al.* Characterization of receptor proteins using affinity cross-linking with biotinylated ligands. *Plant Cell Physiol* **51**, 262-270 (2010).